

Crude Oil Chemistry Effects on Corrosion Inhibition and Phase Wetting in
Oil-Water Flow

A dissertation presented to
the faculty of
the Russ College of Engineering and Technology of Ohio University

In partial fulfillment
of the requirements for the degree
Doctor of Philosophy

François Ayello

November 2010

© 2010 François Ayello. All Rights Reserved.

This dissertation titled
Crude Oil Chemistry Effects on Corrosion Inhibition and Phase Wetting in
Oil-Water Flow

by

FRANÇOIS AYELLO

has been approved for
the Department of Chemical and Biomolecular Engineering
and the Russ College of Engineering and Technology by

Srdjan Nešić

Professor of Chemical and Biomolecular Engineering

Dennis Irwin

Dean, Russ College of Engineering and Technology

ABSTRACT

AYELLO, FRANÇOIS, Ph.D., November 2010, Chemical Engineering

Crude Oil Chemistry Effects on Corrosion Inhibition and Phase Wetting in Oil-Water Flow (181 pp.)

Director of Dissertation: Srdjan Nešić

The presence of water, even in small amounts, is often the cause of internal corrosion problems in crude oil transportation. Understanding the factors influencing steel pipeline corrosion rates is a safety as well as an economic matter. The objective of this dissertation is to quantify the effects that are known to have an influence on corrosion in crude oil-brine flow.

- The first effect is the corrosiveness of the brine. Crude oil's compounds can partition between the oil phase and the water phase to create brines with inhibitive or corrosive properties.

- The second effect is related to which phase wets the pipe wall. This depends on steel wettability and also on the flow pattern. Crude oil's polar compounds can change the steel hydrophilic surface nature. They also change the flow properties.

The problem has been investigated at the Institute for Corrosion and Multiphase Technology at Ohio University on a small scale with specifically designed experiments as well as on a large scale, in a 60 meter-long flow loop loaded with 1600 gallons of oil and water. Results show that only a small percentage of the crude oil's complex chemistry controls its corrosion inhibitive and wettability properties. The knowledge generated from these experiments can be used as a useful reference for corrosion engineers and pipeline operators to maintain oil-water flow systems under corrosion-free conditions.

Approved: _____

Srdjan Nešić

Professor of Chemical and Biomolecular Engineering

ACKNOWLEDGEMENTS

Though the following dissertation is the result of my own work, many people have helped and directed me. I would like to express my most sincere appreciation to my supervisor Dr. Srdjan Nešić for his direction and encouragements. I have been privileged to have a supervisor who gave me both the freedom to explore on my own and guidance when it was needed. I am pleased to thank Dr. Winston Robbins for his insightful comments and direction in the chemical aspect of this dissertation. I would like to thank Dr. Jiyong Cai and Dr. Sonja Richter, both deeply engaged in the “Water Wetting” program at the Institute for Corrosion and Multiphase Technology (ICMT) at Ohio University. I am also thankful to Dr. David Young for his advice and for proofreading this dissertation. I would like to acknowledge the students and other staff members at the ICMT; Bruce Brown, for solving daily problems and Chong Li, Xuanping Tang and Pankaj Ajmera for their teamwork over the last four years. I recognize the financial support of the sponsors of the “Water Wetting” program at the ICMT; BP, Conoco-Phillips, ENI, Exxon Mobil, Petrobras, Saudi Aramco, Shell and Total; without which no research could have been done. Finally, my deepest and warmest appreciation goes to my parents for their unconditional support.

PREFACE

This thesis is submitted in partial fulfillment of the requirements for the PhD degree at the department of Chemical and Biomolecular Engineering, Russ College of Engineering and Technology, Ohio University. The work has been carried out at the Institute for Corrosion and Multiphase Technology (ICMT) at Ohio University from 2005 to 2008. My supervisor was Dr Srdjan Nešić, professor at Ohio University and director of the ICMT.

I started working for the ICMT as a PhD student, and became part of the “Water Wetting” project sponsored by Saudi Aramco from 2005 to 2006. This project then transformed into the “Water Wetting” Joint Industry Project (JIP) in the period from 2006 to 2009. The sponsors of this JIP were BP, ConocoPhillips, ENI, Saudi Aramco, Shell, Total and Petrobras. My work has been published at various conferences including the following:

- Society of Petroleum Engineers annual conference (2005) in Dallas, TX, USA
- NACE annual conference (2006) in San Diego, CA, USA
- 11th Middle East conference (2006) in Manama Bahrain, SAUDI ARABIA
- NACE annual conference (2007) in Nashville, TN, USA
- NACE annual conference (2008) in New Orleans, LA, USA
- International Corrosion Congress (2008) in Las Vegas, NV, USA

Portions of this dissertation come from the publications I submitted to the above conferences as well as ICMT internal publications. No further referencing to these articles will be done in this dissertation as I am a co-author of these publications¹⁻⁶.

TABLE OF CONTENTS

	Page
ABSTRACT	3
ACKNOWLEDGEMENTS	4
PREFACE	5
LIST OF TABLES	10
LIST OF FIGURES	11
LIST OF SYMBOLS	21
CHAPTER 1 INTRODUCTION	23
<i>Motivation</i>	23
<i>Research objectives</i>	24
<i>Thesis outline</i>	26
CHAPTER 2 LITERATURE REVIEW	27
<i>Introduction</i>	27
<i>Carbon dioxide corrosion mechanism</i>	27
<i>Phase wetting in oil-water flow: adaptation of Hinze's model</i>	29
Introduction	29
Overview of the phase wetting model	29
Droplet size calculations	31
Model predictions	41
<i>Crude oil chemistry effects on carbon dioxide corrosion</i>	49
Effect of crude oil chemistry on corrosion inhibition	49
Effects of crude oil chemistry on steel wettability	50

	7
Effect of crude oil chemistry on steel wettability; at the metal surface.....	50
Effect of crude oil chemistry on steel wettability; In the bulk flow	51
Crude oil chemistry, choice of few representative chemicals.....	52
General crude oil chemistry	52
Aromatic compounds	52
Oxygen compounds	53
Sulfur compounds	54
Nitrogen compounds.....	55
 CHAPTER 3 CRUDE OIL CHEMISTRY EFFECT ON CORROSION INHIBITION..	 57
<i>Introduction</i>	57
<i>Experimental technique: glass cell</i>	57
<i>Experimental results</i>	61
The baseline	61
Aromatics.....	64
Oxygen containing compounds.....	65
Small chain organic acids	65
Long chain organic acids	68
Sulfur containing compounds	72
Nitrogen containing compounds.....	78
<i>Modeling the crude oil inhibition of corrosion</i>	84
Corrosion inhibition model.....	84
Calculation of the parameters α_i and β_i	86
Model validation	91
Validation of assumption 1: Adsorption measurements	91
Validation of assumption 2: Corrosion measurements	94
Model validation with crude oil.....	95
<i>Discussion</i>	96
<i>Conclusion</i>	99

CHAPTER 4 CRUDE OIL CHEMISTRY EFFECTS ON PHASE WETTING.....	100
<i>Introduction</i>	100
<i>Part 1 - Study of flow pattern</i>	100
Introduction.....	100
Experimental technique: Tensiometer	102
Experimental results.....	103
Discussion	106
Conclusion	107
<i>Part 2 - Study of steel wettability</i>	107
Introduction.....	107
Experimental technique: Static contact angle measurement.....	108
Experimental results.....	110
Aromatic compounds.....	115
Oxygen containing compounds.....	115
Sulfur containing compounds	116
Nitrogen containing compounds.....	116
Discussion	116
Conclusion	117
<i>Part 3 – Study of the synergy between steel wettability and flow pattern</i>	118
Introduction.....	118
Experimental technique	118
Small scale: Doughnut cell	118
Large scale: Flow loop.....	121
Experimental results.....	126
Small scale results.....	126
Large scale results.....	133
<i>Phase wetting prediction</i>	157
Introduction.....	157
Model prediction for hydrophilic steel	157

	9
Model prediction for hydrophobic steel.....	159
Model calibration.....	163
Summary of the prediction.....	170
CHAPTER 5 CONCLUSION.....	171
<i>Achievements</i>	171
<i>Recommendations for future work</i>	172
BIBLIOGRAPHY.....	174

LIST OF TABLES

	Page
Table 1. <i>Steel composition in wt.% (Fe is in balance)</i>	57
Table 2. <i>LPR, EIS, and polarization sweep main parameters to study the adsorption of surface active compound from the water phase</i>	59
Table 3. <i>LPR, EIS, and polarization sweep main parameters to study the adsorption of surface active compounds from the water phase</i>	60
Table 4. <i>Model oil (LVT-200) properties</i>	60
Table 5. <i>“Acridine like” compounds tested</i>	82
Table 6. <i>Summary of the inhibitive effect of the compounds tested in this study</i>	87
Table 7. <i>Inhibition model’s constants calculated from experiments</i>	89
Table 8. <i>Inhibition model’s constants calculated from experiments for asphaltene</i>	89
Table 9. <i>Inhibition model’s constants calculated from experiments for corrosion inhibitors</i>	90
Table 10. <i>Evolution of the corrosion rate for different ratios of acridine / myristic acid</i>	95
Table 11. <i>Crude oil tested. Chemical composition and corrosion inhibition</i>	96
Table 12. <i>Oil-water interfacial tension testing</i>	103
Table 13. <i>Evolution of the oil-water interfacial tension function of the polar compound added to the oil phase (exception: acetic acid)</i>	104
Table 14. <i>Static contact angle measurements test matrix</i>	110
Table 15. <i>Contact angle measurements</i>	113
Table 16. <i>Doughnut cell test matrix</i>	120
Table 17. <i>Composition of the crude oil from the North Sea tested in the doughnut cell</i>	131
Table 18. <i>Test matrix: model oil test in large flow loop</i>	133
Table 19. <i>Test matrix: myristic acid tests in large flow loop</i>	144
Table 20. <i>Contact angle measurement: water droplet in model oil (the steel is previously wetted by crude oil) with the empirical value of IW</i>	169
Table 21. <i>pH effect on carboxylic acid and pyridine</i>	173

LIST OF FIGURES

	Page
<i>Figure 1.</i> Schematic representation of a horizontal pipe.....	33
<i>Figure 2.</i> Evolution of the maximum droplet size in dispersed systems as a function of water cut and flow velocity, calculated with $\rho_c = 800 \text{ kg}\cdot\text{m}^{-3}$, $\rho_w = 1000 \text{ kg}\cdot\text{m}^{-3}$, $\sigma = 0.04 \text{ N}\cdot\text{m}^{-1}$, $D = 0.1 \text{ m}$, friction factor calculated for smooth pipe using Colebrook formula.....	34
<i>Figure 3.</i> Evolution of the maximum droplet size in dense systems as a function of water cut and flow velocity, calculated with $\rho_c = 800 \text{ kg}\cdot\text{m}^{-3}$, $\rho_w = 1000 \text{ kg}\cdot\text{m}^{-3}$, $\sigma = 0.04 \text{ N}\cdot\text{m}^{-1}$, $D = 0.1 \text{ m}$, friction factor calculated for smooth pipe using Colebrook formula.....	36
<i>Figure 4.</i> Schematic representation of an inclined pipe, with forces applied to a water droplet.....	37
<i>Figure 5.</i> Evolution of the maximum droplet size in dense systems as a function of water cut and flow velocity, calculated with $\rho_c = 800 \text{ kg}\cdot\text{m}^{-3}$, $\rho_w = 1000 \text{ kg}\cdot\text{m}^{-3}$, $\sigma = 0.04 \text{ N}\cdot\text{m}^{-1}$, $D = 0.1 \text{ m}$, horizontal pipe, friction factor calculated for smooth pipe using Colebrook formula.....	39
<i>Figure 6.</i> Evolution of d_{\max}^{dilute} (light blue) and d_{\max}^{dense} (dark blue) as a function of water cut and flow velocity, calculated with $\rho_c = 800 \text{ kg}\cdot\text{m}^{-3}$, $\rho_w = 1000 \text{ kg}\cdot\text{m}^{-3}$, $\sigma = 0.04 \text{ N}\cdot\text{m}^{-1}$, $D = 0.1 \text{ m}$, friction factor calculated for smooth pipe using Colebrook formula.....	42
<i>Figure 7.</i> Evolution of the $\min\{d_{\text{crit}}^{\text{gravity}}, d_{\text{crit}}^{\text{creaming}}\}$ as a function of water cut and flow velocity, calculated with $\rho_c = 800 \text{ kg}\cdot\text{m}^{-3}$, $\rho_w = 1000 \text{ kg}\cdot\text{m}^{-3}$, $\sigma = 0.04 \text{ N}\cdot\text{m}^{-1}$, $D = 0.1 \text{ m}$, horizontal pipe, friction factor calculated for smooth pipe using Colebrook formula.....	43
<i>Figure 8.</i> Evolution of $\min\{d_{\text{crit}}^{\text{gravity}}, d_{\text{crit}}^{\text{creaming}}\}$ (green), d_{\max}^{dilute} (light blue) and d_{\max}^{dense} (dark blue) as a function of water cut and flow velocity, calculated with $\rho_c =$	

800 kg·m ⁻³ , $\rho_w = 1000 \text{ kg}\cdot\text{m}^{-3}$, $\sigma = 0.04 \text{ N}\cdot\text{m}^{-1}$, $D = 0.1\text{m}$, friction factor calculated for smooth pipe using Colebrook formula.....	44
<i>Figure 9.</i> Transition of the phase wetting map from 3-dimensions to 2-dimensions, calculated with $\rho_c = 800 \text{ kg}\cdot\text{m}^{-3}$, $\rho_w = 1000 \text{ kg}\cdot\text{m}^{-3}$, $\sigma = 0.04 \text{ N}\cdot\text{m}^{-1}$, $D = 0.1 \text{ m}$, friction factor calculated for smooth pipe using Colebrook formula.....	45
<i>Figure 10.</i> Evolution of $\min\{d_{crit}^{gravity}, d_{crit}^{creaming}\}$ (green) and d_{max}^{dense} (dark blue) as a function of water cut and flow velocity, calculated with $\rho_c = 800 \text{ kg}\cdot\text{m}^{-3}$, $\rho_w = 1000 \text{ kg}\cdot\text{m}^{-3}$, $\sigma = 0.04 \text{ N}\cdot\text{m}^{-1}$, $D = 0.1 \text{ m}$, friction factor calculated for smooth pipe using Colebrook formula.	47
<i>Figure 11.</i> Phase wetting map in 2-dimensions without the d_{max}^{dilute} equation, calculated with $\rho_c = 800 \text{ kg}\cdot\text{m}^{-3}$, $\rho_w = 1000 \text{ kg}\cdot\text{m}^{-3}$, $\sigma = 0.04 \text{ N}\cdot\text{m}^{-1}$, $D = 0.1 \text{ m}$, friction factor calculated for smooth pipe using Colebrook formula.	48
<i>Figure 12.</i> Interfacial tension forces applied to a water droplet in model oil resting on a steel surface. The shape of the droplet is determined by the interaction of the interfacial forces of oil-water ($\sigma_{o/w}$), steel-oil ($\sigma_{s/o}$) and steel-water ($\sigma_{s/w}$).....	50
<i>Figure 13.</i> Crude oil's aromatic compound examples, from left to right: benzene, naphthalene, phenanthrene and benz(a)anthracene.....	53
<i>Figure 14.</i> Structure of 1,2,3,4-tetrahydronaphthalene used as model compound for the aromatic class.....	53
<i>Figure 15.</i> Crude oil's carboxylic acid examples, from left to right, cyclohexyl carboxylic acid and 2-phenanthrene carboxylic acid.....	54
<i>Figure 16.</i> Structure of acetic acid and myristic acid used as model compound for the oxygen compounds class.....	54
<i>Figure 17.</i> Crude oil's sulfur compound examples, from left to right 1-butanethiol, thiophenol and 4,6 dimethyldibenzothiophene.....	55
<i>Figure 18.</i> Structure of sulfur compound used as model compound, dioctyl sulfide, dibenzothiophene and 1-tetradecanethiol.	55
<i>Figure 19.</i> Crude oil's sulfur compound examples, from left to right, quinoline, 9-propyl-9H-carbazole and 2(1H)-quinolinone.	56

	13
<i>Figure 20.</i> Structure of the nitrogen compounds used as model compounds, carbazole, and acridine.....	56
<i>Figure 21.</i> Representation of glass cell apparatus.	58
<i>Figure 22.</i> Corrosion rate for the base line experiment recoded by LPR. Conditions: 1 wt.% NaCl, 1 bar CO ₂ , pH 5.0.	61
<i>Figure 23.</i> EIS measurement of the impedance, Nyquist plot. Base line (1 wt.% NaCl, 1 bar CO ₂ , pH 5.0).....	62
<i>Figure 24.</i> Polarization sweep: base line (1 wt.% NaCl, 1 bar CO ₂ , pH 5.0).	62
<i>Figure 25.</i> Evolution of the corrosion rate in water (1 wt.% NaCl, 1 bar CO ₂ , pH 5.0) after the steel coupon has been immersed in model oil 20 min.	63
<i>Figure 26.</i> EIS measurement of the impedance, Nyquist plot. EIS experiments in water (1 wt.% NaCl, 1 bar CO ₂ , pH 5.0) after the steel coupon has been immersed in model oil for 20 min.....	64
<i>Figure 27.</i> Corrosion measurements by LPR for aromatics added to the model oil (Base Line: model oil, no tetrahydronaphthalene), water phase: 1%NaCl, 1 bar CO ₂ , pH 5.0.	65
<i>Figure 28.</i> Evolution of the corrosion rate as a function of the amount of acetic acid added to the water phase (0 ppm baseline, then 10 ppm, 100 ppm and 1000 ppm) conditions: 1 wt.% NaCl, 1 bar CO ₂ , pH 5.0.	66
<i>Figure 29.</i> EIS measurement of the impedance, Nyquist plot. EIS experiments in water (1 wt.% NaCl, 1 bar CO ₂ , pH 5.0) base line has no acetic acid, and 10 ppm, 100 pm and 1000 ppm acetic acid.	67
<i>Figure 30.</i> Polarization sweep function of the amount of acetic acid added to the water phase (0 ppm baseline, then 10 ppm, 100 ppm and 1000 ppm) conditions: 1 wt.% NaCl, 1 bar CO ₂ , pH 5.0.....	68
<i>Figure 31.</i> Evolution of the corrosion rate function of acid added to the water phase (10 ppm). Conditions: 1 wt.% NaCl, 1 bar CO ₂ , pH 5.0.	69
<i>Figure 32.</i> EIS measurement of the impedance, Nyquist plot. EIS experiments in water (1 wt.% NaCl, 1 bar CO ₂ , pH 5.0) for different high molecular weight	

	14
organic acids. Base line has no organic acid, 10 ppm myristic acid and 10 ppm naphthenic acid (TCI).....	70
<i>Figure 33.</i> Polarization sweep function of the long chain organic acid added to the water phase (10 ppm). Conditions: 1 wt.% NaCl, 1 bar CO ₂ , pH 5.0.....	70
<i>Figure 34.</i> Corrosion measurements by LPR for long chain organic acids added to the model oil phase, water phase 1 wt.% NaCl, 1 Bar CO ₂ , pH 5.0.	71
<i>Figure 35.</i> EIS measurement of the impedance, Nyquist plot. EIS experiments for long chain organic acids added to the model oil phase, water phase 1 wt.% NaCl, 1 bar CO ₂ , pH 5.0.....	72
<i>Figure 36.</i> Evolution of the corrosion rate function of sulfur containing compounds added to the water phase (10 ppm). Conditions: 1 wt. % NaCl, 1 bar CO ₂ , pH 5.0.....	73
<i>Figure 37.</i> EIS measurement of the impedance, Nyquist plot. EIS experiments in water (1 wt.% NaCl, 1 bar CO ₂ , pH 5.0) for different sulfur containing compounds. Base line has no sulfur containing compounds, 10 ppm dibenzothiophene,10 ppm dioctyl-sulfide and 10 ppm 1-tetradecanethiol.....	74
<i>Figure 38.</i> Full scale for <i>Figure 37</i>	74
<i>Figure 39.</i> Polarization sweep function of the sulfur containing compound added to the water phase (10 ppm) conditions: 1 wt.% NaCl, 1 bar CO ₂ , pH 5.0.....	75
<i>Figure 40.</i> Corrosion measurements by LPR for sulfur containing compounds added to the model oil phase, water phase 1 wt.% NaCl, 1 bar CO ₂ , pH 5.0.	76
<i>Figure 41.</i> EIS measurement of the impedance, Nyquist plot. EIS experiments for sulfur containing compounds added to the model oil phase, water phase 1% NaCl, 1 bar CO ₂ , pH 5.0.....	76
<i>Figure 42.</i> Chemical structure comparison of myristic acid (left) with 1-tetradecanethiol (right).....	77
<i>Figure 43.</i> Evolution of the corrosion rate function of the nitrogen added to the water phase (10 ppm). Conditions: 1 wt.% NaCl, 1 bar CO ₂ , pH 5.0.....	78
<i>Figure 44.</i> EIS measurement of the impedance, Nyquist plot. EIS experiments in water (1 wt.% NaCl, 1 bar CO ₂ , pH 5.0) for different nitrogen containing	

compounds. Base line has no nitrogen containing compounds, 10 ppm carbazole and 10 ppm acridine.	15 79
<i>Figure 45.</i> Full scale for <i>Figure 44</i>	79
<i>Figure 46.</i> Polarization sweep function of the nitrogen containing compound added to the water phase (10 ppm). Conditions: 1 wt.% NaCl, 1 bar CO ₂ , pH 5.0.	80
<i>Figure 47.</i> Corrosion measurements by LPR for nitrogen containing compounds added to the model oil phase, water phase 1 wt.% NaCl, 1 bar CO ₂ , pH 5.0.....	81
<i>Figure 48.</i> EIS measurement of the impedance, Nyquist plot. EIS experiments for different nitrogen containing compounds added to the model oil phase, water phase 1 wt.% NaCl, 1 bar CO ₂ , pH 5.0.	81
<i>Figure 49.</i> Corrosion measurements by LPR for pyridinic compounds added to the model oil phase, water phase 1 wt.% NaCl, 1 bar CO ₂ , pH 5.0.	83
<i>Figure 50.</i> EIS measurement of the impedance, Nyquist plot. EIS experiments in water (1 wt.% NaCl, 1 bar CO ₂ , pH 5.0) after the steel coupon has been immersed in model oil mixed with 3 different pyridinic compounds.....	83
<i>Figure 51.</i> Inhibition of corrosion calculated from Table 6 for the naturally occurring chemicals in crude oil that have induced significant corrosion inhibition.....	88
<i>Figure 52.</i> Iron coated quartz crystal used in the Quartz Crystal Microbalance.	92
<i>Figure 53.</i> Evolution of the mass adsorbed for different surface active compounds as a function of time.	93
<i>Figure 54.</i> Relationship between mass adsorbed and inhibition of corrosion.....	94
<i>Figure 55.</i> Comparison between inhibitions of corrosion calculated and measured for oxygen, sulfur, nitrogen containing compounds, asphaltenes and corrosion inhibitors.	99
<i>Figure 56.</i> Representation of a polar molecule with a hydrophilic head group and hydrophobic tail, C14 chain organic acid: myristic acid.	101
<i>Figure 57.</i> Platinum ring tensiometer used in these experiments.	103
<i>Figure 58.</i> Evolution of the transition line calculated using the water wetting model for three concentrations of TCI added to model oil (0 wt.%, 0.1 wt.% and 1 wt.%).	105

<i>Figure 59.</i> Drawing of the contact angle measurement setup ⁸⁰ , the cell is made of acrylic to allow the camera on the right to video.....	109
<i>Figure 60.</i> 3D picture of the metal surface after polishing with 600 grit sandpaper, roughness: 1.1 μm	110
<i>Figure 61.</i> Evolution of a water droplet in model oil during the first 10 minutes as the contact angle evolves from 180° to 58°.....	111
<i>Figure 62.</i> Water-Steel contact angle after 5 minutes. Organic acids have the strongest effect on steel wettability.....	114
<i>Figure 63.</i> Water-Steel contact angle after 120 minutes. Organic acid effect on steel wettability is not time dependent.....	114
<i>Figure 64.</i> Phase wetting experiment apparatus called the ‘doughnut cell’.....	119
<i>Figure 65.</i> The bottom of the doughnut cell shows conductivity probes.....	119
<i>Figure 66.</i> One conductivity probe, 160 conductivity probes are used in the doughnut cell.....	120
<i>Figure 67.</i> Schematic of the flow loop.....	121
<i>Figure 68.</i> Picture of the flow loop in horizontal position.....	122
<i>Figure 69.</i> Picture of the flow loop in 15° position.....	122
<i>Figure 70.</i> Representation of the test section.....	124
<i>Figure 71.</i> Example of flow visualization picture, water appears green under UV light, oil is black.....	125
<i>Figure 72.</i> Representation of the instrumentation of the test section.....	126
<i>Figure 73.</i> Phase wetting map obtained in a doughnut cell with pure model oil. No chemicals are added to the oil phase. Points are measurements, line is just an indicator separating oil and water wetting regions.....	127
<i>Figure 74.</i> Phase wetting map obtained in a doughnut cell with 0.01 wt.% myristic acid added to the oil phase. Points are measurements, line is just an indicator separating oil and water wetting regions.....	127
<i>Figure 75.</i> Phase wetting map obtained in a doughnut cell with 0.05 wt.% myristic acid added to the oil phase. Points are measurements, line is just an indicator separating oil and water wetting regions.....	128

<i>Figure 76.</i> Phase wetting map obtained in a doughnut cell with 0.1 wt.% myristic acid added to the oil phase.....	128
<i>Figure 77.</i> Phase wetting map of Middle Eastern crude oils API 50 to 34. Experiment done by Li ⁶⁶	129
<i>Figure 78.</i> Phase wetting map comparison between model oil and crude oil API37, doughnut cell experimental results. Experiment done by Li ⁶⁶	131
<i>Figure 79.</i> Phase wetting map comparison between model oil mixed with myristic acid and crude oil API37, similar organic acid concentration.....	132
<i>Figure 80.</i> Model oil phase wetting map measured in large flow loop in horizontal position. Points are measurements, line is just an indicator separating oil and water wetting regions.....	134
<i>Figure 81.</i> Picture of the flow in 4 inch pipe, oil-water mixture velocity $0.5 \text{ m}\cdot\text{s}^{-1}$, water cut 5%.	135
<i>Figure 82.</i> Picture of the flow in 4 inch pipe, oil-water mixture velocity $0.5 \text{ m}\cdot\text{s}^{-1}$, water cut 10%.	135
<i>Figure 83.</i> Picture of the flow in 4 inch pipe, oil-water mixture velocity $0.5 \text{ m}\cdot\text{s}^{-1}$, water cut 15%.	136
<i>Figure 84.</i> Picture of the flow in 4 inch pipe, oil-water mixture velocity $0.5 \text{ m}\cdot\text{s}^{-1}$, water cut 20%.	136
<i>Figure 85.</i> Picture of the flow in 4 inch pipe, oil-water mixture velocity $1 \text{ m}\cdot\text{s}^{-1}$, water cut 5%.	137
<i>Figure 86.</i> Picture of the flow in 4 inch pipe, oil-water mixture velocity $1 \text{ m}\cdot\text{s}^{-1}$, water cut 10%.	138
<i>Figure 87.</i> Picture of the flow in 4 inch pipe, oil-water mixture velocity $1 \text{ m}\cdot\text{s}^{-1}$, water cut 15%.	138
<i>Figure 88.</i> Picture of the flow in 4 inch pipe, oil-water mixture velocity $1 \text{ m}\cdot\text{s}^{-1}$, water cut 20%.	139
<i>Figure 89.</i> Picture of the flow in 4 inch pipe, oil-water mixture velocity $1.5 \text{ m}\cdot\text{s}^{-1}$, water cut 5%.	140

	18
<i>Figure 90.</i> Picture of the flow in 4 inch pipe, oil-water mixture velocity $1.5 \text{ m}\cdot\text{s}^{-1}$, water cut 10%.	140
<i>Figure 91.</i> Picture of the flow in 4 inch pipe, oil-water mixture velocity $1.5 \text{ m}\cdot\text{s}^{-1}$, water cut 15%.	141
<i>Figure 92.</i> Flow pattern map with model oil, horizontal flow through a 4" pipe.....	142
<i>Figure 93.</i> Phase wetting map measured in a large flow loop (4" ID, horizontal flow), with 0.01 wt.% myristic acid added to the model oil. Points are measurements, line is just an indicator separating oil and water wetting regions.	145
<i>Figure 94.</i> Phase wetting map measured in a large flow loop (4" ID, horizontal flow), with 0.05 wt.% myristic acid added to the model oil. Points are measurements, line is just an indicator separating oil and water wetting regions.	145
<i>Figure 95.</i> Phase wetting map measured in a large flow loop (4" ID, horizontal flow), with 0.08 wt.% myristic acid added to the model oil. Points are measurements, line is just an indicator separating oil and water wetting regions.	146
<i>Figure 96.</i> Evolution of the transition line oil wetting to intermittent wetting as a function of the quantity of myristic acid added to the oil phase.	147
<i>Figure 97.</i> Flow loop experiment, phase wetting map of Middle Eastern oil API 50. Points are measurements, line is just an indicator separating oil and water wetting regions.	148
<i>Figure 98.</i> Flow loop experiment, phase wetting map of Middle Eastern oil API 40. Points are measurements, line is just an indicator separating oil and water wetting regions.	149
<i>Figure 99.</i> Flow loop experiment, phase wetting map of Middle Eastern oil API 34. Points are measurements, line is just an indicator separating oil and water wetting regions.	151
<i>Figure 100.</i> Flow loop experiment, phase wetting map of Middle Eastern oil API 30. Points are measurements, line is just an indicator separating oil and water wetting regions.	152
<i>Figure 101.</i> Composite of 16 pictures taken with a microscope of the water in oil emulsion.	154

<i>Figure 102.</i> Flow loop experiment, phase wetting map of Middle Eastern oil API 27. Points are measurements, line is just an indicator separating oil and water wetting regions.....	155
<i>Figure 103.</i> Phase wetting maps of Middle Eastern crude oils API 27 to 50.....	156
<i>Figure 104.</i> Comparison: transition line oil wetting to intermittent wetting function for the model oil (dashed line) with water wetting model's prediction (solid line).....	158
<i>Figure 105.</i> Comparison: size of water droplet measured experimentally and prediction of the water wetting model oil (Equation 21).....	159
<i>Figure 106.</i> Comparison of transition lines for oil wetting to intermittent wetting as a function of the concentration of myristic acid including the water wetting model prediction.	160
<i>Figure 107.</i> Evolution of the transition line oil wetting to intermittent wetting as a function of the inhibition of wettability (IW).....	162
<i>Figure 108.</i> Picture of a water droplet (1 wt.% NaCl, pH 5.0) immersed in model oil mixed with 1 wt.% myristic acid on a steel surface. The water droplet is gently moving on a slightly inclined steel surface, the water droplet does not wet the steel surface.....	163
<i>Figure 109.</i> Comparison between large scale tests (with myristic acid) and modified water wetting model (values of IW are empirical).....	164
<i>Figure 110.</i> Comparison of the wettability alteration (IW), experimental results vs. the prediction made by Equation 49.	165
<i>Figure 111.</i> Large scale experiment results with Middle Eastern oil API 50 from <i>Figure 97</i> and the prediction from the water wetting model ($IW = 0$) and the prediction from the corrected water wetting model with $IW = 0.3$	166
<i>Figure 112.</i> Large scale experiment results with Middle Eastern oil API 40 from <i>Figure 98</i> and the prediction from the water wetting model ($IW = 0$) and the prediction from the corrected water wetting model with $IW = 0.3$	166

- Figure 113.* Large scale experiment results with Middle Eastern oil API 34 from *Figure 99* and the prediction from the water wetting model ($IW = 0$) and the prediction from the corrected water wetting model with $IW = 0.3$167
- Figure 114.* Large scale experiment results with Middle Eastern oil API 30 from *Figure 100* and the prediction from the water wetting model ($IW = 0$) and the prediction from the corrected water wetting model with $IW = 0.3$167
- Figure 115.* Large scale experiment results with Middle Eastern oil API 27 from *Figure 102* and the prediction from the water wetting model ($IW = 0$) and the prediction from the corrected water wetting model with $IW = 0.3$168

LIST OF SYMBOLS

Latin Symbol		Dimensions
d	Droplet diameter	L
D	Pipe internal diameter	L
e	Turbulent energy dissipation	M/t ³
f	Friction factor	-
F	Force	ML/t ²
g	Gravitational acceleration	L/t ²
K	Arbitrary constant	-
l	Length	L
L	Pipe length	L
m	Mass	M
N	Number	-
P	Pressure	M/Lt ²
Q	Volumetric flow rate	L ³ /t
T	Temperature	T
u	Velocity	L/t
Greek Symbol		
α	Constant	-
β	Constant	-
τ	Viscous shear stress	M/Lt ²
σ	Interfacial tension	M/t ²
ρ	Density	M/L ³
ε	Fraction of liquid	-

θ	Contact angle	-
θ	Surface coverage	-
Δ	Difference	-

Superscript

'	Turbulent
---	-----------

Subscript

<i>crit</i>	Critical
-------------	----------

<i>droplets</i>	Droplets
-----------------	----------

<i>k</i>	Kolmogoroff
----------	-------------

<i>m</i>	Mixture
----------	---------

max	Maximum
-----	---------

<i>o</i>	Oil
----------	-----

<i>w</i>	Water
----------	-------

<i>wc</i>	Water Cut
-----------	-----------

*	Friction
---	----------

∞	Infinity
----------	----------

CHAPTER 1 INTRODUCTION

Motivation

Oil and gas pipelines are generally made out of carbon steel. Such pipelines are vulnerable in the presence of small amounts of water due to corrosion. The oil industry pays a heavy price every year. On March 2nd 2006 267,000 US gallons of crude oil were spilled over a little less than 2 acres in Prudhoe Bay, Alaska. The spill originated from a quarter inch hole in BP's production line. "Early indications are that water accumulated in the pipeline, causing the corrosion"⁷. The spill had a major impact on BP's image and induced a major financial loss. On May 21st 2008 in Anchorage, Alaska a relatively small oil leak, 170 gallons, was discovered on a ConocoPhillips' pipeline. The leak was a surprise because the installation was only eight years old. Ed Meggert, the Department of Environmental Conservation coordinator, said that corrosion was "caused by water settling in low parts of the line"⁸. Often, the water phase contains dissolved corrosive species such as carbon dioxide, hydrogen sulfide and organic acids. Therefore, the water is corrosive. In the past, low volume fractions of water were associated with non-corrosive situations because the flowing oil phase can sweep out the water from the bottom of the pipe and therefore oil prevents the water from corroding the bottom of the pipe. However, recent incidents, such as in Prudhoe Bay and Anchorage show that even low volume fractions of water can lead to corrosion problems and large financial losses. All the more so when the volume fraction of water increases, water drops out of the oil phase and forms a continuous water layer corroding the bottom of the pipe. The complete understanding of the transition from oil wetting to water wetting in mild steel pipelines is necessary for engineers to improve their ability to combat corrosion.

The first significant research on the transition from water wetting conditions to oil wetting conditions in oil-water flows was published in 1975 by Wicks and Fraser⁹. Wicks proposed a model predicting the minimum velocity required to sweep out settled water on the bottom of the pipe. This assumption makes the model suitable only for low water

volume fraction as the model significantly underestimates the minimum velocity at high water volume fractions. In 1987, Smith *et al.*¹⁰ stated that crude oil has the capability to carry up to 20% water at a velocity larger than $1 \text{ m}\cdot\text{s}^{-1}$. Water wetting as a function of fluid velocity and water cut have been studied in the 1990s. C. de Waard and Lotz¹¹ (1993) estimated that oil wetting occurred only for a water volume fraction lower than 30% at oil velocity larger than $1 \text{ m}\cdot\text{s}^{-1}$. Adams *et al.*¹² suggested that at below 30% water volume fractions, only oil wetting occurs, and that at over 50% water volume fractions only water wetting is possible. Obviously, these first studies on water wetting conditions oversimplified the picture complicated by multiple and interconnected effects such as crude oil properties and flow regimes. Moreover, case studies show that corrosion can happen in a pipeline carrying less than 2% of water while in other instances no corrosion was found for a line carrying more than 50% water.

Research objectives

The objective of this study is to determine which class of chemicals present in crude oil have an effect on inhibition of corrosion and phase wetting. This information is necessary in order to predict corrosion rates in wells and pipelines where crude oil and water are flowing in a mild steel pipe. However, the molecular composition of crude oil is very complex and crude oil chemistry varies from field to field. It is therefore impossible to study the effect of each and every chemical present in crude oil.

The main phenomenon studied here was the adsorption of particular surface active compounds naturally present in crude oil: aromatics, oxygen, sulfur, and nitrogen containing compounds. Surface active compounds are known for their affinity towards iron surfaces, where they can adsorb either via weak interactions such as van der Waals forces (characteristic of physisorption) or strong covalent bonding (characteristic of chemisorption)^{13,14}. Adsorption processes can create a very thin organic film on metal surfaces. This accumulation of surface active compounds at the metal surface, where the oxidation of iron by protons occurs, can slow down corrosion rates, leading to corrosion

inhibition¹⁵⁻¹⁷. Furthermore, the accumulation of the hydrophobic surface active compounds can change the wettability of iron, which is hydrophilic by nature^{18,19}. Wettability has a direct effect on the corrosion rate²⁰, *i.e.* steel wet by oil does not corrode.

Another phenomenon studied was the accumulation of surface active compounds at the oil-water interface. This accumulation of surface active compounds changes the oil-water interfacial tension^{21,22} which influences the break-up process of the water phase by the oil phase²³ thereby lowering the velocity needed in order to disperse the water phase into droplets.

Therefore, the current study has focused on two possible effects that crude oil has on corrosion in oil-water flow:

- 1 – Corrosion inhibition induced by the accumulation of surface active compounds at the metal surface.

- 2 – Wetting alteration due to different steel surface wettability (affected by accumulation of surface active compounds at the steel surface) and modification of the flow pattern (due to accumulation of surface active compounds at the oil-water interface).

Surface active compound's adsorption effects on inhibition of corrosion and wettability have been studied both qualitatively and quantitatively in the past²⁴⁻²⁹. However, these effects were studied only by using corrosion measurements. The use of a single type of experiment cannot distinguish which effect has the dominant influence on corrosion: corrosion inhibition or the change in steel wettability. Therefore, in this study each effect will be investigated separately without the interference of the others. The main aim is to achieve a better understanding of corrosion in oil-water flow.

Thesis outline

A literature review is presented in Chapter 2. First a background on CO₂ corrosion and a two-phase flow model are presented. Then, general crude oil chemistry is analyzed. This enables the choice of the few crude oils chemical compounds that will be used in this study.

The Chapter 3 presents the research about the effect of crude oil's chemistry on pure corrosion inhibition. The experimental results presented in this chapter are used as calibrating factors for a mechanistic model of corrosion inhibition. Then real crude oils are tested in order to validate the model.

The Chapter 4 presents crude oil's effects on phase wetting in oil-water flow. Firstly, the crude oil's naturally occurring surface active chemicals effect on flow pattern is qualified. Secondly, the crude oil's naturally occurring surface active compounds effect on steel wettability is discussed. Finally, the synergy of the two effects is studied on a large scale in a 60 m long inclinable flow loop. Finally, a phase wetting model is presented. The parameters of the model are calibrated using experimental results.

Conclusions and suggestions for future work are presented in Chapter 5.

CHAPTER 2 LITERATURE REVIEW

Introduction

A literature review of the effects of crude oil chemistry on corrosion in oil-water flow has been conducted. The first part presents carbon dioxide corrosion mechanism. The second part of the literature review covers phase wetting in oil-water flow, as knowing which phase wets the pipe is a major issue in predicting corrosion rates. Finally, the last part of this literature review focuses on the crude oil naturally occurring chemicals and their effects on corrosion inhibition and phase wetting.

Carbon dioxide corrosion mechanism

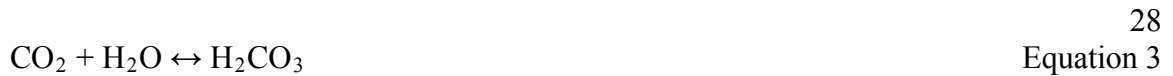
Carbon dioxide corrosion happens under different forms such as uniform corrosion, localized corrosion, galvanic corrosion and erosion-corrosion³⁰. All of these types of attack involve only one anodic chemical reaction, the oxidation of iron (Equation 1).



The oxidation of iron requires one or more balancing reductions. Few cathodic reactions are possible in aqueous solutions saturated with carbon dioxide.

- Protons can be reduced (Equation 2),
- Carbon dioxide can dissolve into the aqueous phase (Equation 3) and lead to the formation of reducible carbonic acid (Equation 4)³¹.
- Water can be directly reduced at the metal surface (Equation 5)
- Also, if oxygen is present, reduction of oxygen molecules happens (Equation 6).





It should be noted that at low pH (<pH4) and low partial pressure of CO₂ (<1 bar), the reduction of carbonic acid and water molecules onto the metal surface is negligible compared to the proton reduction^{32, 33}.

Nešić³⁴ indicated that carbonic acid (like many other weak acids) is more aggressive than a strong acid at the same pH. This phenomenon is due to the large reservoir of carbonic acid present in solution replenishing the solution in protons as they are consumed. Carbonic acid can dissociate to bicarbonate ion and bicarbonate (Equation 7) to carbonate ion (Equation 8).



These chemical/electrochemical reactions are a foundation of the processes happening in the bulk water as well as on the metal surface. It is therefore possible to calculate mild steel corrosion rate quite accurately if the concentration of the involved species, temperature, pressure, and flowing conditions are known.

Introduction

Hinze studied the effect of turbulence on the mechanism of drops splitting. He published a model³⁵ predicting droplet size as a function of turbulence. Taitel³⁶⁻³⁹, Barnea⁴⁰⁻⁴⁵ and Brauner⁴⁶ used Hinze's model to predict the minimum velocity required to entrain air bubbles in water flow. Finally, this model was modified by Nešić *et al.*⁴⁷ in order to calculate the minimum velocity required to entrain water droplets in oil-water flow. This minimum velocity is critical from a corrosion point of view. Below it, the water droplets settle on the bottom of the pipe, corroding it. Above this minimum velocity, the water droplets are entrained in the oil phase and the likelihood of corrosion is decreased.

Overview of the phase wetting model

The model is based on the comparison of the size of two droplets. The *maximum* water droplet size possible in the oil-water pipe flow, and the *critical* water droplet size that can stay suspended in such a flow. If the maximum water droplet size possible is smaller than the critical water droplet size that can be sustained by the flow, all the water droplets are dispersed in the oil flow. Consequently, the water phase does not wet the pipe wall and the pipe is free from corrosion.

Maximum droplet size: Hinze's model for droplet breakage was used by Taitel and Barnea to determinate the maximum droplet size (d_{\max}) possible in two-phase flow. Balance between turbulence in the pipe flow and surface tension determine the maximum droplet size possible in the pipe. Bigger droplets than the maximum droplet size will be broken by the turbulence into smaller droplets. This balance between turbulence and surface tension must be evaluated for two cases: first for dilute dispersions (when the effect of turbulence on a single droplet is considered), and secondly for dense dispersions (when the interaction of turbulence with a multitude of droplets is considered). These two types of balance give two maxima for droplet size, one for dilute dispersion (d_{\max}^{dilute}) and one for dense dispersion (d_{\max}^{dense}).

Critical droplet size: The critical droplet size (d_{crit}) represents the maximum size droplet which can be sustained in the flow. Bigger droplets than the critical droplet size will migrate toward the pipe wall, smaller droplets than the critical droplet size will flow suspended in the pipe (possibly impinging the pipe wall). The critical droplet size is found by two different approaches.

First, for near-horizontal flow when the turbulent forces acting on droplets overcome the gravity forces: droplets will be sustained in the flow. Vice versa when gravity overpowers turbulence, the droplets will “sink” (water droplet in flowing oil) and form a water layer on the bottom of the pipe. This criterion is called *gravity* driven critical droplet size ($d_{crit}^{gravity}$).

Second, as Taitel³⁹ explains: “if the bubble size produced by the breakup process is large enough to permit deformation, then the Taylor bubbles characteristic of slug flow are formed by the process of coalescence. Thus, the turbulence breakup process can prevent agglomeration only if the bubble size produced is small enough to cause the bubbles to remain spherical”. This criterion is called *creaming* critical droplet size ($d_{crit}^{creaming}$). If droplets are bigger than the creaming critical droplet size, droplets deform. The droplets deformation leads to larger droplets, because the turbulence breaking process is less efficient on a deformable sphere than on a rigid sphere. Indeed, the large non-spherical water droplets move randomly in the flow with significant components of the velocity being perpendicular to the main flow (picture a falling leaf in the wind). This makes it more likely to reach the wall of the pipe, even in the absence of gravity effects – typical for near-vertical flow. It should be noted that Taitel studied air-water systems; however the physics are valid for any two-phase or immiscible two-fluid system.

Criterion of transition dispersed flow to stratified flow: Knowing the maximum droplet size that can exist in the pipe without further breaking up in dilute (d_{\max}^{dilute}) or dense (d_{\max}^{dense}) solutions and the critical droplet size that can be sustained in the flow without sinking ($d_{crit}^{gravity}$) or creaming ($d_{crit}^{creaming}$) is enough to determine the two-phase flow pattern.

In a two-phase flow, when the maximum droplet size is smaller than the minimum critical droplet size, the turbulence is high enough to maintain the droplet in the flow without sinking or creaming. Therefore, when the condition below is satisfied, the water phase will flow as dispersed droplets in the oil phase. However, if the condition is not satisfied, some water droplets will settle out of the flow and wet the pipe wall. It is likely then that the water phase which settles on the bottom of the pipe may create a continuous water layer.

$$\max\{d_{\max}^{dilute}, d_{\max}^{dense}\} < \min\{d_{crit}^{gravity}, d_{crit}^{creaming}\} \quad \text{Equation 9}$$

In a dispersed flow the water droplets may randomly impinge the pipe wall, particularly at flow disturbances, but overall, the pipe is wet by oil and corrosion is unlikely. In stratified flow, the water phase wets the bottom of the pipe and oil wets the top of the pipe. In such conditions corrosion happens only on the bottom of the pipe.

Droplet size calculations

Maximum droplet size in a dilute dispersion system: The calculation of the maximum droplet size that can flow in a pipe without further breakup is based on the assumption that some of the energy of the oil phase is used to break up the water phase into droplets. Therefore we can make the turbulent kinetic energy of the oil flow (proportional to $\rho_o u'^2$) proportional to the surface energy necessary to break the water phase (proportional to σ/d_{\max}).

$$\rho_o u'^2 \propto \frac{\sigma}{d_{\max}^{dilute}} \quad \text{Equation 10}$$

In this equation d_{\max}^{dilute} is the unknown, ρ_o (oil density) and σ (oil-water interfacial tension) are physical constants. In order to calculate d_{\max}^{dilute} it is necessary to determine the factor of proportionality between turbulence and surface energy and calculate u' , the turbulent velocity.

In isotropic homogeneous turbulence: “the main contribution of the kinetic energy is made by the fluctuations in the region of wave lengths where the Kolmogorov energy distribution law is valid. In this region the turbulence pattern is solely determined by the energy input per unit mass and unit time.”³⁵ Therefore, the energy input is a function of the turbulent kinetic energy (u'):

$$e = \frac{[\text{energy input}]}{[\text{mass}] \cdot [\text{time}]} = \frac{\frac{1}{2} m_o u_o'^2}{m_o \cdot \frac{l_k}{u_o'}} = \frac{1}{2} \cdot \frac{u_o'^3}{l_k} \quad \text{Equation 11}$$

Consequently:

$$u_o'^2 = K_1 \cdot (e \cdot l_k)^{2/3} \quad \text{Equation 12}$$

By assuming that eddies of the same size as the droplets are the most effective in the breaking-up process, we find that $l_k = d_{\max}^{dilute}$, where l_k represent the Kolmogorov length scale. Consequently: $K_1 = 2^{2/3}$. However, Batchelor found by experiments⁴⁸ that $K_1 = 2$. The energy (e) input can be calculated as follows:

$$e = \frac{[Pressure\ drop] \cdot [Volume]}{[Mass] \cdot [Time]} = \frac{\frac{4L\tau}{D} \cdot \frac{1}{4}\pi D^2 L}{\frac{1}{4}\pi D^2 L \varepsilon_o \rho_o \cdot \frac{L}{u_m}} = \frac{4\tau u_m}{D \rho_o \varepsilon_o} \quad \text{Equation 13}$$

The expression of the energy (e) can be rearranged by using the shear stress (τ),

$$\tau = \frac{1}{2} f \rho_m u_m^2 \quad \text{Equation 14}$$

and by using a force balance on a section of pipe as shown on *Figure 1*:

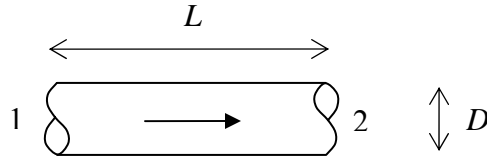


Figure 1. Schematic representation of a horizontal pipe.

$$Area_1 \cdot P_1 - Area_2 \cdot P_2 + Surface \cdot \tau = 0 \quad \text{Equation 15}$$

to find:
$$\Delta P = \frac{4L\tau}{D} \quad \text{Equation 16}$$

Therefore:
$$e = \frac{2u_m^3 f}{D} \frac{\rho_m}{\rho_c} \frac{1}{\varepsilon_o} \quad \text{Equation 17}$$

Equations 16 and 17 become:
$$d_{\max}^{dilute} \left(\frac{\rho_o}{\sigma} \right)^{0.6} e^{0.4} = K_2 \quad \text{Equation 18}$$

Clay found an experimental value for this constant⁴⁹: 0.725.

Therefore, Equation 18 becomes:

$$d_{\max}^{\text{dilute}} = 0.725 \cdot \left(\frac{\rho_c}{\sigma} \right)^{-0.6} \cdot \left(\frac{2u_o^3 f}{D} \cdot \frac{\rho_m}{\rho_c} \cdot \frac{1}{\varepsilon_o} \right)^{-0.4} \quad \text{Equation 19}$$

This constant 0.725 is supposed to represent what fraction of the turbulent kinetic energy is used to break up the water phase. *Figure 2* shows the evolution of the maximum droplet size in a dilute system as a function of the water cut (fraction of water in the mix) and mixture flow velocity. The Figure shows that flow velocity has a major impact on the maximum droplet size in dilute systems, while water cut has only a small effect.

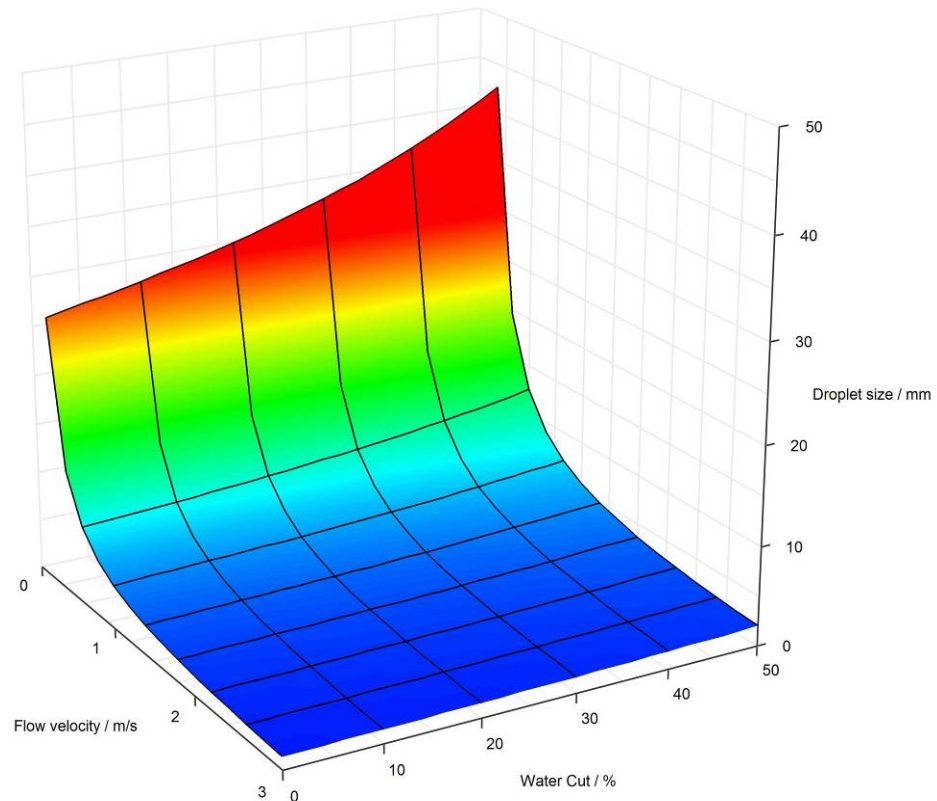


Figure 2. Evolution of the maximum droplet size in dispersed systems as a function of water cut and flow velocity, calculated with $\rho_c = 800 \text{ kg}\cdot\text{m}^{-3}$, $\rho_w = 1000 \text{ kg}\cdot\text{m}^{-3}$, $\sigma = 0.04 \text{ N}\cdot\text{m}^{-1}$, $D = 0.1 \text{ m}$, friction factor calculated for smooth pipe using Colebrook formula.

Maximum droplet size in a dense dispersion system: The calculation of the maximum droplet size in a dense dispersion system that can flow in a pipe without further breaking is based on the assumption that: “The energy of the oil phase is used to break the totality of the water phase in droplets”⁴⁶. In dilute solution the balance is done on one droplet and then summed over all droplets, while in dense solution the balance has to be done on all the droplets to account for the interaction between droplets. The oil flow turbulence kinetic energy ($\frac{1}{2}\rho_o u'^2 \cdot Q_o$) is proportional to the surface energy of the droplets (Es):

$$Es = area \cdot \sigma \cdot N_{droplets} = \pi d_{max}^2 \cdot \sigma \cdot \frac{Q_w}{\pi d_{max}^{dense3} / 6} = \frac{6 \cdot \sigma}{d_{max}^{dense}} \cdot Q_w \quad \text{Equation 20}$$

Therefore

$$\frac{1}{2} \rho_c u'^2 Q_o = K_3 \frac{6\sigma}{d_{max}^{dense}} Q_w \quad \text{Equation 21}$$

The turbulent kinetic energy u' is calculated in the same way as for dilute solutions. Consequently:

$$d_{max}^{dense} = 2.22 \cdot K_3^{3/5} \cdot D \cdot \left(\frac{\rho_c u_c^2 D}{\sigma} \right)^{-0.6} \left(\frac{\varepsilon_d}{\varepsilon_o} \right)^{0.6} \left(\frac{\rho_m}{\rho_c} \cdot \frac{1}{\varepsilon_o} \cdot f \right)^{-0.4} \quad \text{Equation 22}$$

Brauner⁴⁶ pointed out that the constant K_3 is in the order of 1. Therefore Equation 22 becomes:

$$d_{max}^{dense} = 2.22 \cdot D \cdot \left(\frac{\rho_c u_c^2 D}{\sigma} \right)^{-0.6} \left(\frac{\varepsilon_d}{\varepsilon_o} \right)^{0.6} \left(\frac{\rho_m}{\rho_c} \cdot \frac{1}{\varepsilon_o} \cdot f \right)^{-0.4} \quad \text{Equation 23}$$

As for the dilute solution, the constant 2.22 is affected by the ratio ‘flow turbulent kinetic energy’ / ‘energy used to break the water phase’. *Figure 3* shows the evolution of the maximum droplet size in a dense system as a function of the water cut and flow velocity. The Figure shows that water droplet size depends on both water cut and flow velocity. Moreover, at high water cut and low flow velocity, the model predicts water droplets bigger than 50 mm, which is unrealistic. Above 10 mm, water droplets in oil cannot be assumed to remain as rigid spheres – they deform.

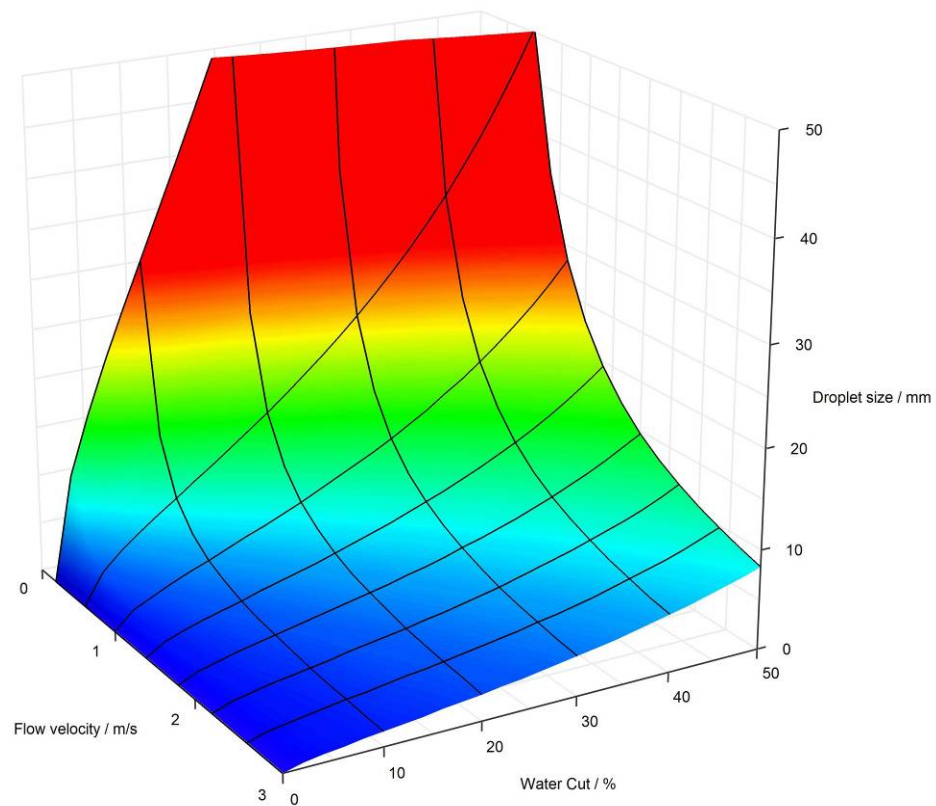


Figure 3. Evolution of the maximum droplet size in dense systems as a function of water cut and flow velocity, calculated with $\rho_c = 800 \text{ kg}\cdot\text{m}^{-3}$, $\rho_w = 1000 \text{ kg}\cdot\text{m}^{-3}$, $\sigma = 0.04 \text{ N}\cdot\text{m}^{-1}$, $D = 0.1 \text{ m}$, friction factor calculated for smooth pipe using Colebrook formula.

Gravity critical droplet size: The calculation of the biggest water droplet than can be sustained in an oil flow because of the turbulence is based on the assumption that: “droplets will be sustained in the flow only if the turbulence is strong enough to counteract the gravity”⁴⁴. The turbulence is in all directions, but in these equations we consider only the vertical component directed upward (direction opposite to gravity).

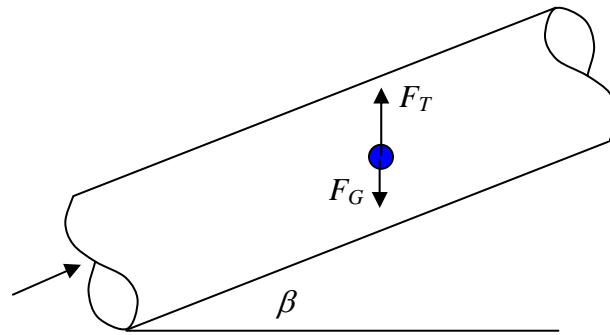


Figure 4. Schematic representation of an inclined pipe, with forces applied to a water droplet.

$$\text{Gravity force: } F_G = \text{Volume} \cdot \Delta\rho \cdot g \cdot \cos \beta \quad \text{Equation 24}$$

$$\text{Turbulence force: } F_T = \text{Droplet cross section area} \cdot \frac{1}{2} \rho_o u'^2 \quad \text{Equation 25}$$

The gravity critical droplet size is found when the force of the gravity equals the force of the turbulence ($F_G = F_T$). The only unknown is the turbulent velocity (u'). If we assume that “The radial velocity fluctuation (...) is estimated to be approximately equal the friction velocity u_* ”⁴⁴ we can write:

$$|u'| = u_* = u_m \cdot \sqrt{\frac{f}{2}} \quad \text{Equation 26}$$

It should be noted that this equation uses the radial fluctuation of velocity and not the space averaged velocity fluctuation, which is 2 to 4 times bigger.

Finally, the gravity critical droplet size is found when $F_G = F_T$:

$$d_{crit}^{gravity} = \frac{3}{8} \cdot \frac{\rho_o}{\Delta\rho} \cdot \frac{f \cdot u_m^2}{g \cdot \cos\beta} \quad \text{Equation 27}$$

The analysis demonstrates that 3/8 is not an empirical constant in the same way as the constant found in the maximum droplet size calculations in dilute and dense system given above. It should be noted that the main approximation here has been made during the calculation of the radial velocity fluctuation.

Figure 5 shows the evolution of the gravity critical droplet size as a function of water cut and flow velocity. As it should be expected, the highest gravity critical droplets size are found for high velocity (high turbulence) and low water cut.

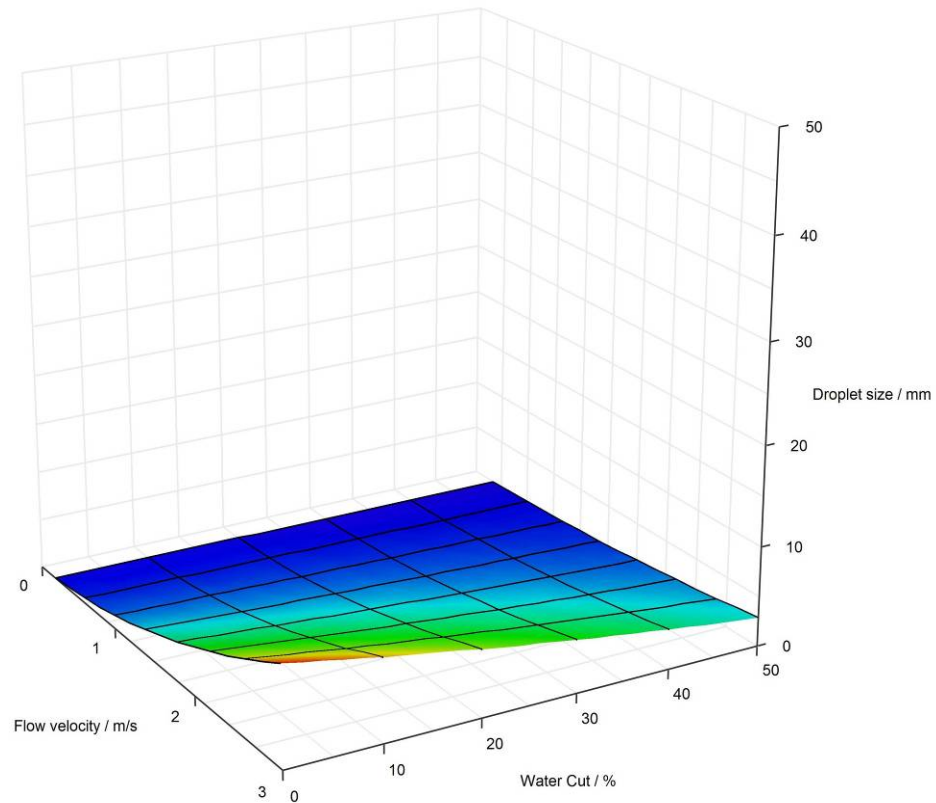


Figure 5. Evolution of the maximum droplet size in dense systems as a function of water cut and flow velocity, calculated with $\rho_c = 800 \text{ kg}\cdot\text{m}^{-3}$, $\rho_w = 1000 \text{ kg}\cdot\text{m}^{-3}$, $\sigma = 0.04 \text{ N}\cdot\text{m}^{-1}$, $D = 0.1 \text{ m}$, horizontal pipe, friction factor calculated for smooth pipe using Colebrook formula.

Creaming critical droplet size: The creaming critical droplet size ($d_{crit}^{creaming}$) represents the maximum droplet size before deformation of the droplet. Droplets smaller than the creaming critical droplet are spherical, and droplets bigger than the creaming critical droplet are deformable. This droplet size was used by Brodkey⁵⁰ and calculated by Bond⁵¹. The critical droplet size before deformation is calculated using the theory of the terminal velocity of a rigid sphere compared to a deformable sphere.

The terminal velocity of a rigid sphere in a viscous Newtonian fluid was calculated by Stokes in 1851 by solving the Navier-Stokes equations:

$$V_{\infty} = \frac{2}{9} \cdot \frac{d \cdot g \cdot \Delta\rho}{\mu} \quad \text{Equation 28}$$

However, for a non rigid droplet (non spherical), the terminal velocity of the droplet differs from the velocity calculated from Stokes' Law. Bond assumed that the small difference come from a slow circulation inside the droplet generating friction and heat. Therefore, Bond⁵² wrote a new equation:

$$V_{\infty} = k \cdot \frac{2}{9} \cdot \frac{d \cdot g \cdot \Delta\rho}{\mu} \quad \text{Equation 29}$$

In this equation k is a constant dependent on the viscosity of the droplet. Bond solved the Navier-Stokes equations inside the droplet and outside (main phase: oil) to obtain a value for the constant. Bond found by dimensional analysis the critical diameter near which the transition between Stokes' Law *i.e.* rigid droplets and deformable droplets should be expected.

$$d_{crit}^{creaming} = \sqrt{\frac{\sigma}{(\rho_{water} - \rho_{air}) \cdot g}} \quad \text{Equation 30}$$

Bond studied rising air bubbles in water and recorded the bubbles diameter and terminal velocity to find the following equation:

$$d_{crit}^{creaming} = \sqrt{0.4 \cdot \frac{\sigma}{(\rho_{water} - \rho_{air}) \cdot g}} \quad \text{Equation 31}$$

Therefore 0.4 is an empirical value for air-water systems. Brauner⁴⁶ added the effect of the pipe inclination in the previous equation:

$$d_{crit}^{creaming} = \sqrt{0.4 \cdot \frac{\sigma}{(\rho_{water} - \rho_{air}) \cdot \cos \beta' \cdot g}} \quad \text{Equation 32}$$

$$\beta' = \beta, \text{ if } \beta < 45^\circ \quad \text{Equation 33a}$$

$$\beta' = 90 - \beta, \text{ if } \beta > 45^\circ \quad \text{Equation 33b}$$

Brauner's explanation⁴⁶ is: "The value of β' is the inclination angle to the horizontal (positive for downward inclination). The value of β' in Equation 33-a and 33-b reflects the notion that in horizontal and lightly inclined tubes, drop distortion results mainly from the lateral gravity force (pushing the bubbles/drops toward the upper or lower tube wall respectively), whereas in vertical and off-vertical inclined tubes, distortion is due to the axial buoyant forces. It is to be noted however, that the inclusion of $(\cos \beta')^{1/2}$ in $d_{crit}^{creaming}$ is not critical, since the effect is of the same order as uncertainty in the value of the constant parameter".

Therefore, Equation 34 should be used to calculate the creaming critical droplet size. In this equation the constant 0.632 is an empirical value calculated for air-water systems.

$$d_{crit}^{creaming} = 0.632 \cdot \sqrt{\frac{\sigma}{(\rho_{water} - \rho_{air}) \cdot \cos \beta' \cdot g}} \quad \text{Equation 34}$$

This equation does not depend on water cut or flow velocity.

Model predictions

The model predicts that if the larger of the two maximum droplet sizes (for dilute and dense system) is smaller than the critical droplet size as affected by gravity and creaming,

then the flow is dispersed. *Figure 6* shows the maximum droplet size in dilute and dense systems.

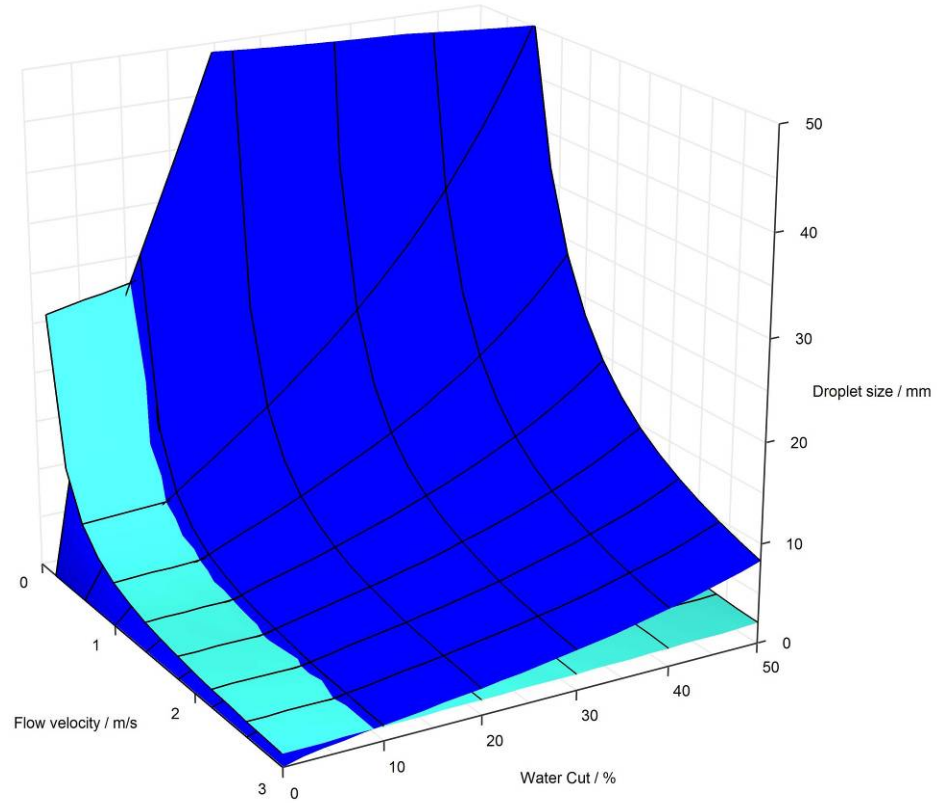


Figure 6. Evolution of d_{\max}^{dilute} (light blue) and d_{\max}^{dense} (dark blue) as a function of water cut and flow velocity, calculated with $\rho_c = 800 \text{ kg}\cdot\text{m}^{-3}$, $\rho_w = 1000 \text{ kg}\cdot\text{m}^{-3}$, $\sigma = 0.04 \text{ N}\cdot\text{m}^{-1}$, $D = 0.1 \text{ m}$, friction factor calculated for smooth pipe using Colebrook formula.

The maximum value is then compared to the critical droplet size shown in *Figure 7*. The red area is flat on the Figure, this is due to the creaming critical droplet size which has only one value on the graph as it does not depend on water cut and flow velocity.

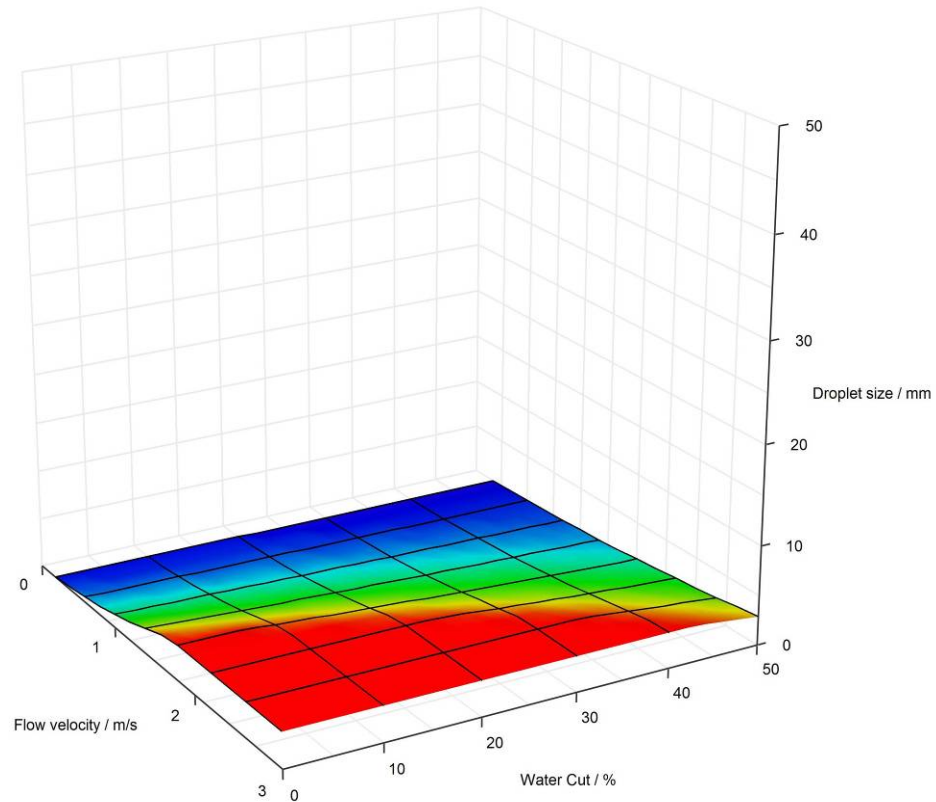


Figure 7. Evolution of the $\min\{d_{crit}^{gravity}, d_{crit}^{creaming}\}$ as a function of water cut and flow velocity, calculated with $\rho_c = 800 \text{ kg}\cdot\text{m}^{-3}$, $\rho_w = 1000 \text{ kg}\cdot\text{m}^{-3}$, $\sigma = 0.04 \text{ N}\cdot\text{m}^{-1}$, $D = 0.1 \text{ m}$, horizontal pipe, friction factor calculated for smooth pipe using Colebrook formula.

Figure 6 and *Figure 7* are superimposed to create a phase wetting map. When $\min\{d_{crit}^{gravity}, d_{crit}^{creaming}\}$ is “higher” on the graph than d_{max}^{dilute} and d_{max}^{dense} the water phase is dispersed and flows as droplets. This can be seen on *Figure 8*. Therefore, the green area represents “oil wetting” conditions, when the water phase flows as droplets in the oil and only oil wets the pipe wall. Inversely, the blue area represents “water wetting” conditions, when the water droplets settle on the bottom of the pipe and wet the bottom of the pipe. It should be noted that in oil wetting conditions the entire pipe is wet by oil while in water wetting conditions only the bottom of the pipe is wet by water (in near-horizontal flow). In near-vertical flow there is no top or bottom of the pipe and when the water wetting

happens it is randomly oriented. Indeed, if there is so much water in the line that it becomes the continuous phase (water cut > 50% typically), water wetting is encountered at most of the pipe surface irrespective of its orientation.

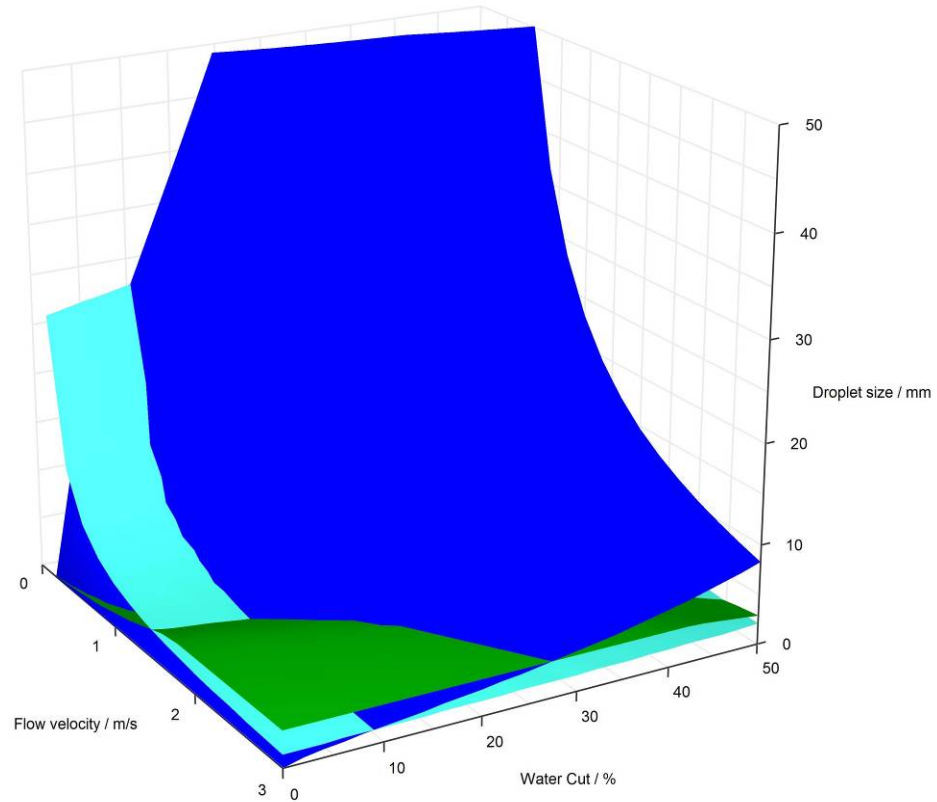


Figure 8. Evolution of $\min\{d_{crit}^{gravity}, d_{crit}^{creaming}\}$ (green), d_{max}^{dilute} (light blue) and d_{max}^{dense} (dark blue) as a function of water cut and flow velocity, calculated with $\rho_c = 800 \text{ kg}\cdot\text{m}^{-3}$, $\rho_w = 1000 \text{ kg}\cdot\text{m}^{-3}$, $\sigma = 0.04 \text{ N}\cdot\text{m}^{-1}$, $D = 0.1\text{m}$, friction factor calculated for smooth pipe using Colebrook formula.

Figure 9 shows the transition of the phase wetting map from 3-dimensions (flow velocity, water cut and droplet size) to 2-dimensions (flow velocity and water cut).

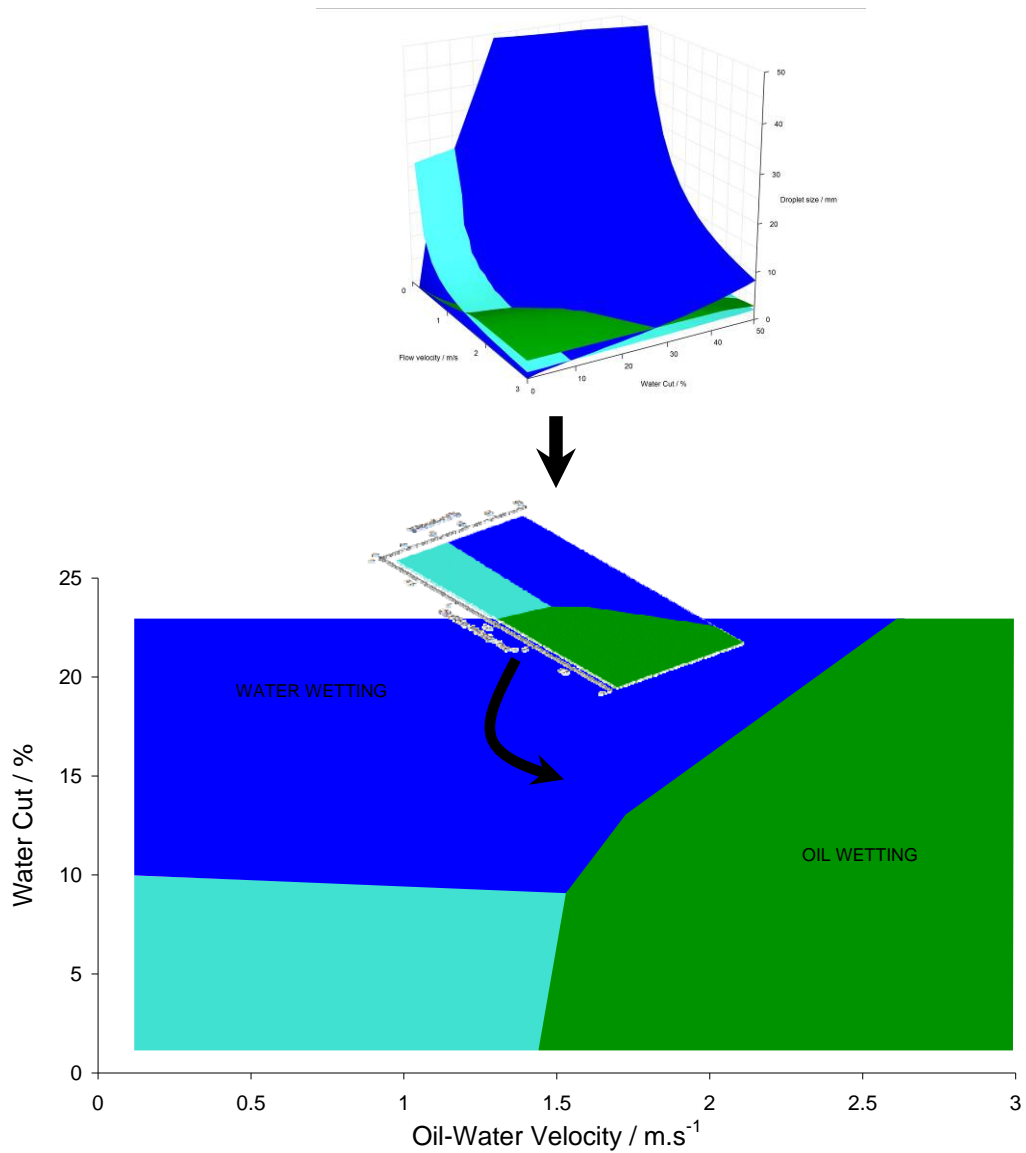


Figure 9. Transition of the phase wetting map from 3-dimensions to 2-dimensions, calculated with $\rho_c = 800 \text{ kg}\cdot\text{m}^{-3}$, $\rho_w = 1000 \text{ kg}\cdot\text{m}^{-3}$, $\sigma = 0.04 \text{ N}\cdot\text{m}^{-1}$, $D = 0.1 \text{ m}$, friction factor calculated for smooth pipe using Colebrook formula.

On the right of *Figure 9*, at high flow velocity ($> 1.5 \text{ m}\cdot\text{s}^{-1}$) oil wetting occurs; the water phase is broken into droplets by the turbulence of the oil phase. On the contrary, at low velocities ($> 1.5 \text{ m}\cdot\text{s}^{-1}$) water wetting is predominant. This is due to the low turbulence unable to break water droplets in smaller droplets and unable to entrain the water droplets in the flow.

There is however, one problem on the phase wetting map presented in *Figure 9*. At very low water cuts, the minimum velocity needed to entrain the water phase is predicted to be about $1.4 \text{ m}\cdot\text{s}^{-1}$. Later in this study it was found that the minimum velocity needed to entrain the water phase is much lower. Also, it should be noted that the original model was developed for air bubbles rising in vertical water pipes. Therefore, in such conditions the maximum droplet size in dilute systems has a physical meaning; few air bubbles randomly dispersed through the entire cross section of the pipe have little chance to interact. However, in horizontal pipes, when all the water droplets are concentrated in the region close to the bottom of the pipe, water droplets interact and the equation of the maximum droplet size in dilute systems loses its physical meaning.

Therefore a new phase wetting map has been generated without the equation of the maximum droplet size in dilute systems. It can be seen in 3-dimensions on *Figure 10*.

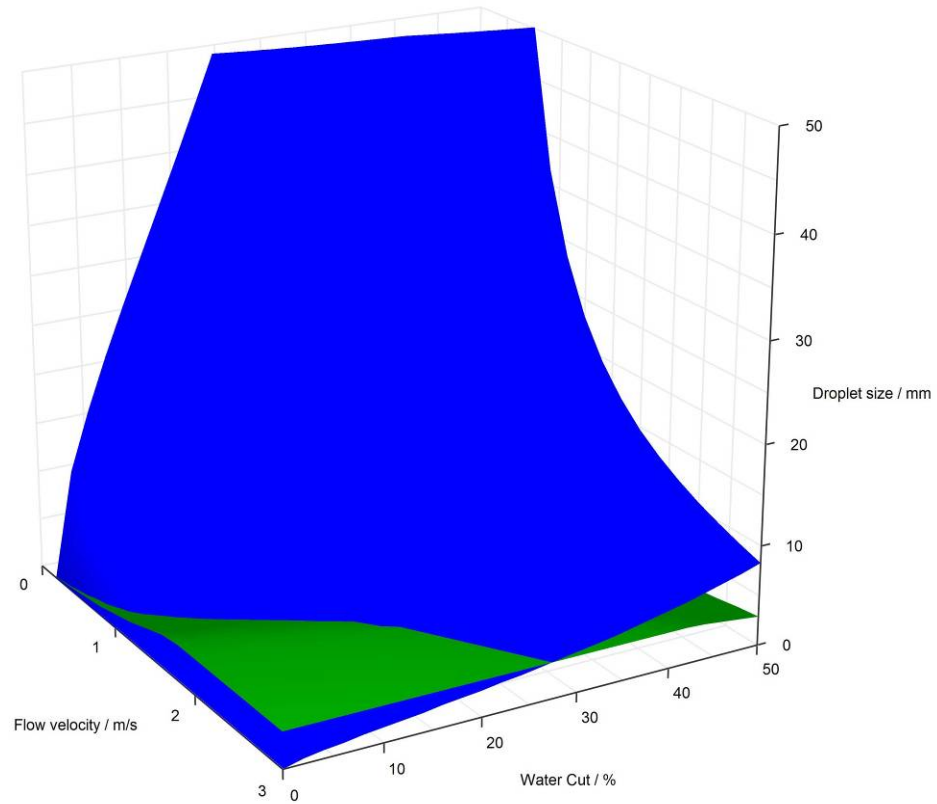


Figure 10. Evolution of $\min\{d_{crit}^{gravity}, d_{crit}^{creaming}\}$ (green) and d_{max}^{dense} (dark blue) as a function of water cut and flow velocity, calculated with $\rho_c = 800 \text{ kg}\cdot\text{m}^{-3}$, $\rho_w = 1000 \text{ kg}\cdot\text{m}^{-3}$, $\sigma = 0.04 \text{ N}\cdot\text{m}^{-1}$, $D = 0.1 \text{ m}$, friction factor calculated for smooth pipe using Colebrook formula.

As it was done for the previous phase 3-dimension wetting map, a new phase wetting map in 2-dimensions is created and shown in *Figure 11*.

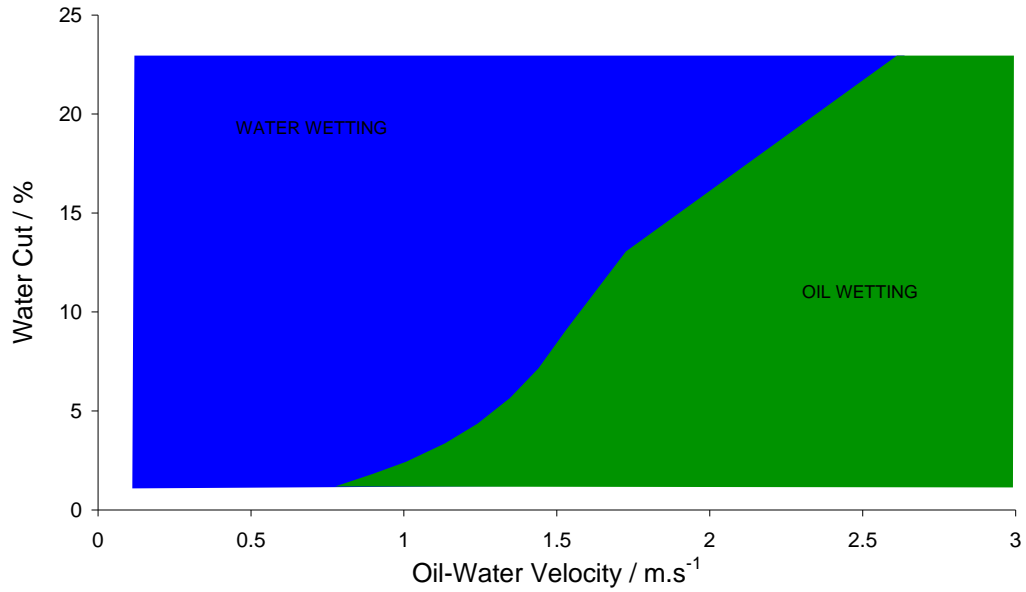


Figure 11. Phase wetting map in 2-dimensions without the d_{\max}^{dilute} equation, calculated with $\rho_c = 800 \text{ kg}\cdot\text{m}^{-3}$, $\rho_w = 1000 \text{ kg}\cdot\text{m}^{-3}$, $\sigma = 0.04 \text{ N}\cdot\text{m}^{-1}$, $D = 0.1 \text{ m}$, friction factor calculated for smooth pipe using Colebrook formula.

The phase wetting map presented in *Figure 11* is calculated using Equation 35. Further referencing to Equation 35 will be made as the “water wetting model”. The model predicts the transition between water wetting and oil wetting.

Water wetting model

$$2.22 \cdot D \cdot \left(\frac{\rho_o u_o^2 D}{\sigma} \right)^{-0.6} \cdot \left(\frac{\varepsilon_w}{\varepsilon_o} \right)^{0.6} \cdot \left(\frac{\rho_m}{\rho_o} \cdot \frac{1}{\varepsilon_o} \cdot f \right)^{-0.4} < \min \left\{ \begin{array}{l} \frac{3}{8} \cdot \frac{\rho_o}{\Delta\rho} \cdot \frac{f \cdot u_m^2}{g \cdot \cos \beta} \\ 0.632 \cdot \sqrt{\frac{\sigma}{(\rho_w - \rho_o) \cdot \cos \beta' \cdot g}} \end{array} \right\}$$

Equation 35

Crude oil chemistry effects on carbon dioxide corrosion

Effect of crude oil chemistry on corrosion inhibition

In pure carbon dioxide corrosion, it is assumed that the metal surface is bare of any precipitates or other impurities. Hence, the diffusion of the protons to the metal surface is uninhibited and corrosion is at its maximum. However, if the metal surface is coated with an organic layer, protons cannot reach the metal surface as easily and corrosion is minimal. Between these two idealized scenarios are real situations; the metal surface is partially covered with uneven layers of precipitates, asphaltenes, waxes and other substances coming from crude oil. In such conditions it is much harder to predict corrosion rates.

As stated in Chapter 1, the first objective of this study is to quantify the corrosion inhibition induced by the accumulation of surface active compounds at the metal surface. The polar molecules naturally present in crude oil are called surface active compounds because of their ability to interact with the metal surface. These molecules are the most likely to have an effect on corrosion and wettability. Efir and Jasinski⁵³ published a simple regression model for the corrosion rate in oil water flow as a function of the concentration of some polar compounds (nitrogen compounds and sulfur compounds) present in the crude oil. In their study, the corrosion rate is seen decreasing with the increase of nitrogen and sulfur compounds concentration. Since then, many have taken the challenge of predicting the evolution of the corrosion rate as a function of the crude oil chemistry. Hernandez *et al.* developed a linear model for crude oil corrosion inhibition in oil-water flow²⁵. The model was improved in 2002 using a non-linear regression²⁶, and in 2005 an artificial neural network was used to model the interaction between molecules²⁷. In all these models, surface active compounds are a significant part of the model input.

Effects of crude oil chemistry on steel wettability

Effect of crude oil chemistry on steel wettability; at the metal surface

Hydrocarbons are hydrophobic. Their adsorption at the metal surface can change the normal affinity of the steel, from hydrophilic to hydrophobic (*Figure 12*). This alteration of phase wetting at the metal surface is caused by a change of steel-oil and steel-water interfacial tension²⁴. The difference between the steel-oil interfacial tension and the steel-water interfacial tension is termed the equilibrium spreading coefficient, ψ ²⁸ and is determined by Young's equation (Equation 36).

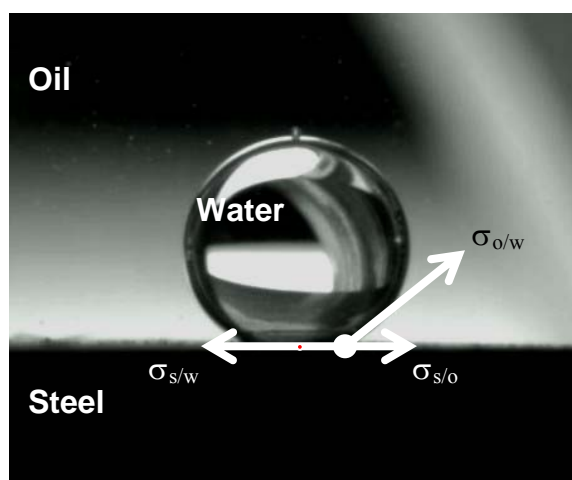


Figure 12. Interfacial tension forces applied to a water droplet in model oil resting on a steel surface. The shape of the droplet is determined by the interaction of the interfacial forces of oil-water ($\sigma_{o/w}$), steel-oil ($\sigma_{s/o}$) and steel-water ($\sigma_{s/w}$).

$$\text{Young's equation: } \psi = -\sigma_{o/w} \cos \theta = \sigma_{s/o} - \sigma_{s/w} \quad \text{Equation 36}$$

If the contact angle is larger than 90° the equilibrium spreading coefficient ψ is positive. Therefore, the affinity of the steel for water ($\sigma_{s/w}$) is stronger than the affinity of the steel for oil ($\sigma_{s/o}$). On the other hand, if the affinity for the steel is stronger for oil, the water droplet will have a contact angle smaller than 90° . A strong affinity of the steel for

oil is beneficial for preventing corrosion. In this condition, a water droplet approaching the wall surface will not wet the metal and therefore will not be corrosive.

The second goal of this study is to quantify the phase wetting alteration of steel by the accumulation of surface active compounds at the metal surface. Surface active compounds such as oxygen compounds, sulfur compounds, and nitrogen compounds were identified by Neumann, *et al.* as factor affecting the wettability preference of a crude oil⁵⁴. Phase wetting is known for having a direct effect on corrosion in oil-water flow⁴⁷. Steel wet by water corrodes faster than steel wet by oil.

Effect of crude oil chemistry on steel wettability; in the bulk flow

When the effect of crude oil chemistry on wettability was studied in the past, very little research was focused on the connection with the flow regime. Wicks and Fraser⁹, Wu⁵⁵, Adams *et al.*¹² and C. de Waard *et al.*^{10,11,56} published independently four simple empirical models to calculate the minimum flow velocity needed to entrain the water settled on the bottom of a pipe, based on experimental results. However, these models have all oversimplified the effect of flow and the effect of the crude oil chemistry is not even mentioned. This explains the inability to predict different wetting conditions for two crude oils with similar physical properties (density, viscosity) but different wetting properties. On the other hand, in field experience water wetting (and corrosion) has been seen with less than 2% water cut, and on the other extreme, oil wetting occurred (no corrosion) with water cuts larger than 50%.

Nešić *et al.*²⁰ published a variation of Hinze's model. This model requires the physical properties of the crude oil, such as oil density, viscosity and oil-water interfacial. The oil-water interfacial tension can be greatly changed by the crude oil composition. Polar compounds such as naphthenic acids can accumulate at the oil-water interface and decrease the oil-water interfacial tension. The effect of polar compounds on oil-water interfacial tension is further developed in this dissertation.

Crude oil chemistry, choice of few representative chemicals

General crude oil chemistry

Crude oil is formed from a large variety of living organisms, buried with sediments. After a long period of time, the decomposition of these organisms produces a wide range of organic species⁵⁷. Therefore the study of “the crude oil chemistry effect on phase wetting and corrosion inhibition” compound-by-compound is not possible⁵⁸. Efrid⁵³ proposed three ways to characterize crude oil chemistry:

- by the boiling point (Light Ends, < 32°C; Light Naphtha, 32°C to 171°C; Kerosene, 171°C to 260°C; Diesel, 260°C to 353°C; Light Distillate, 353°C to 409°C; Medium Distillate, 409°C to 464°C; Heavy Distillate, 464°C to 520°C; and Residue, > 520°C);
- by the percentage of paraffins, aromatics and naphthenes; and
- by chemical compounds in the crude oil: n-alkanes, iso-alkanes, mono- and poly-nuclear naphthenes, mono- and poly-nuclear naphthenoaromatics, hetero-compounds, asphaltenes, and carbenes.

In this work the third approach has been used. The four main classes of surface active compounds naturally present in crude oil will be studied (aromatic compounds, oxygen compounds, sulfur compounds and nitrogen compounds.). For each class, sub-classes will be identified and one molecule representative of these sub-classes will be chosen: for corrosion inhibition testing as well as for phase wetting testing.

Aromatic compounds

Aromatic compounds naturally present in crude oil are made of 1 to 4 fused rings, rarely more. Almost never present are peri-condensed rings or linear fused rings. *Figure 13* shows examples of aromatics found in crude oil. Aromatic compounds adsorb onto the steel surface by sharing π -electron density from the aromatic ring with the metal surface¹⁴. This binding can possibly decrease corrosion rates or change the steel-oil interfacial tension.

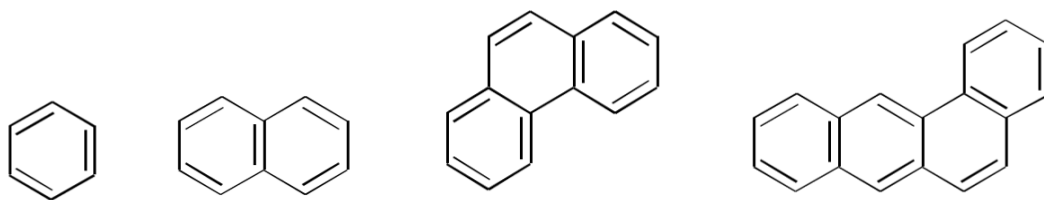


Figure 13. Crude oil's aromatic compound examples, from left to right: benzene, naphthalene, phenanthrene and benz(a)anthracene.

The aromatic chosen for this study is 1,2,3,4-tetrahydronaphthalene ($C_{10}H_{12}$, $132.2 \text{ g}\cdot\text{mol}^{-1}$) shown in *Figure 14*.

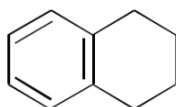


Figure 14. Structure of 1,2,3,4-tetrahydronaphthalene used as model compound for the aromatic class.

Oxygen compounds

Oxygen compounds adsorb onto the steel surface by the interaction of electron density, as manifested by unshared electron pairs on the carbonyl oxygen within the molecule, with the metallic surface⁵⁹. The resulting physical interaction blocks the metal's active site and therefore decreases the corrosion rate⁶⁰. The class of oxygen containing compounds with the highest potential for adsorption are organic acids. Other classes such as phenols, ethers and furans are either present in minute amounts or are not surface active. While small chain organic acids are known to increase corrosion rates⁶¹, long chain organic acids are used as corrosion inhibitors in the industry⁶². *Figure 15* shows the representations of carboxylic acid present in crude oil.

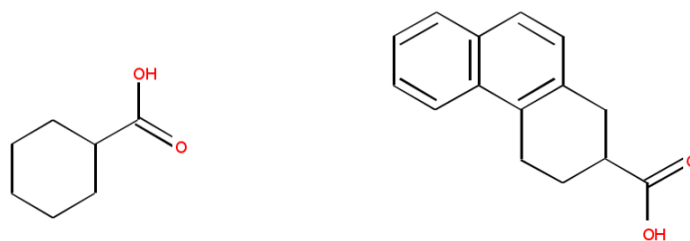


Figure 15. Crude oil's carboxylic acid examples, from left to right, cyclohexyl carboxylic acid and 2-phenanthrene carboxylic acid.

Two model compounds will be tested: acetic acid (CH_3COOH , $60.05 \text{ g}\cdot\text{mol}^{-1}$) and myristic acid ($\text{CH}_3(\text{CH}_2)_{12}\text{COOH}$, $228.37 \text{ g}\cdot\text{mol}^{-1}$), represented on *Figure 16*. Finally, tests will be run with a mixture of naphthenic acids extracted from kerosene sold by Tokyo Chemicals International (TCI). The molecular formula is $\text{R-CH}_2\text{-COOH}$ where R represents a mixture of 0 to 3 saturated rings. The average molecular weight for the TCI is $214 \text{ g}\cdot\text{mol}^{-1}$. Mass spectrometry suggests that two ring structures are prevalent.

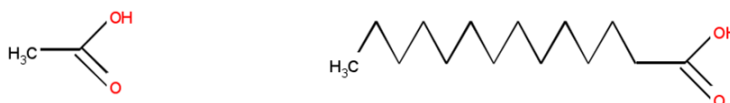


Figure 16. Structure of acetic acid and myristic acid used as model compound for the oxygen compounds class.

Sulfur compounds

Sulfur compounds can adsorb in an analogous fashion to oxygen containing compounds, using unshared electrons, although they have a greater tendency to chemisorb *via* formation of sulfur-metal bonds. Sulfur containing compounds present in crude oil are thiols (commonly known as mercaptans), sulfides, disulfides, thiophenols and thiophenic compound⁵⁸. *Figure 17* shows the representations of sulfur compounds present in crude oil. The rule of thumb is sulfur hetero-cycles (thiophene, dibenzothiophene, and benzologs) form about 2/3 of the total sulfur in crude oils. The other third of the sulfur compounds are sulfides and thiols. Sulfides and thiols are reactive; the sulfur atom has

two pairs of electrons in non-bonding orbital bonds to adsorb at the metal surface. The thiols are more reactive than sulfides because of their active hydrogen. In sulfur heterocycles, the sulfur atom has only one bond to adsorb at the metal surface. Therefore, sulfur heterocycles are less surface active than sulfide.

Figure 18 shows a representation of the sulfur compounds tested in this study. Dioctyl sulfide ($\text{CH}_3(\text{CH}_2)_7\text{S}(\text{CH}_2)_7\text{CH}_3$, $258.51 \text{ g}\cdot\text{mol}^{-1}$), dibenzothiophene ($\text{C}_{12}\text{H}_8\text{S}$, $184.26 \text{ g}\cdot\text{mol}^{-1}$), and tetradecanethiol ($\text{CH}_3(\text{CH}_2)_{13}\text{SH}$, $230.45 \text{ g}\cdot\text{mol}^{-1}$) were tested to represent sulfide, thiophenes and mercaptans respectively.

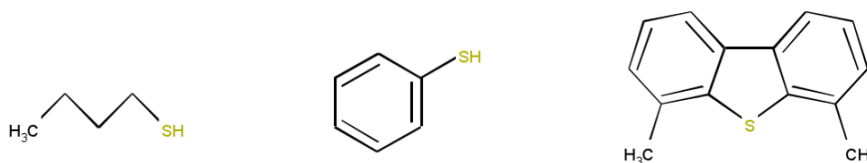


Figure 17. Crude oil's sulfur compound examples, from left to right 1-butanethiol, thiophenol and 4,6 dimethyldibenzothiophene.

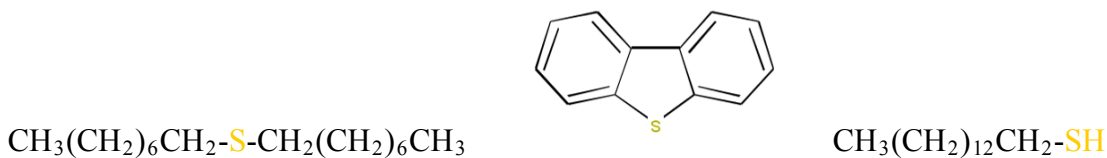


Figure 18. Structure of sulfur compound used as model compound, dioctyl sulfide, dibenzothiophene and 1-tetradecanethiol.

Nitrogen compounds

Nitrogen containing compounds can adsorb in an analogous fashion to both oxygen and sulfur containing compounds. Nitrogen containing compounds are subdivided in two categories: pyridinic forms (known as basic nitrogen compounds) and pyrrolic forms (known as neutral nitrogen compounds)⁵⁸. The rule of thumb is that pyridinic compounds form about one third of the total nitrogen while pyrrolic compounds form the other two thirds. A representation of typical nitrogen compounds present in crude oil is shown in Figure 19.



Figure 19. Crude oil's sulfur compound examples, from left to right, quinoline, 9-propyl-9H-carbazole and 2(1H)-quinolinone.

Acridine ($C_{13}H_9N$, $179.2 \text{ g}\cdot\text{mol}^{-1}$) was chosen to represent pyridinic compounds and carbazole ($C_{12}H_9N$, $167.2 \text{ g}\cdot\text{mol}^{-1}$) to represent pyrrolic compounds. The molecules are represented on *Figure 20*.



Figure 20. Structure of the nitrogen compounds used as model compounds, carbazole, and acridine.

CHAPTER 3 CRUDE OIL CHEMISTRY EFFECT ON CORROSION INHIBITION

Introduction

In this chapter the corrosion inhibition effect of crude oil is studied. Initially, a few chosen model compounds are tested individually, then mixtures of model compounds and finally, real crude oil. This approach enables us to calibrate a mechanistic corrosion inhibition model and use the results obtained with real crude oil to test the accuracy of the model.

Experimental technique: glass cell

A glass cell apparatus as represented in *Figure 21* mounted with a rotating cylindrical electrode (diameter 1.5 cm) is used for the corrosion measurements. The working electrode is made from carbon steel. The composition of the steel is shown in Table 1. The counter electrode is a platinum ring and the reference electrode a silver/silver-chloride electrode connected to the solution by a salt bridge. Linear polarization resistance (LPR), electrochemical impedance spectroscopy (EIS) and potentiodynamic sweep data are recorded.

Table 1. *Steel composition in wt.% (Fe is in balance)*

Al	As	B	C	Ca	Co	Cr	Cu	Mn	Mo	Nb
0.004	0.010	0.0002	0.19	0.002	0.007	0.13	0.16	0.83	0.042	0.003
Ni	P	Pb	S	Sb	Si	Sn	Ta	Ti	V	Zr
0.16	0.015	0.017	0.013	0.015	0.22	0.021	<0.001	<0.001	0.058	0.002

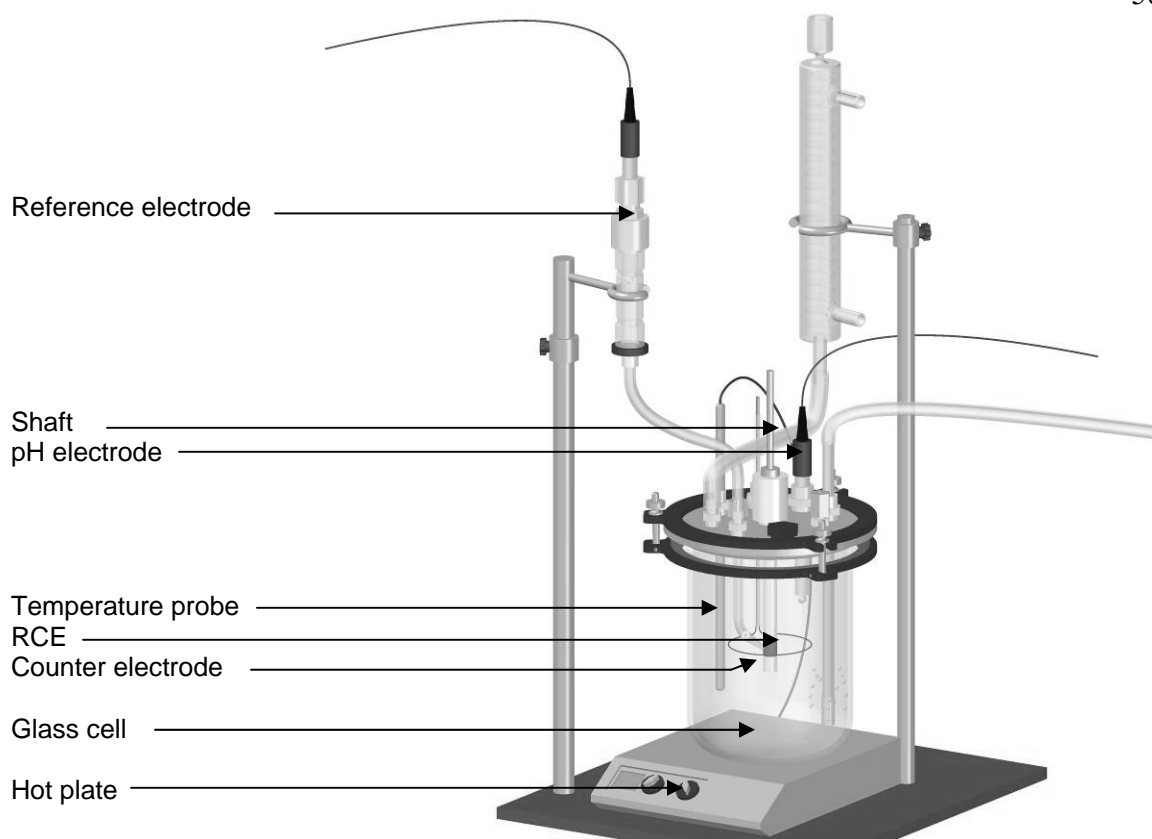


Figure 21. Representation of glass cell apparatus.

Two tests were performed:

Test 1 – Adsorption from the water phase

A procedure was designed to determine if a model compound can dissolve in water and inhibit corrosion. In a 2 L glass cell, aqueous electrolyte is introduced (1 wt.% NaCl, 1 bar CO₂, pH 5.0). The working electrode is sequentially polished with 400 and 600 grit sandpaper then cleaned with acetone and 2-propanol in an ultrasonic bath. The working electrode is then inserted into the glass cell and rotated at 2000 rpm with flowing CO₂. The corrosion rate is recorded by LPR for 20 hours after introduction of a tested chemical (10 ppm unless specified). The pH is adjusted to pH 5.0 using a 1 M sodium-bicarbonate solution; pH is measured every hour and readjusted if necessary. Then, EIS and polarization sweep are performed. The electrochemical measurements details are shown

in Table 2. It should be noted that pH 5.0 is chosen because no iron carbonate film can be formed.

Table 2. *LPR, EIS, and polarization sweep main parameters to study the adsorption of surface active compound from the water phase*

LPR				
Total time	Repeat time	Initial Potential	Final Potential	Scan rate
20 h	20 min	-5 mV vs. OCP	+5mV vs. OCP	0.125 mV·s ⁻¹
EIS				
Initial Frequency	Final Frequency	Points/ decade	AC Voltage	DC Voltage
5000 Hz	0.02 Hz	10	5 mV	0 V vs. OCP
Anodic Sweeps				
Initial Potential	Final Potential	Scan rate		
0 V vs. OCP	0.2 V vs. OCP	0.125 mV·s ⁻¹		
Cathodic Sweeps				
Initial Potential	Final Potential	Scan rate	OCP: Open Circuit Potential	
0 V vs. OCP	-0.4 V vs. OCP	0.125 mV·s ⁻¹		

Test 2– Adsorption from the oil phase

A specific experimental procedure was designed to understand the adsorption onto the metal surface of a surface active compound present in the oil phase. In a 2 L glass cell, 1.8 L of aqueous electrolyte is introduced (1 wt.% NaCl, 1 bar CO₂, pH 5.0), the solution is prepared according to the same procedure as in Test 1. The working electrode is sequentially polished with 400 and 600 grit sandpaper then cleaned with acetone and 2-propanol in an ultrasonic bath. The working electrode is then inserted into the aqueous phase in the glass cell and rotated at 2000 rpm with flowing CO₂. The corrosion rate is measured for 20 min using LPR, after which 200 mL of model oil containing a surface active compound is introduced in the glass cell. The rotating working electrode is moved up into the oil phase for 20 minutes, and then moved down into the water phase. The

corrosion rate is recorded every 5 minutes by LPR for 20 minutes. The electrochemical measurements details are shown in Table 3.

Table 3. *LPR, EIS, and polarization sweep main parameters to study the adsorption of surface active compounds from the water phase*

LPR				
Total time	Repeat time	Initial Potential	Final Potential	Scan rate
20 h	20 min	-5 mV vs. OCP	+5mV vs. OCP	0.125 mV·s ⁻¹
EIS				
Initial Frequency	Final Frequency	Points/ decade	AC Voltage	DC Voltage
5000 Hz	0.02 Hz	10	5 mV	0 V vs. OCP

A model oil, LVT-200 (refined oil sold by Penreco), is used as the oil phase. The properties of the model oil are measured and summarized in Table 4. However, nitrogen containing compounds such as acridine or carbazole are not soluble in LVT-200 because of the oil's low aromaticity. Therefore, a modified model oil is used in the test of nitrogen containing compounds. The new oil is made of 60% LVT-200 and 40% 1,2,3,4-tetrahydronaphthalene .

Table 4. *Model oil (LVT-200) properties*

Chemical composition	Only saturates
Density / API	825 kg·m ⁻³ / 40.1
Viscosity	2 cP
Surface tension	29.9 dyne·cm ⁻¹ at 26°C
Oil-water interfacial tension	38.4 dyne·cm ⁻¹ at 26°C

Experimental results

*The baseline**Test 1 – Adsorption from the water phase*

The baseline experiment is performed with tap water, 1 wt.% sodium chloride, 1 bar CO₂, and the pH is adjusted to 5.0. The corrosion rate is recorded for 20 hours using LPR and the results are shown from *Figure 22* to *Figure 24*. The corrosion potential was found stable at about -0.70V (reference: silver / silver chloride electrode +0.25 V vs. hydrogen electrode). The corrosion rate is stable at about 0.85mm/year.

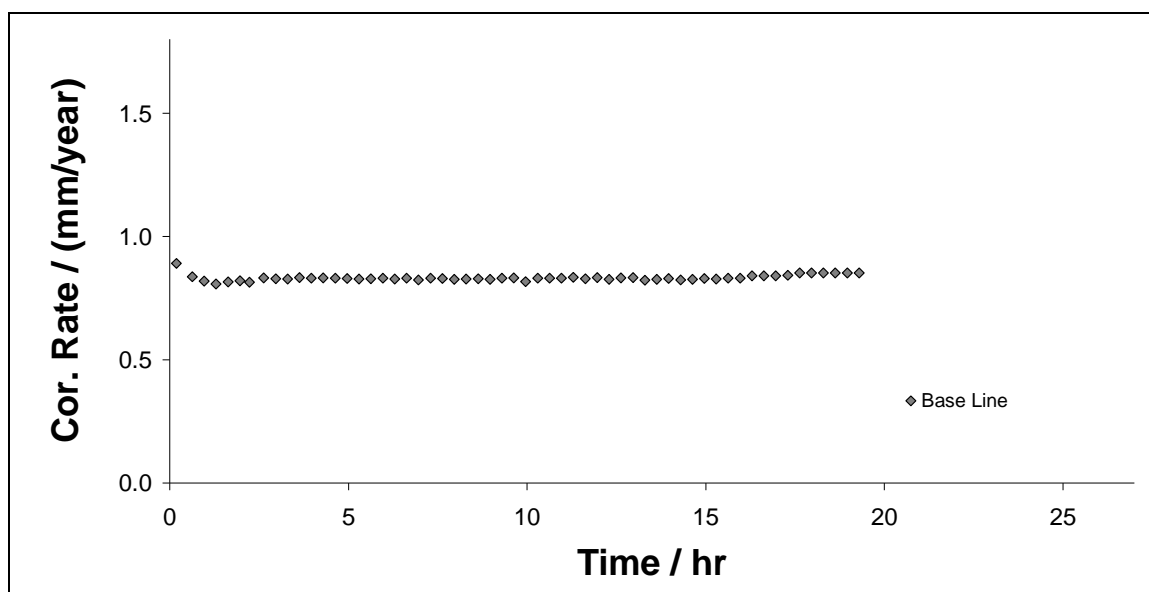


Figure 22. Corrosion rate for the base line experiment recorded by LPR. Conditions: 1 wt.% NaCl, 1 bar CO₂, pH 5.0.

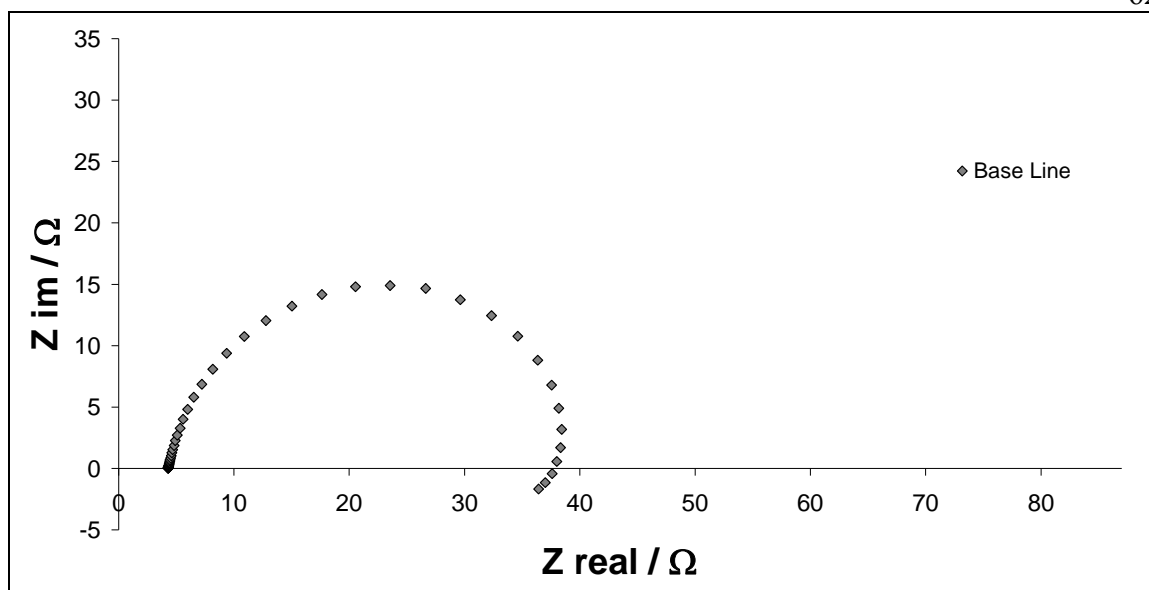


Figure 23. EIS measurement of the impedance, Nyquist plot. Base line (1 wt.% NaCl, 1 bar CO₂, pH 5.0).

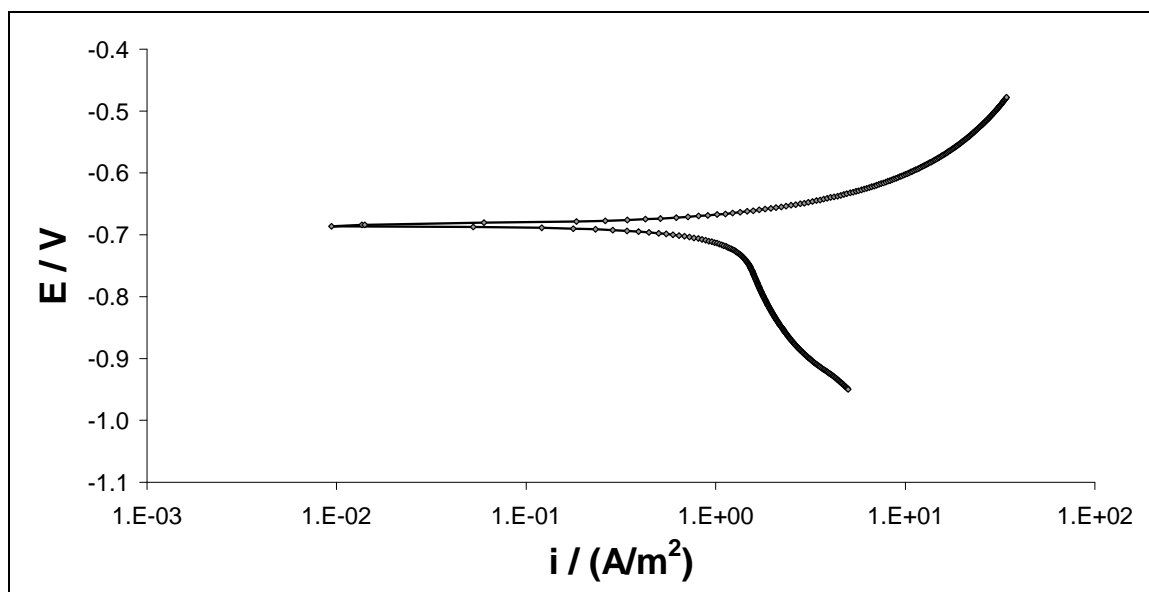


Figure 24. Polarization sweep: base line (1 wt.% NaCl, 1 bar CO₂, pH 5.0).

Test 2 – Adsorption from the oil phase

The corrosion rate is recorded in water (1 wt.% NaCl, 1 bar CO₂, pH 5.0) after the electrode has been wet in model oil. The corrosion rate is recorded for 15 min, 4 times (once every 5 min). As shown on *Figure 25* and *Figure 26* a stable corrosion rate was obtained at 0.9 mm/year. The very small difference of the corrosion rate obtained in test 1 and test 2 (about 5%) is due to minute amount of model oil “attached” onto the metal surface slightly decreasing the surface area. Since the model oil used in this test is a mixture of saturates, and the corrosion rate is the same between test 1 (no oil) and test 2 (oil), the comparison between test 1 and test 2 proves that none of the compounds present in the oil phase have an effect on corrosion.

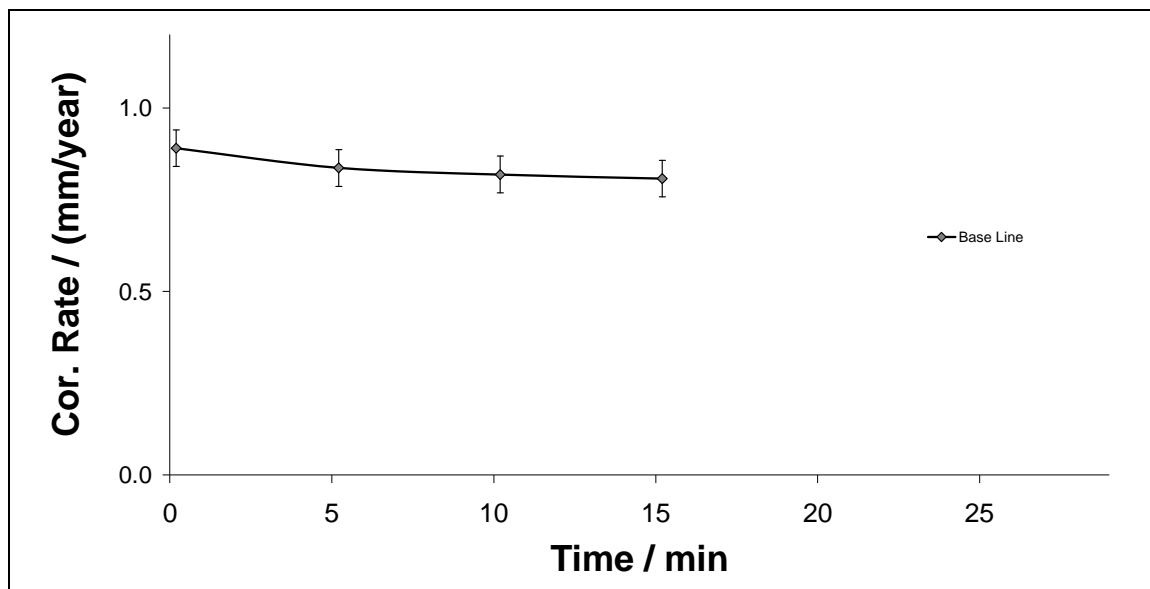


Figure 25. Evolution of the corrosion rate in water (1 wt.% NaCl, 1 bar CO₂, pH 5.0) after the steel coupon has been immersed in model oil 20 min.

The experiment has been repeated 3 times on *Figure 25* the top error bar represents the highest corrosion rate recorded, and the bottom error bar represents the lowest value measured.

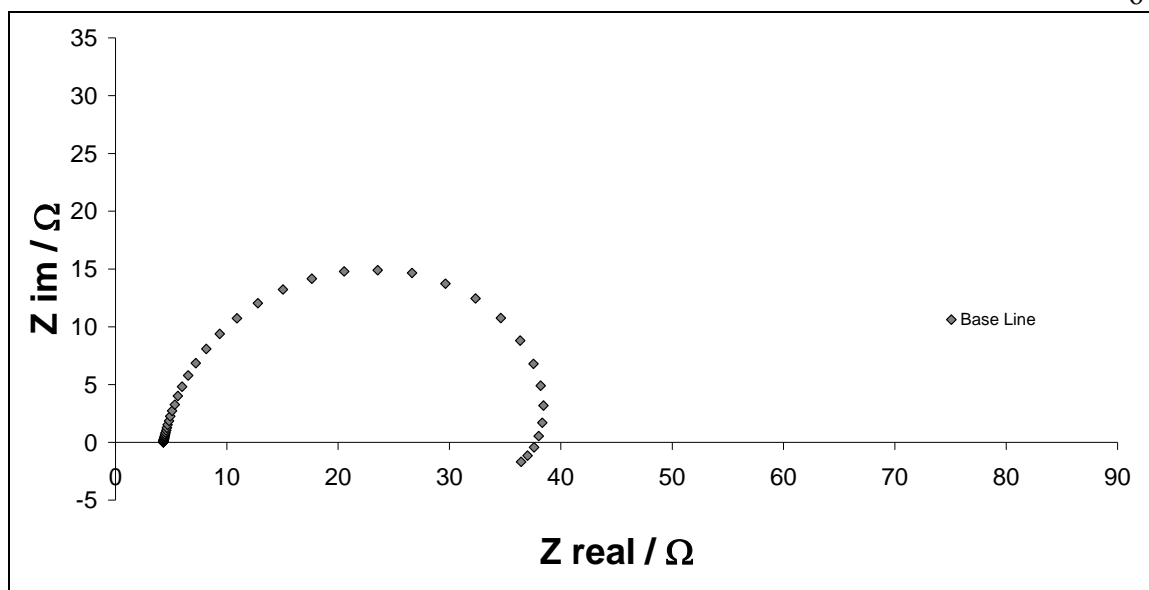


Figure 26. EIS measurement of the impedance, Nyquist plot. EIS experiments in water (1 wt.% NaCl, 1 bar CO₂, pH 5.0) after the steel coupon has been immersed in model oil for 20 min.

Aromatics

Test 1 – Adsorption from the water phase

Tetrahydronaphthalene is not soluble in water and test 1, which measures the inhibition of corrosion of a chemical dissolved in the water phase, is therefore not relevant. Figure 27 shows the corrosion rate measured during test 2. The measurement of the inhibition of corrosion due to tetrahydronaphthalene dissolved in the oil phase. A carbon steel coupon is immersed in model oil (base line) and a mixture of model oil (60 wt.%) and tetrahydronaphthalene (40 wt.%) for 20 minutes. Even with 40 wt.% tetrahydronaphthalene, the corrosion rate does not change. Aromatics can adsorb onto a metal surface¹³, but the molecule-surface interactions created are insufficiently strong to replace the water molecules adsorbed onto the iron surface, and therefore do not significantly decrease the corrosion rate.

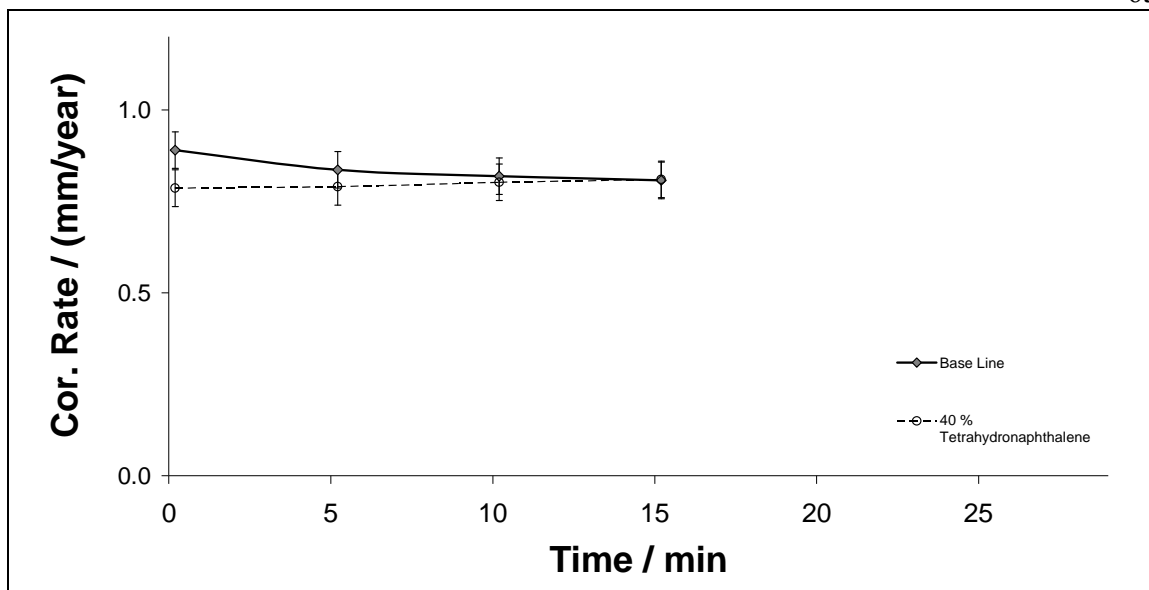


Figure 27. Corrosion measurements by LPR for aromatics added to the model oil (Base Line: model oil, no tetrahydronaphthalene), water phase: 1%NaCl, 1 bar CO₂, pH 5.0.

Oxygen containing compounds

Small chain organic acids

Test 1 – Adsorption from the water phase

Small chain organic acids such as formic acid (HCOOH) or acetic acid (CH₃COOH) are known to increase corrosion⁶³. The corrosion rate of acetic acid is recorded by LPR experiments. The conditions are identical to those outlined in a previous section for the same test. The corrosion rate is recorded for 0 ppm (base line), 10 ppm, 100 ppm and 1000 ppm acetic acid and the results are shown from *Figure 28* to *Figure 30*. 10 ppm of acetic acid increases the corrosion rate after 20 hours by 5%. 100 ppm increases the corrosion rate by 20% and 1000 ppm of acetic acid increases the corrosion rate by almost 85%.

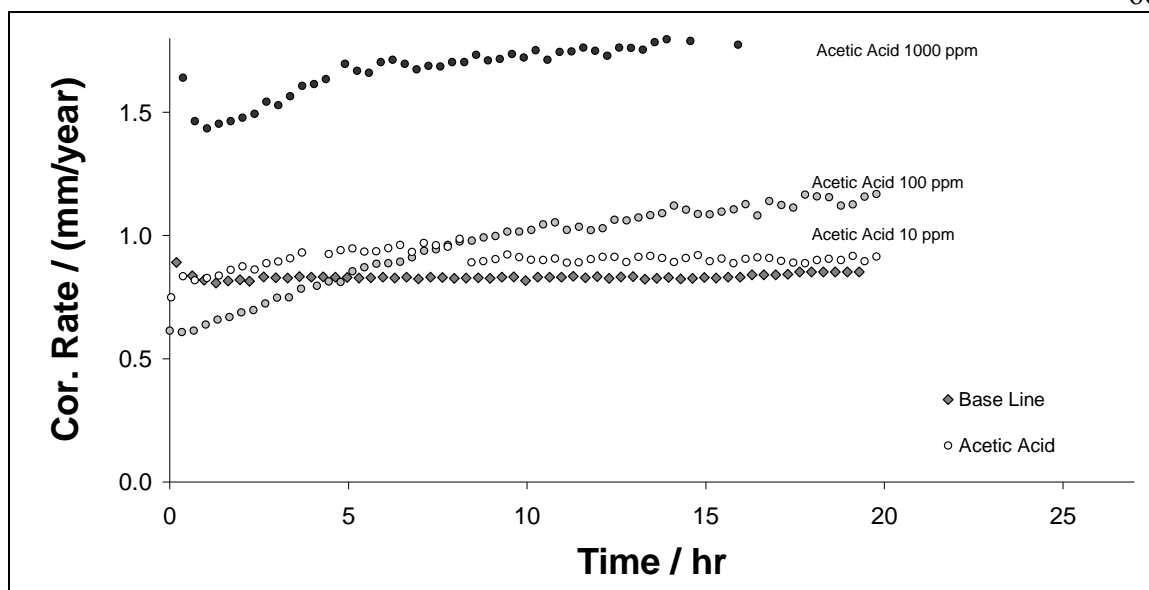


Figure 28. Evolution of the corrosion rate as a function of the amount of acetic acid added to the water phase (0 ppm baseline, then 10 ppm, 100 ppm and 1000 ppm) conditions: 1 wt.% NaCl, 1 bar CO₂, pH 5.0.

The Nyquist plot on *Figure 29* is unchanged with or without acetic acid. This shows that acetic acid does not change the corrosion mechanism; even if the increased corrosion rates reflect a change in mass transport of corrosive species to the metal surface.

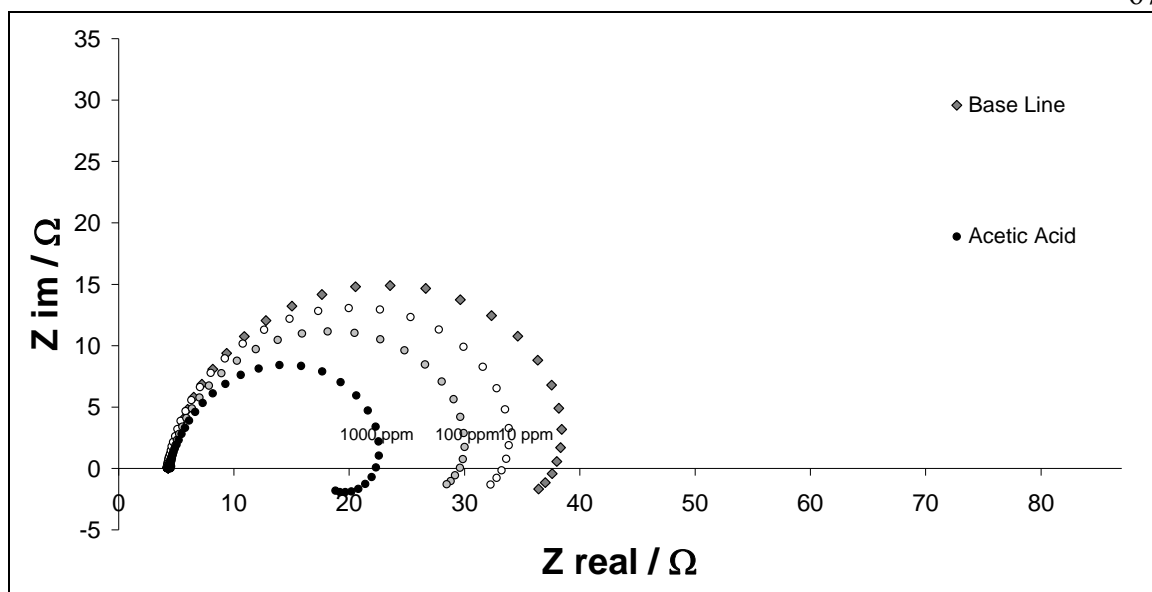


Figure 29. EIS measurement of the impedance, Nyquist plot. EIS experiments in water (1 wt.% NaCl, 1 bar CO₂, pH 5.0) base line has no acetic acid, and 10 ppm, 100 pm and 1000 ppm acetic acid.

The polarization sweep on *Figure 30* shows that acetic acid has an effect only the cathodic reaction, while the anodic reaction is unchanged.

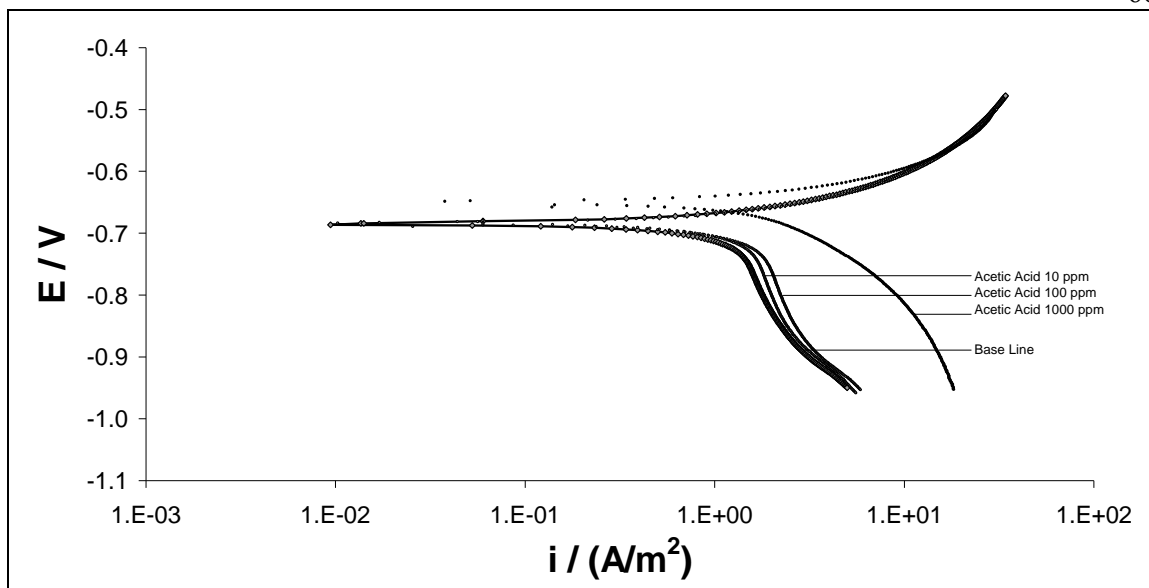


Figure 30. Polarization sweep function of the amount of acetic acid added to the water phase (0 ppm baseline, then 10 ppm, 100 ppm and 1000 ppm) conditions: 1 wt.% NaCl, 1 bar CO₂, pH 5.0.

Long chain organic acids

Test 1 – Adsorption from the water phase

Interestingly, even though the corrosion rate increases with acetic acid concentration, this is not the case with every organic acid. As shown in *Figure 31* to *Figure 33*, long chain organic acids such as myristic acid (CH₃(CH₂)₁₂COOH) and naphthenic acids (TCI) decrease the corrosion rate. As shown on *Figure 31*, 10 ppm of myristic acid is able to decrease the corrosion rate by 12%. Naphthenic acids have the same effect. It should be noted that only 10 ppm of organic acids were added to the solution because of the very low solubility of organic acids in aqueous solutions.

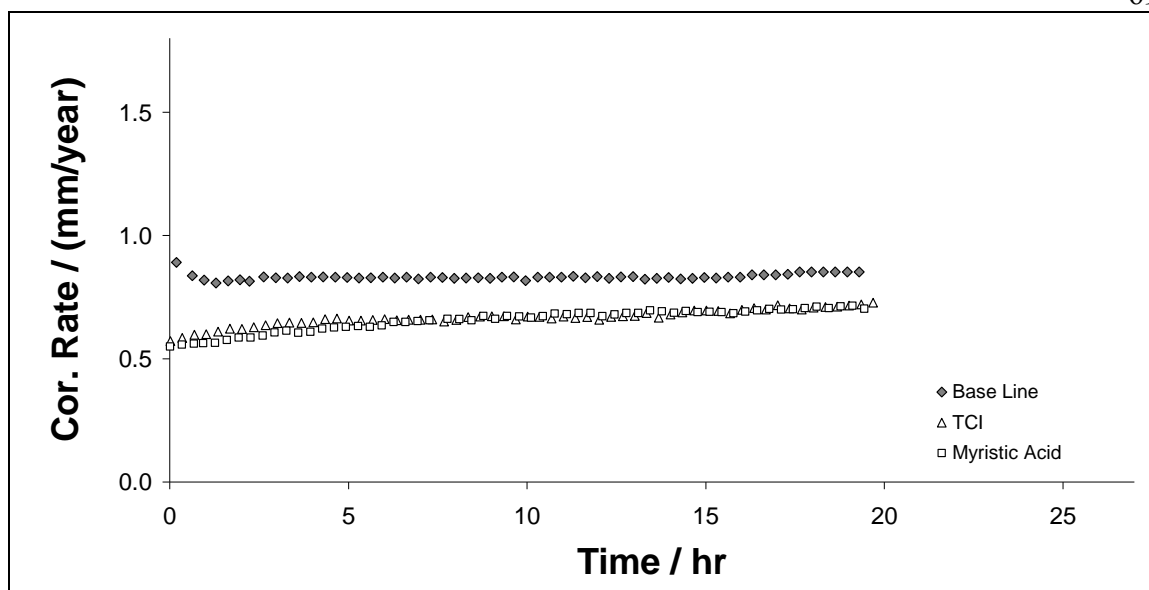


Figure 31. Evolution of the corrosion rate function of acid added to the water phase (10 ppm). Conditions: 1 wt.% NaCl, 1 bar CO₂, pH 5.0.

As with the short chain organic acids, the EIS experiments for the long chain organic acids showed no effect on the corrosion mechanism as depicted in *Figure 32*. The polarization sweeps on *Figure 33* showed that only the cathodic reaction is inhibited by organic acid while the anodic reaction stays unchanged.

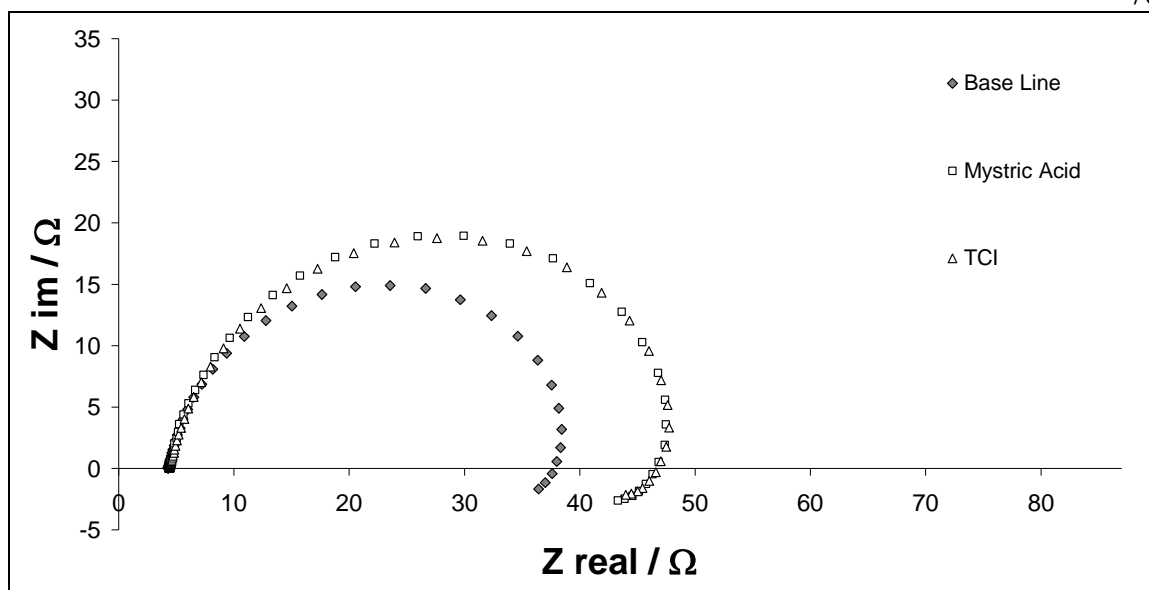


Figure 32. EIS measurement of the impedance, Nyquist plot. EIS experiments in water (1 wt.% NaCl, 1 bar CO_2 , pH 5.0) for different high molecular weight organic acids. Base line has no organic acid, 10 ppm myristic acid and 10 ppm naphthenic acid (TCI).

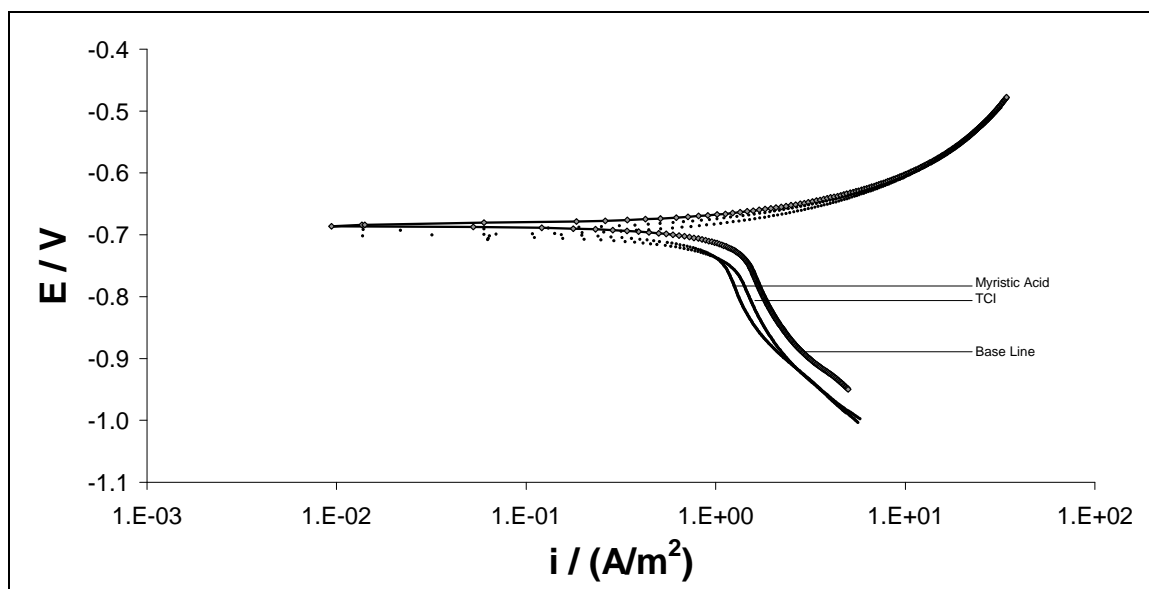


Figure 33. Polarization sweep function of the long chain organic acid added to the water phase (10 ppm). Conditions: 1 wt.% NaCl, 1 bar CO_2 , pH 5.0.

Test 2 – Adsorption from the oil phase

Long chain organic acids are able to significantly decrease the corrosion rate when the steel is in direct contact with the oil phase as shown on *Figure 34* and *Figure 35*. Only 0.1 wt.% concentration of myristic acid in oil gives a 48% inhibition of corrosion when the steel coupon is immersed in the water phase, while a 1 wt.% concentration of myristic acid gives 88% of inhibition of corrosion. Naphthenic acids present similar behavior. These results were expected, the protection against corrosion by high molecular weight organic acids is well known^{15,53}.

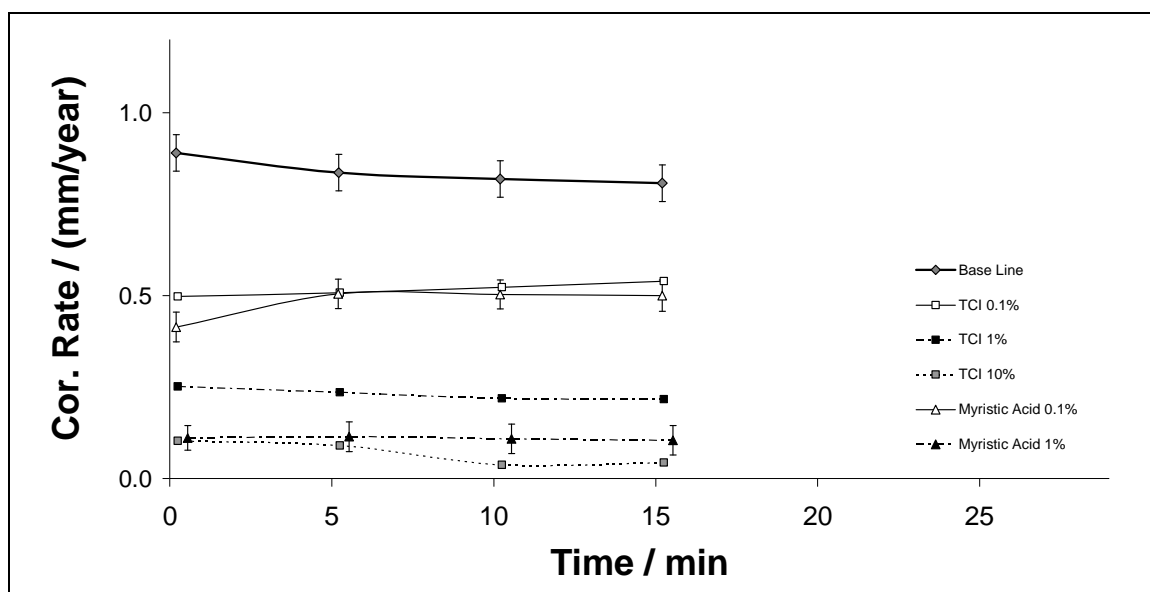


Figure 34. Corrosion measurements by LPR for long chain organic acids added to the model oil phase, water phase 1 wt.% NaCl, 1 Bar CO₂, pH 5.0.

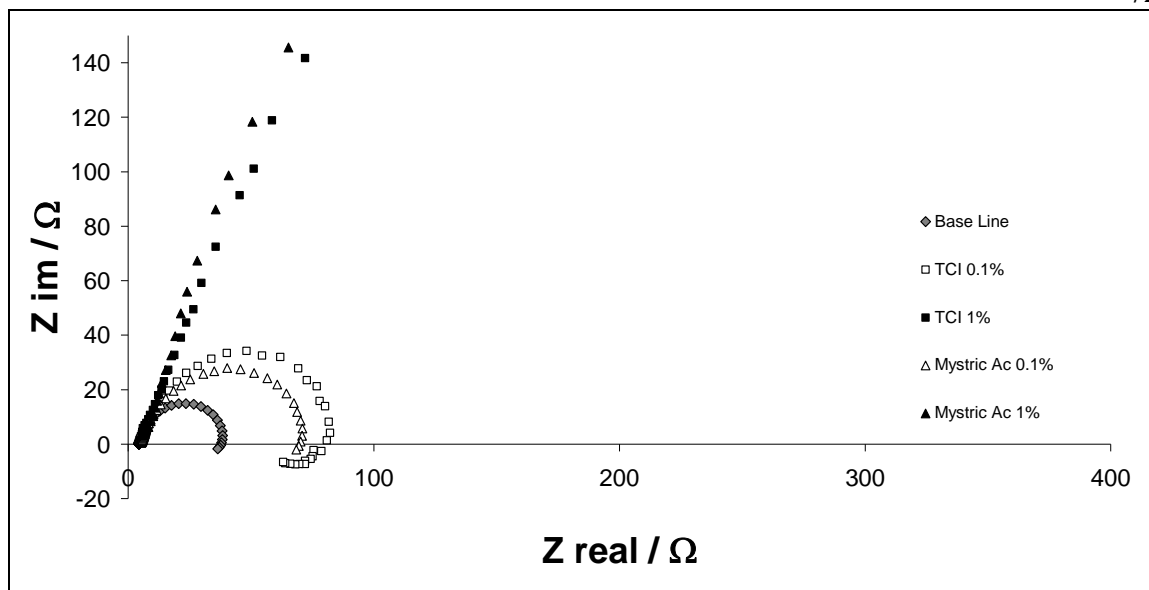


Figure 35. EIS measurement of the impedance, Nyquist plot. EIS experiments for long chain organic acids added to the model oil phase, water phase 1 wt.% NaCl, 1 bar CO₂, pH 5.0.

Despite the fact that high molecular weight acids exist in oil phase predominantly as dimers and are virtually insoluble in water, it appears that interaction with the metal surface still occurs. Results proved that high molecular weight organic acids are able to adsorb onto the metal surface and decrease corrosion rates.

Sulfur containing compounds

Test 1 – Adsorption from the water phase

Figure 36 to Figure 39 show the results obtained with sulfur containing compounds added to the water phase. The compounds tested (dibenzothiophene, dioctyl-sulfide and 1-tetradecanethiol) have very low solubility in water, therefore only 10 ppm of these compounds are added to the water phase during test 1. Dibenzothiophene, dioctyl-sulfide had virtually no effect on the corrosion rate. However, 1-tetradecanethiol has strong inhibitive properties; 10 ppm induces almost 100% inhibition of corrosion.

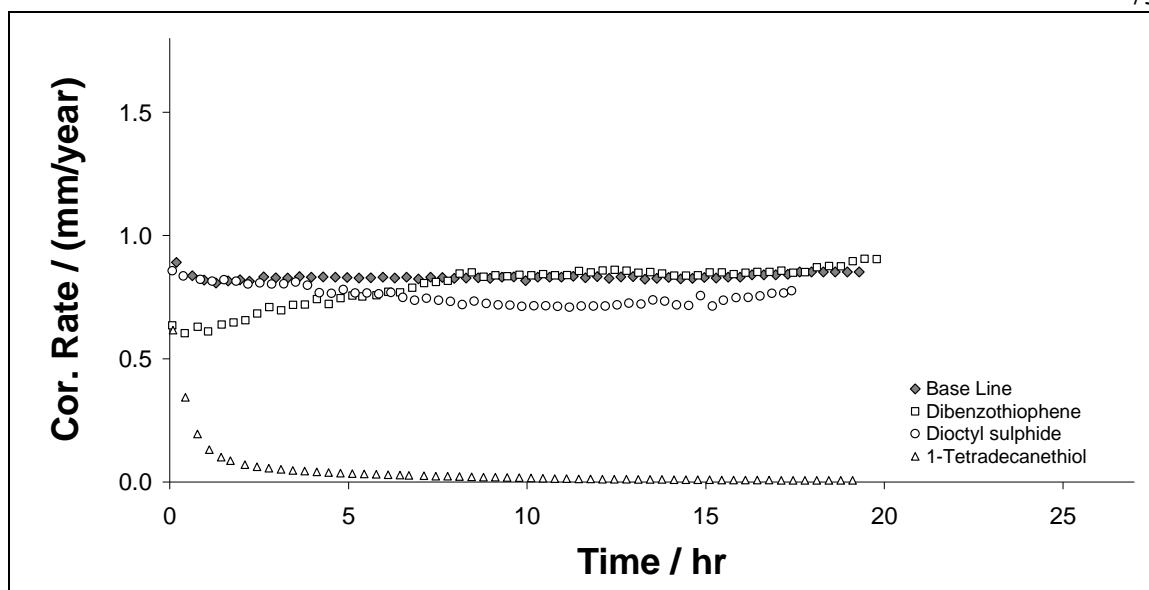


Figure 36. Evolution of the corrosion rate function of sulfur containing compounds added to the water phase (10 ppm). Conditions: 1 wt. % NaCl, 1 bar CO₂, pH 5.0.

As for the organic acids, EIS measurements with sulfur containing compounds show that the corrosion mechanism is unchanged (*Figure 36*). When the scale is expanded, it appears that the mechanism is also unchanged for the 1-tetradecanethiol (*Figure 37* and *Figure 38*).

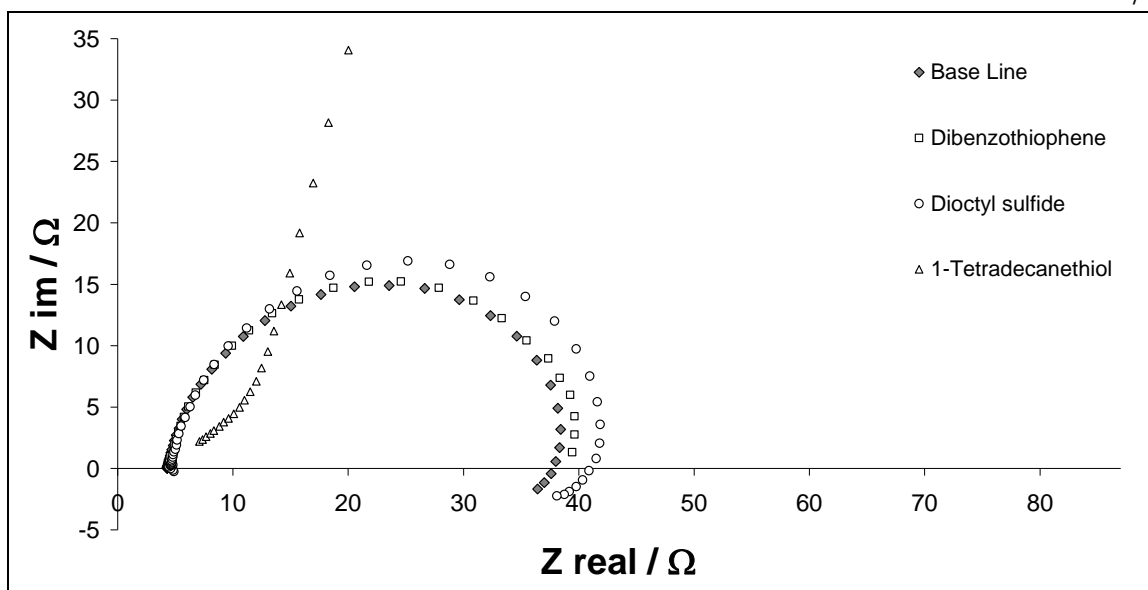


Figure 37. EIS measurement of the impedance, Nyquist plot. EIS experiments in water (1 wt.% NaCl, 1 bar CO₂, pH 5.0) for different sulfur containing compounds. Base line has no sulfur containing compounds, 10 ppm dibenzothiophene, 10 ppm dioctyl-sulfide and 10 ppm 1-tetradecanethiol.

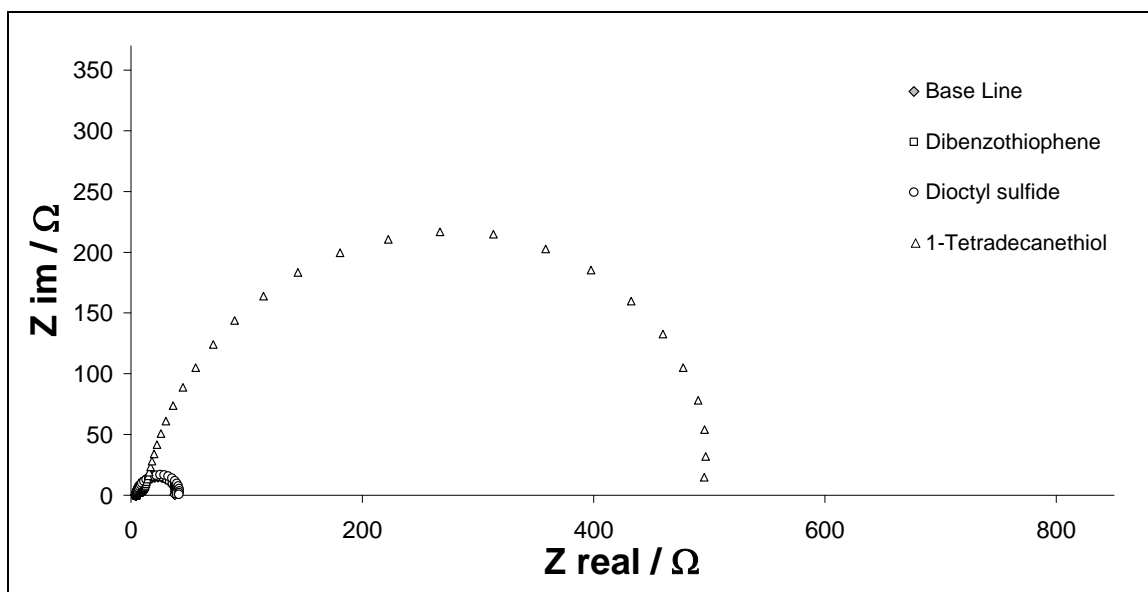


Figure 38. Full scale for Figure 37.

Polarization sweep (*Figure 39*) shows that 1-tetradecanethiol induces a strong inhibition of both the anodic and cathodic processes, while dibenzothiophene and dioctyl-sulfide have no effect on polarization curves.

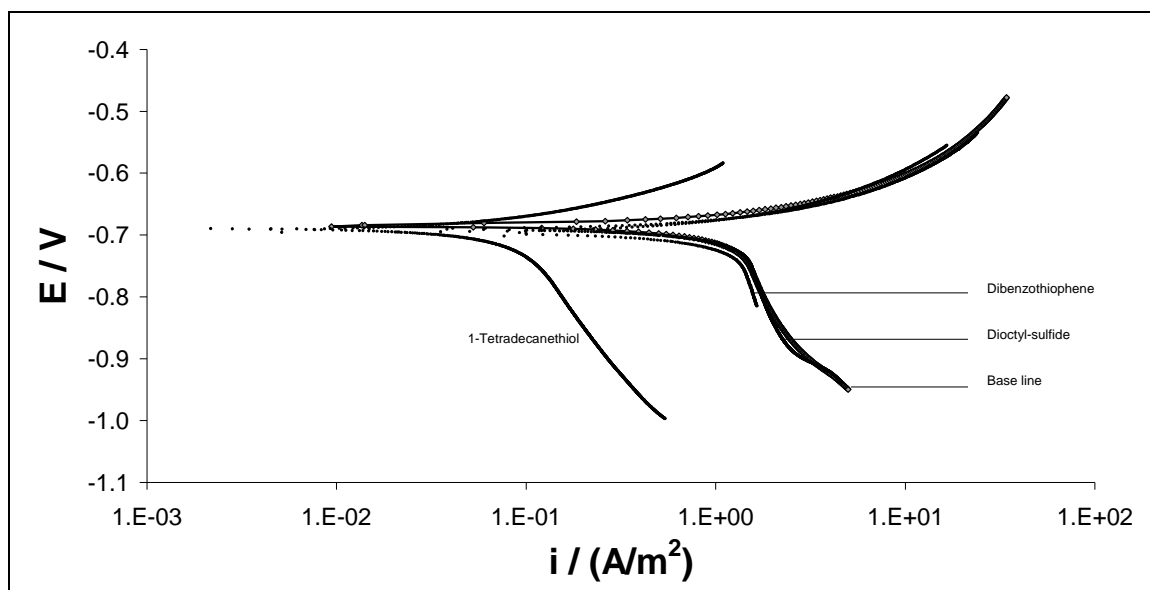


Figure 39. Polarization sweep function of the sulfur containing compound added to the water phase (10 ppm) conditions: 1 wt.% NaCl, 1 bar CO₂, pH 5.0.

Test 2 – Adsorption from the oil phase

Figure 40 and *Figure 41* show the results obtained with sulfur containing compounds. Just as for the results obtained in test 1, dibenzothiophene and dioctyl-sulfide have no significant effect on the corrosion rate. However, with the addition of 1-tetradecanethiol the corrosion rate decreases significantly. Only 0.1 wt.% of 1-tetradecanethiol produces a 44% inhibition of corrosion and 1 wt.% of 1-tetradecanethiol gives 84% of inhibition of corrosion. This is in agreement with the literature about mercaptans⁶⁴.

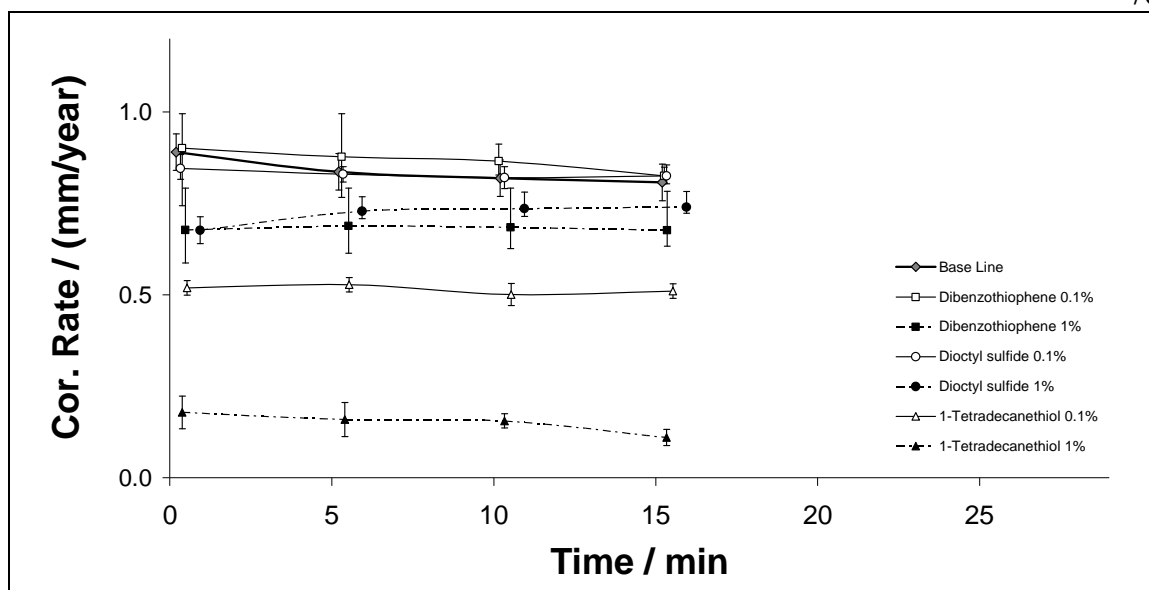


Figure 40. Corrosion measurements by LPR for sulfur containing compounds added to the model oil phase, water phase 1 wt.% NaCl, 1 bar CO₂, pH 5.0.

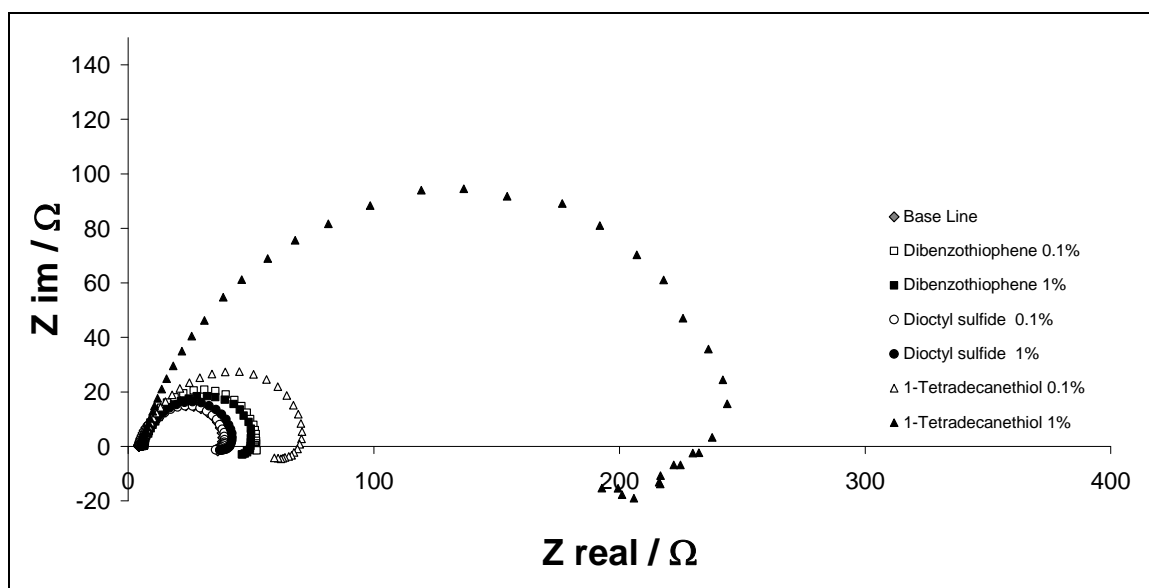


Figure 41. EIS measurement of the impedance, Nyquist plot. EIS experiments for sulfur containing compounds added to the model oil phase, water phase 1% NaCl, 1 bar CO₂, pH 5.0.

Three sulfur containing compounds were tested; each chemical representative of a chemical class. Dibenzothiophene (representing sulfur heterocycles) and dioctyl-sulfide (representing thio-ethers or sulfides) did not show any inhibitive properties. In contrast, 1-tetradecanethiol (representing thiols or mercaptans), has very strong inhibitive properties.

It is interesting to compare the results obtained with myristic acid and 1-tetradecanethiol. These two molecules were chosen because of their similarities in chemical structure. A representation of the two molecules is shown in *Figure 42*. They both have a linear saturated chain made up of 14 atoms of carbon. The inhibitions found for these compounds are similar: for 0.1 wt.% of 1-tetradecanethiol or myristic acid added in the oil phase a 44% inhibition of corrosion is achieved. For 1 wt.% added to the oil phase, 1-tetradecanethiol gives 84% inhibition of corrosion while myristic acid was recorded at 88% inhibition of corrosion. The comparison of these chemicals inhibitive properties suggests that once a chemical is adsorbed at the metal surface, its functionality (oxygen or sulfur) may not be important and the length and shape of the carbon chain has the strongest effect on corrosion inhibition. In other words, it is a steric effect.

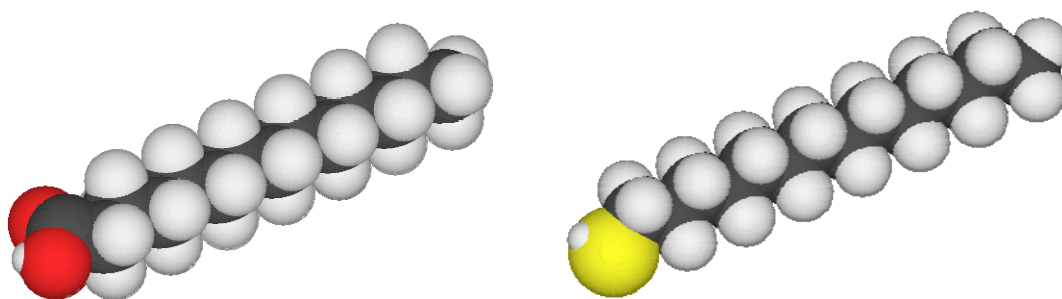


Figure 42. Chemical structure comparison of myristic acid (left) with 1-tetradecanethiol (right).

*Nitrogen containing compounds**Test 1 – Adsorption from the water phase*

Figure 43 to Figure 46 show the results obtained with nitrogen containing compounds added to the water phase (10 ppm). It is interesting that (as for oxygen and sulfur containing compounds) a wide range of corrosion rates is found. Carbazole has no effect on corrosion while acridine has very strong inhibitive properties. During EIS experiments, acridine's polarization resistance as high as 15,000 Ω were recorded. It should be noted that the 100% corrosion inhibition associated with acridine is too high to be representative of all "pyridinic type" compounds found in crude oil. Therefore, three nitrogen containing compounds more representative of crude oil's naturally occurring pyridinic compounds were identified for further study: benzo[h]quinoline, benzo[c]quinoline and 1,10-phenanthroline. Results of these chemicals are shown in test 2.

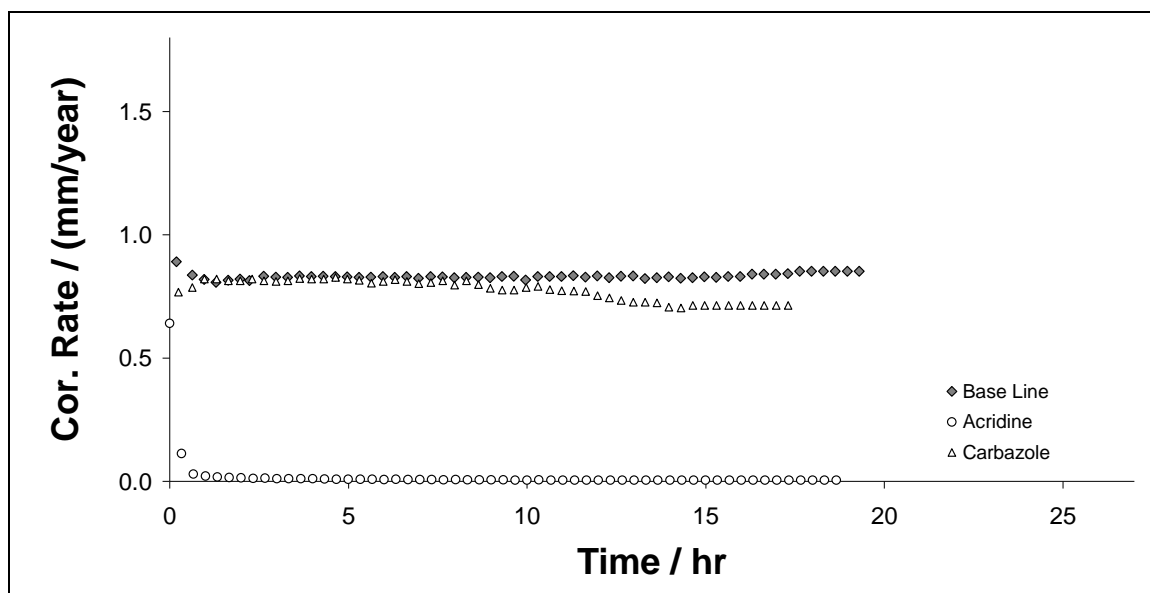


Figure 43. Evolution of the corrosion rate function of the nitrogen added to the water phase (10 ppm). Conditions: 1 wt.% NaCl, 1 bar CO₂, pH 5.0.

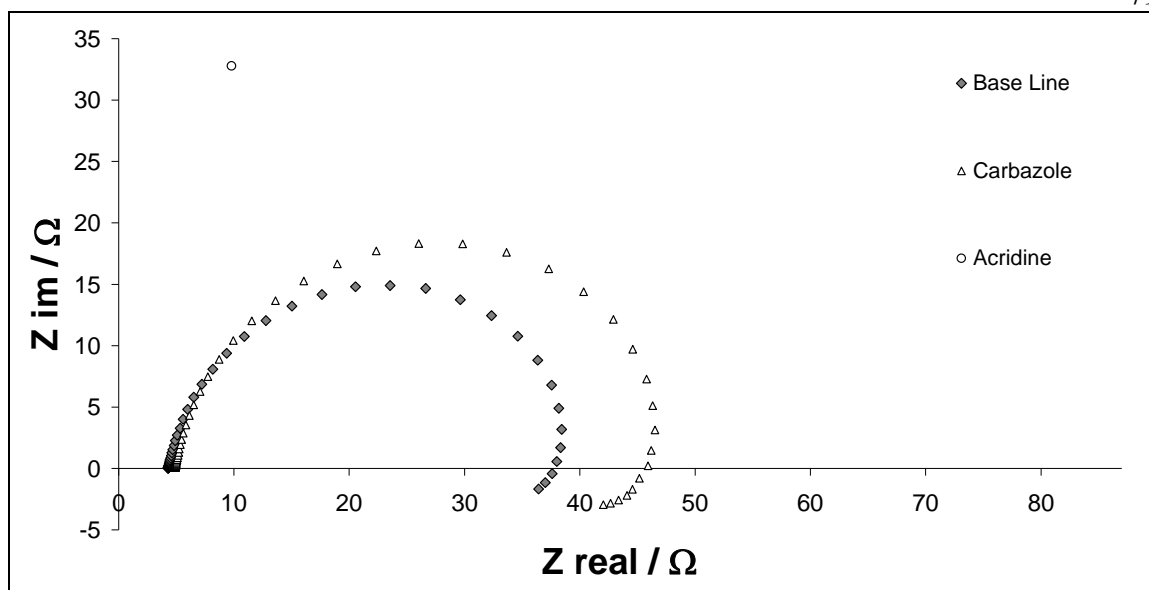


Figure 44. EIS measurement of the impedance, Nyquist plot. EIS experiments in water (1 wt.% NaCl, 1 bar CO_2 , pH 5.0) for different nitrogen containing compounds. Base line has no nitrogen containing compounds, 10 ppm carbazole and 10 ppm acridine.

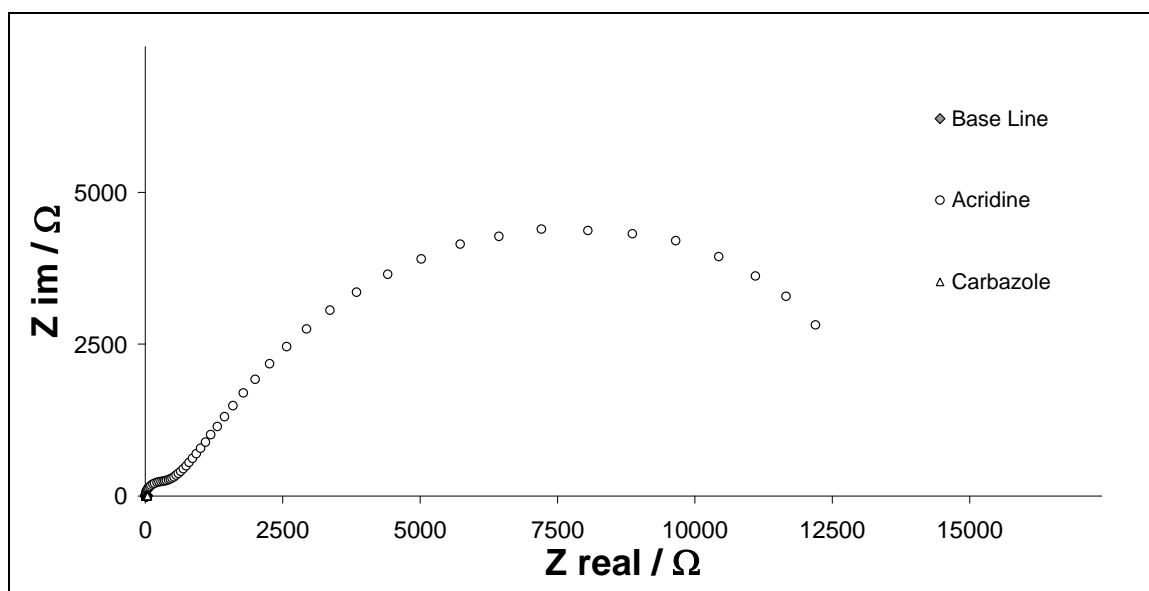


Figure 45. Full scale for Figure 44.

It should be noted that acridine is the only compound that changed the shape of the Nyquist plot, thus changing the corrosion mechanism. One possible explanation would be

the formation of acridine-carbonate salts. Therefore the corrosive species in solution may no longer be simply H^+ and H_2CO_3 but acridine complexes in solution.

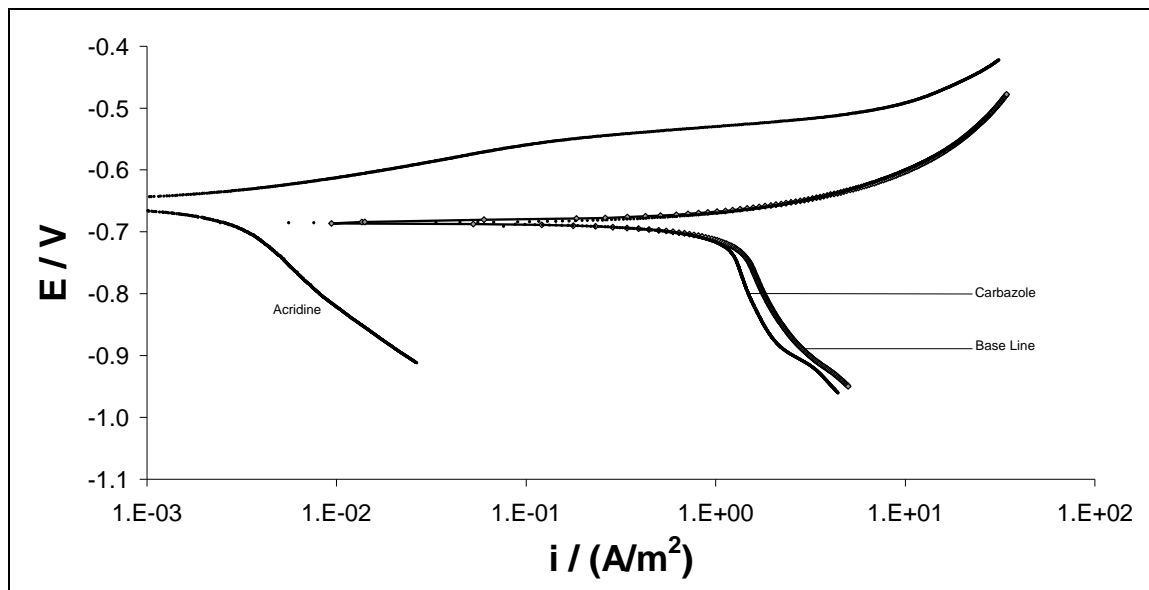


Figure 46. Polarization sweep function of the nitrogen containing compound added to the water phase (10 ppm). Conditions: 1 wt.% NaCl, 1 bar CO_2 , pH 5.0.

It should be noted that acridine inhibits both anodic and cathodic processes. Also, acridine is the only compound tested that increased the corrosion potential.

Test 2 – Adsorption from the oil phase

Figure 47 and Figure 48 depict results obtained with nitrogen containing compounds. While carbazole does not adsorb onto an iron surface and inhibit corrosion, acridine does adsorb at the metal surface and strongly inhibit corrosion. Only 0.01 wt.% of acridine added to the oil phase produces 83% inhibition of corrosion, while 0.1 wt.% acridine present in the oil phase induces 100% corrosion inhibition.

It should be noted that acridine and carbazole are not soluble in the model oil used. Some “aromaticity” is needed to dissolve nitrogen compounds in oil. Therefore, the base line in the test of nitrogen compounds is done, not with pure model oil, but with a mixture of

model oil (60 wt.%) and tetrahydronaphthalene (40 wt.%). It was proven by previous experiments that tetrahydronaphthalene does not induce any corrosion inhibition.

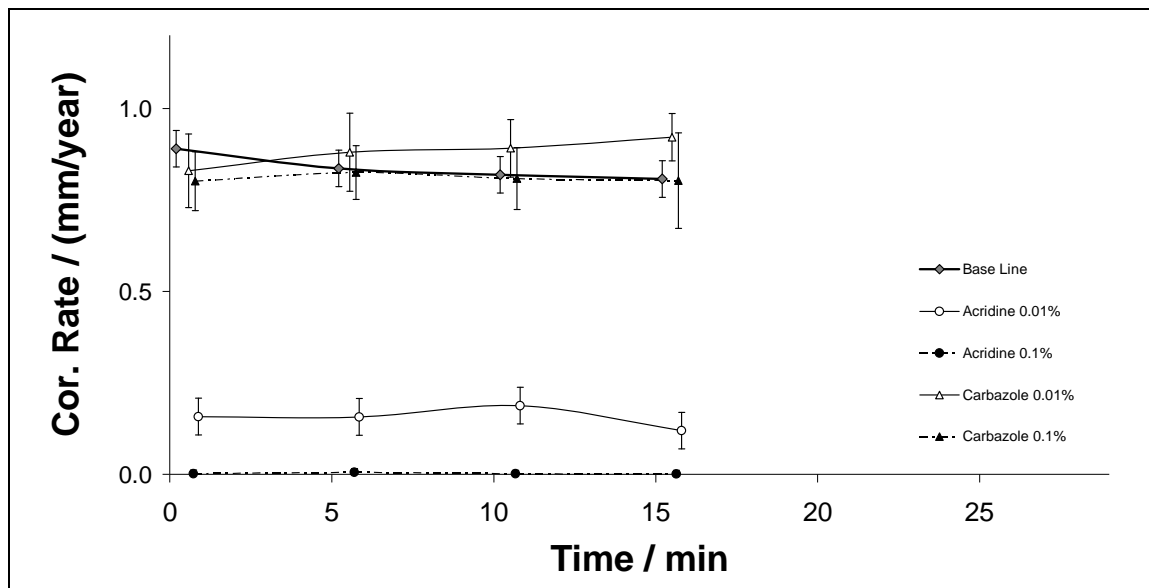


Figure 47. Corrosion measurements by LPR for nitrogen containing compounds added to the model oil phase, water phase 1 wt.% NaCl, 1 bar CO₂, pH 5.0.

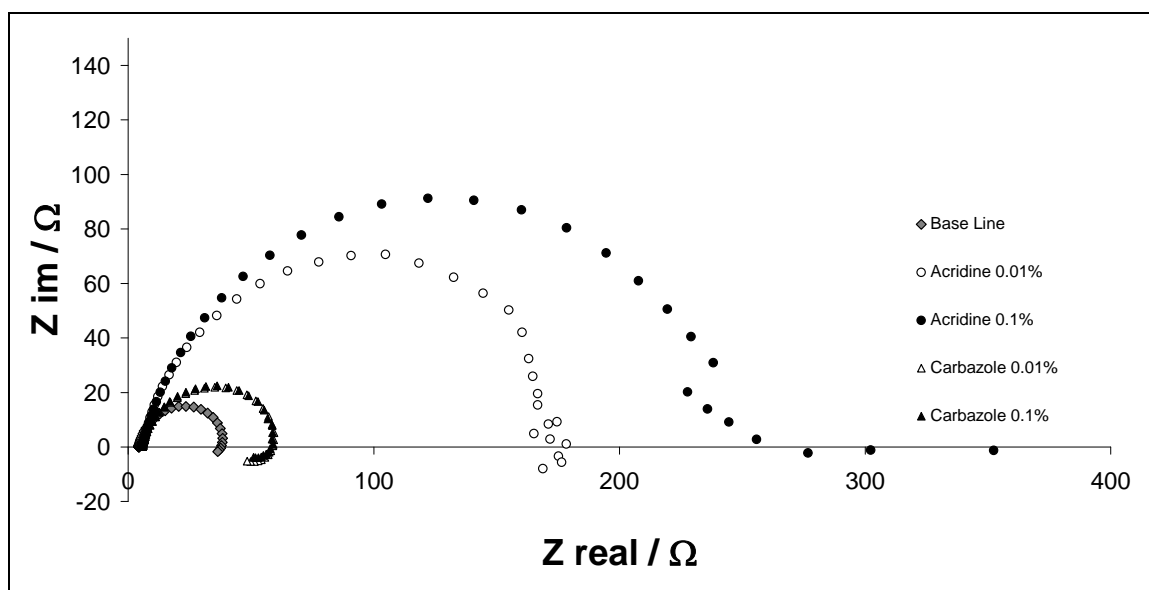
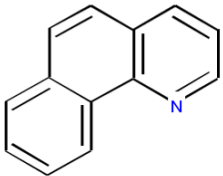
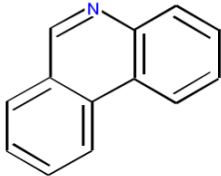
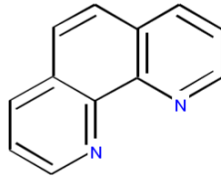


Figure 48. EIS measurement of the impedance, Nyquist plot. EIS experiments for different nitrogen containing compounds added to the model oil phase, water phase 1 wt.% NaCl, 1 bar CO₂, pH 5.0.

In these experiments acridine prove itself to be a very strong corrosion inhibitor, even in minute amounts. Such inhibition of corrosion shows that “pyridinic type” compounds can inhibit corrosion. However, such strong inhibition of corrosion might not be representative of all pyridinic type compounds. Therefore, three more pyridines have been tested: benzo[h]quinoline, benzo[c]quinoline and 1,10-phenanthroline. Structural data for these compounds are shown in Table 5.

Table 5. “Acridine like” compounds tested

Name	benzo[h]quinoline	benzo[c]quinoline	1,10-phenanthroline
Common name	naphthoquinoline	phenanthridine	phenanthroline
Chemical formula	$C_{13}H_9N$ 	$C_{13}H_9N$ 	$C_{13}H_8N_2$ 
Molecular weight	179.22 g·mol ⁻¹	179.22 g·mol ⁻¹	180.21 g·mol ⁻¹

The three “pyridinic type” compounds: benzo[h]quinoline, benzo[c]quinoline and 1,10-phenanthroline have been chosen because they have the same ring structure. The only difference between these three chemicals is the place and number of nitrogen atoms on the molecule. *Figure 49* and *Figure 50* depict results obtained with nitrogen containing compounds. The results show that benzo[h]quinoline is not effective as a corrosion inhibitor. This result can be explained by the location of the active site as the nitrogen is sterically hindered by the aromatic ring. Interestingly, benzo[c]quinoline and 1,10-phenanthroline produce the same amount of inhibition of corrosion, 1% of the chemicals is equivalent to 50% corrosion inhibition. These results suggest, again, that once a

chemical is adsorbed onto the metal surface, the carbon structure is the main factor on the inhibition of corrosion. This is a steric effect.

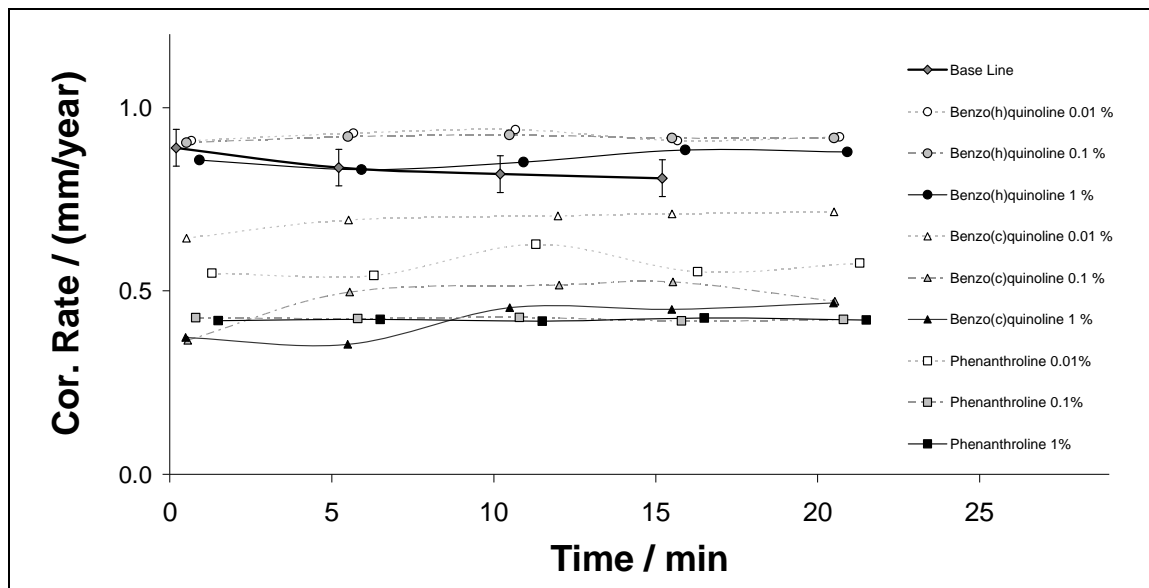


Figure 49. Corrosion measurements by LPR for pyridinic compounds added to the model oil phase, water phase 1 wt.% NaCl, 1 bar CO₂, pH 5.0.

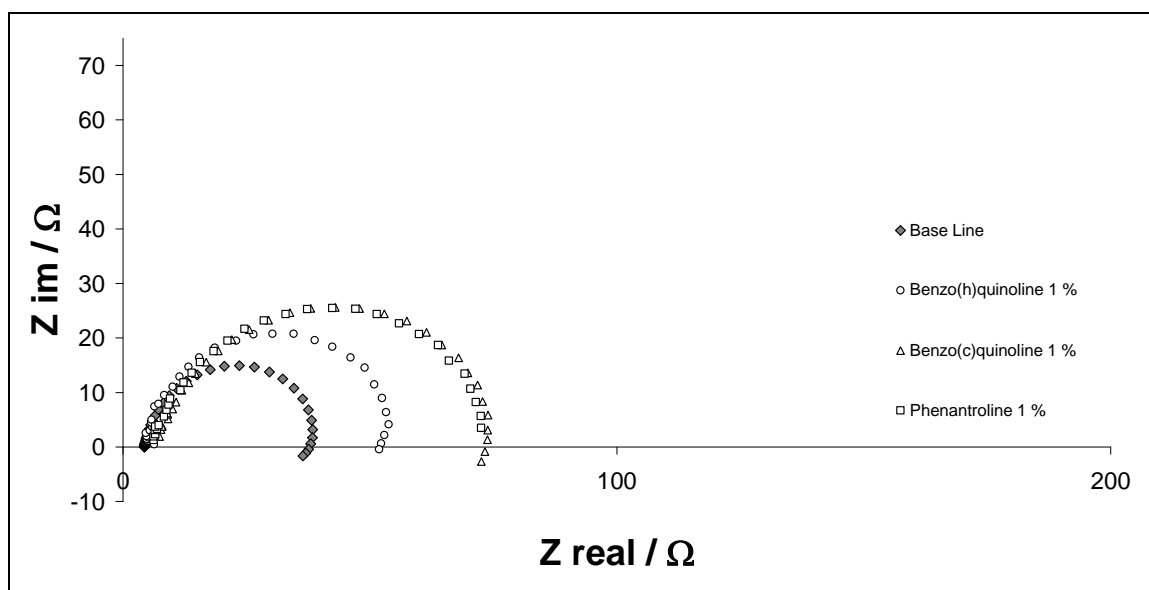


Figure 50. EIS measurement of the impedance, Nyquist plot. EIS experiments in water (1 wt.% NaCl, 1 bar CO₂, pH 5.0) after the steel coupon has been immersed in model oil mixed with 3 different pyridinic compounds.

Modeling the crude oil inhibition of corrosion

Corrosion inhibition model

A simple mechanistic model is developed in order to predict inhibition of corrosion. The inhibition of corrosion (*IC*) has been defined as the ratio of the inhibited corrosion rate divided by the uninhibited corrosion rate.

A simple mechanistic model is developed in order to predict inhibition of corrosion. The inhibition of corrosion has been defined as the ratio of the inhibited corrosion rate divided by the uninhibited corrosion rate.

$$IC_{\%} = \left(1 - \frac{\text{corrosion rate}_{\text{with inhibition}}}{\text{corrosion rate}_{\text{without inhibition}}} \right) \cdot 100 \quad \text{Equation 37}$$

The model is based on two assumptions. The first assumption says that corrosion inhibition is proportional to the fraction of the metal surface covered by the surface active chemicals. Therefore the present model is created using the Langmuir equation. If only one chemical is added to the oil phase the corrosion inhibition can be calculated knowing the chemical group and concentration.

If one chemical *X* is able to adsorb onto a metal surface, the following reaction can be written:



The equilibrium constant (*K*) can be therefore calculated using the equation:

$$K = \frac{[X_{\text{iron}}]}{[X] \cdot [\text{iron}]} \quad \text{Equation 39}$$

If θ represents the percentage coverage of the metal surface, $[X_{iron}]$ is proportional to θ . And the concentration of the chemical X (noted as $[X]$) must be proportional to $1 - \theta$. Therefore, if α is a constant, it is possible to write the following equation:

$$\alpha = \frac{\theta}{[X] \cdot (1 - \theta)} \quad \text{Equation 40}$$

This equation is known as the Langmuir equation. The difference is that $[X]$ represents here the concentration of a chemical present in the oil phases and in the Langmuir equation $[X]$ would be a gas pressure.

It is possible to rearrange the equation above to obtain:

$$\theta = \frac{\alpha \cdot [X]}{1 + \alpha \cdot [X]} \quad \text{Equation 41}$$

The main assumption is that the inhibition of corrosion is proportional to the surface coverage. Therefore using two constants α and β we can write:

$$IC_{\%} = \beta \cdot \frac{\alpha \cdot [X]}{1 + \alpha \cdot [X]} \quad \text{Equation 42}$$

In this equation, α is proportional to the adsorption equilibrium constant of chemical X onto iron, and β represents the proportionality between inhibition of corrosion and surface coverage. The constants α and β can be calculated for each chemical class using the model compound chosen to represent that specific chemical class. If the chemicals tested are well chosen and representative of their chemical class, it is possible to predict the inhibition of corrosion due to one class of chemical (such as organic acids or mercaptans) using the model compound tested in this research for that particular chemical class. However, in real crude oils, more than one chemical class is producing

corrosion inhibition. Therefore, a simplifying assumption will be used: the inhibition of corrosion will be calculated for every chemical class and the highest corrosion inhibition calculated will be the corrosion inhibition predicted by the model.

In consequence, the final equation to predict the corrosion inhibition of each class of chemical i is:

$$IC_{\%} = MAX\left(\beta_i \cdot \frac{\alpha_i \cdot [X_i]}{1 + \alpha_i \cdot [X_i]}\right) \quad \text{Equation 43}$$

In this equation i represents successively long chain organic acids, thiols and pyridinic compounds (and not sulfur heterocycles, thio-ethers and pyrrolic compounds since it was found that these chemicals have no major effect on corrosion).

Calculation of the parameters α_i and β_i

Four classes of compounds have been tested but only three were able to reduce the corrosion rate (oxygen, sulfur and nitrogen containing compounds). Also, the inhibition within each class is not homogeneous, sub-classes produces different corrosion inhibitions. Table 6 summarizes the results obtained in this chapter.

Table 6. Summary of the inhibitive effect of the compounds tested in this study

Chemical class	Chemical sub-class	Chemical compound tested	Con. in oil phase	Cor. Rate mm/year
Base line		pure CO ₂		0.91
Aromatics		Tetrahydronaphthalene	40.00%	0.85
oxygen compounds	Long chain organic acids	Myristic Acid	0.10%	0.48
			1.00%	0.11
		TCI	0.10%	0.52
			1.00%	0.23
10.00%	0.07			
sulfur compounds	Sulfur heterocycles	Dibenzothiophene	0.10%	1.01
			1.00%	0.69
	Thio-ethers (sulfide)	Diocetyl sulfide	0.10%	0.83
			1.00%	0.72
	Thiols (mercaptan)	1-Tetradecanethiol	0.10%	0.51
			1.00%	0.15
nitrogen compounds	Pyridinic (basic nitrogen)	Acridine	0.01%	0.16
			0.10%	0.00
		Benzo(h)quinoline	0.01%	0.92
			0.10%	0.92
			1.00%	0.86
	Benzo(c)quinoline	0.01%	0.69	
		1.00%	0.42	
		0.01%	0.57	
		0.10%	0.42	
		1.00%	0.42	
	Pyrrolic (neutral nitrogen)	Carbazole	0.01%	0.83
			0.10%	0.80

Using Table 6 , α_i and β_i can be calculated for every chemical sub-class tested. However, a prediction for every chemical sub-class is unnecessary since some chemical sub-class have no effect on corrosion inhibition.

- Aromatics were unable to have a significant effect on corrosion even in very large concentration (40 wt.%). Table 6 shows that within the same class of compounds not every sub-class was able to inhibit corrosion.

- Oxygen containing compounds: Small molecule organic acids increase the corrosion rate while large molecule organic acids have inhibitive properties.

- Sulfur containing compounds: Only mercaptans are able to decrease corrosion rates while dialkyl sulfides and thiophenes have no significant effect.

- Nitrogen containing compounds: Pyridinic compounds (basic nitrogen compounds) can adsorb at the metal surface, this is proven by acridine's strong inhibition of corrosion. However, pyrrolic compounds (neutral nitrogen compounds) such as carbazole have no effect on corrosion.

Therefore, the model is calibrated for only three chemical classes: long chain organic acids, thiols (mercaptan), and pyridinic compounds (basic nitrogen) using the results obtained with myristic acid, 1-tetradecanethiol and benzo(c)quinoline shown in *Figure 51*.

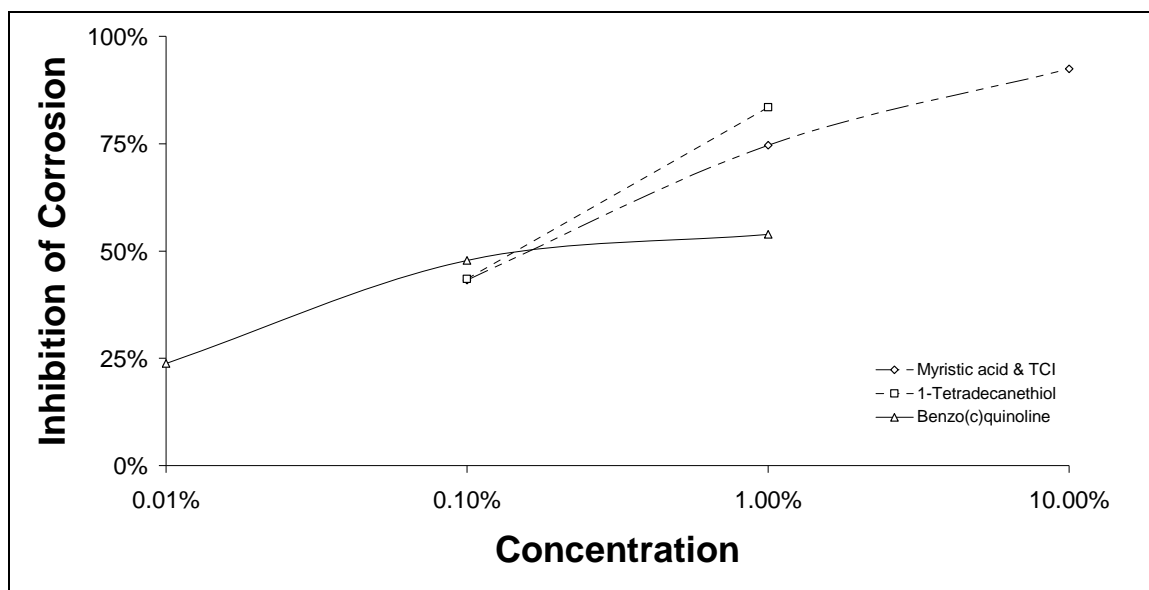


Figure 51. Inhibition of corrosion calculated from Table 6 for the naturally occurring chemicals in crude oil that have induced significant corrosion inhibition.

The values of the constants α_i and β_i are shown in the Table 7 with i representing successively long chain organic acids, thiols and pyridinic compounds.

Table 7. *Inhibition model's constants calculated from experiments*

Chemical class	Chemical tested	α_i	β_i
Long chain organic acids	Myristic Acid	4	1
Thiols (mercaptan)	1-Tetradecanethiol	5	1
Pyridinic (basic nitrogen)	Benzo(c)quinoline	150	0.55

Ajmera⁶⁵ studied the effect of asphaltene on corrosion inhibition. Based on his results the constants α_i and β_i can be calculated for asphaltenes. Results are shown in Table 8.

Table 8. *Inhibition model's constants calculated from experiments for asphaltene*

Chemical class	Concentration	Corrosion inhibition	α_i	β_i
Asphaltene	1 g·L ⁻¹	13%	0.6	1
	10 g·L ⁻¹	48%		
	50 g·L ⁻¹	67%		

Li⁶⁶ studied the effect of corrosion inhibitors on corrosion inhibition. Based on his results the constants α_i and β_i can be calculated for corrosion inhibitors. Results are shown in Table 9.

Table 9. *Inhibition model's constants calculated from experiments for corrosion inhibitors*

Chemical class	Concentration	Corrosion inhibition	α_i	β_i
Amino	2 ppm	85%	1000	1
	3 ppm	87%		
	5 ppm	90%		
	20 ppm	93%		
	60 ppm	94%		
	100 ppm	95%		
	200 ppm	95%		
Quat	5 ppm	36%	75	1
	20 ppm	60%		
	30 ppm	76%		
	40 ppm	83%		
	60 ppm	84%		
	100 ppm	89%		
	200 ppm	94%		

Using Equation 43 for i equaling successively long chain organic acids, thiols, pyridines, asphaltenes and the type of corrosion inhibitor; it is now possible to predict an approximate value of the corrosion inhibition associated with to a particular crude oil. Other types of compounds in crude oils such as aromatics, sulfur heterocycles, thioethers, and pyrroles, have little or no effect on direct corrosion inhibition. However, this does not mean that these compounds do not have an effect on corrosion; some of them

have an effect on crude oil wettability, which has an indirect effect on corrosion rates. This effect will be studied in Chapter 4.

Two assumptions were proposed to predict the effect of crude oil chemistry on corrosion inhibition. First, that corrosion inhibition is proportional to the amount of surface active chemicals adsorbed onto the metal surface. Second, that in a mixture of surface active compounds, the overall corrosion inhibition is equal to the highest corrosion inhibition calculated for each chemical class. Two experimental procedures were developed in order to validate the two main assumptions.

Model validation

Validation of assumption 1: Adsorption measurements

Assumption 1: Corrosion inhibition is proportional to the amount of surface active chemicals adsorbed onto the metal surface.

To test the first assumption, the mass adsorbed onto the metal surface is measured. The adsorption can be recorded as a function of time by a Quartz Crystal Microbalance (QCM). The quartz crystal is covered with an iron layer (*Figure 52*). In each experiment, a new iron-coated quartz crystal is introduced into a 1 L beaker containing 0.5 L of model oil. After the quartz crystal frequency is stabilized, 0.5 L of model oil mixed with one surface active compound is added into the beaker. The frequency of the quartz crystal is recorded throughout the whole experiment. The observed change in frequency is inversely proportional to a change of mass. Therefore, the adsorption of surface active compounds was detected when the frequency of the quartz crystal decreased.

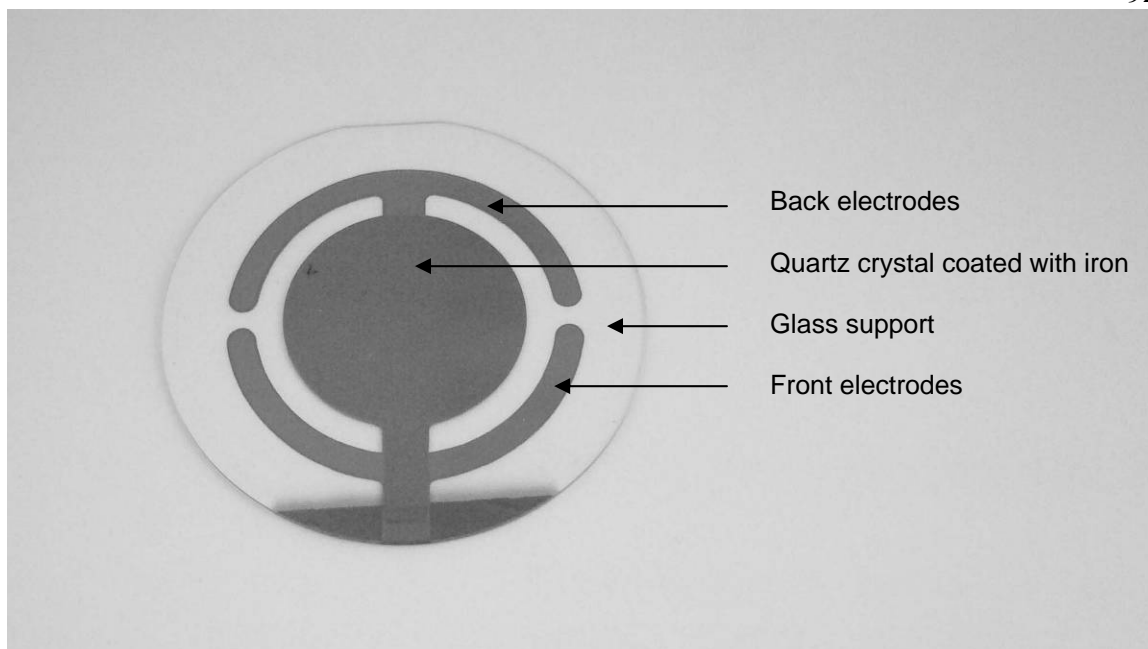


Figure 52. Iron coated quartz crystal used in the Quartz Crystal Microbalance.

The results of the adsorption measured with a QCM are shown in the *Figure 53*. The mass adsorbed has been converted to a film thickness assuming that the film created during the adsorption is homogenous.

Aromatics were not tested since the high concentration of tetrahydronaphthalene changes the viscosity of the model oil. A change in the viscosity implies a change in the quartz crystal's frequency much larger than the effect of the mass adsorbed.

The adsorption results for myristic acid and naphthenic acid (TCI) are similar, a rapid adsorption with a maximum about $1 \mu\text{g}\cdot\text{cm}^{-2}$. This quick response suggests that the adsorption of organic acids is physisorption: *i.e.*, rapid adsorption through weak intermolecular interactions (van der Waals forces). If this is really physisorption, experiments should depend on temperature. Durnie, *et al.*⁶⁷ tested 1,8-octanedicarboxylic acid ($\text{C}_{10}\text{H}_{18}\text{O}_4$) similar in structure and molecular weight with myristic acid. He proved that the logarithm of the concentration needed to induce 50% corrosion inhibition is

inversely proportional to the temperature. This further points to the physisorption of organic acids onto iron surfaces.

The adsorption of sulfur containing compounds showed two different responses. Dibenzothiophene and dioctylsulfide have a rapid adsorption rate with a maximum at about $0.5 \mu\text{g}\cdot\text{cm}^{-2}$. The 1-tetradecanethiol adsorption was slow but steady. The maximum mass adsorbed was measured at $0.9 \mu\text{g}\cdot\text{cm}^{-2}$ after one hour. Such slow adsorption is likely to be chemisorption.

Nitrogen containing compounds were not tested for the same reason as stated for aromatics.

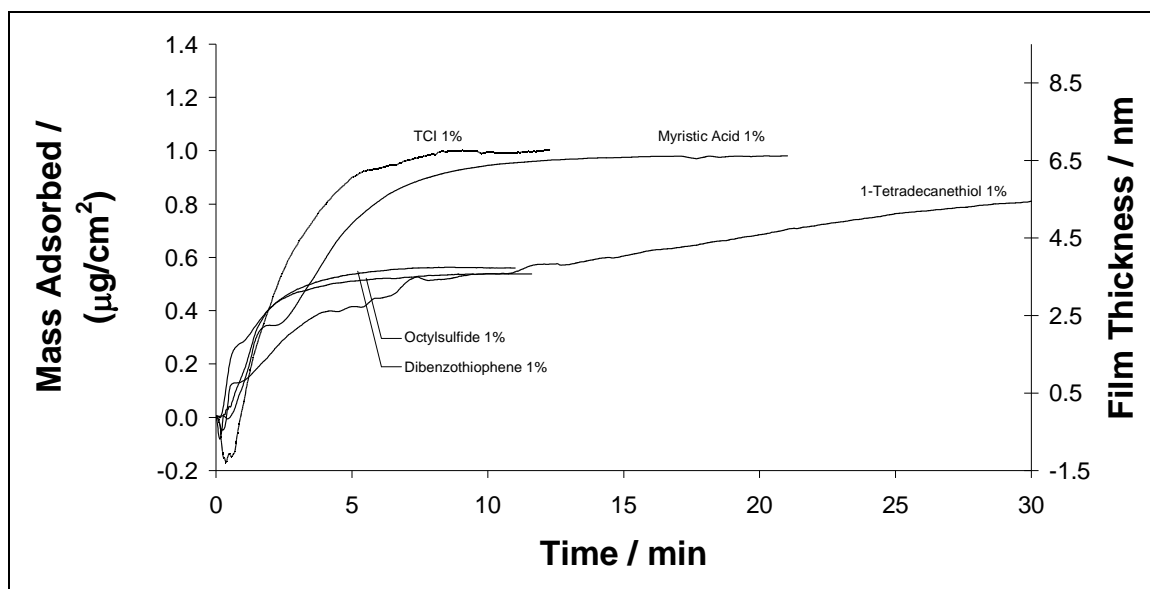


Figure 53. Evolution of the mass adsorbed for different surface active compounds as a function of time.

Using the corrosion measurement from Table 6 and the results of the QCM in *Figure 53*, a graph that correlates inhibition and adsorption can be generated. Each chemical tested produces one data point and the results are shown in *Figure 54*. The results indicate a linear relationship between inhibition of corrosion and the mass adsorbed at the metal

surface. However, testing of only 5 chemicals is insufficient for the development of a universal conclusion.

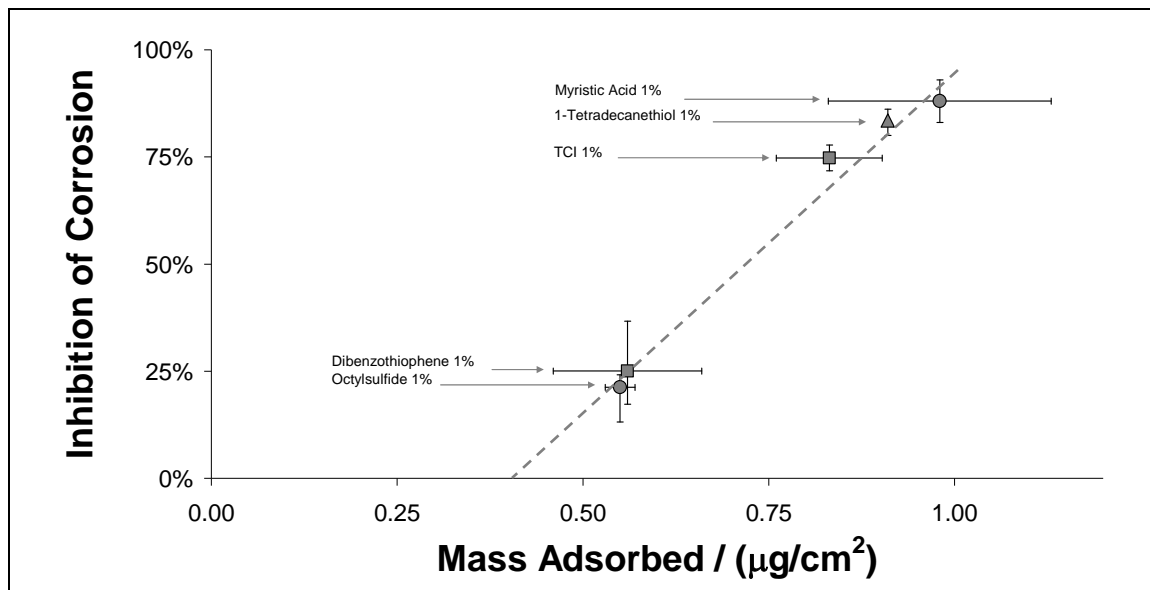


Figure 54. Relationship between mass adsorbed and inhibition of corrosion.

Validation of assumption 2: Corrosion measurements

Assumption 2: In a mixture of surface active compounds, the overall corrosion inhibition is equal to the highest corrosion inhibition calculated for each chemical class.

This assumption is tested using two different compounds, myristic acid and acridine. This combination seems to be possibly the most detrimental, since myristic acid is an acid and acridine is a base. The chemicals could inhibit each other and, overall, produce a lower corrosion inhibition than the best of the two. Table 10 shows the results obtained with these chemicals using the procedure described as test 2.

Table 10. *Evolution of the corrosion rate for different ratios of acridine / myristic acid*

Myristic acid	Acridine	Corrosion rate	Rp
0.0%	0.1%	0.0 mm/year	16,200 Ω
0.1%	0.1%	0.0 mm/year	11,400 Ω
1.0%	0.1%	0.1 mm/year	350 Ω

The results in Table 10 show that myristic acid does lower the corrosion inhibition of acridine. This proves that, hypothesis 2 is incorrect. However myristic acid needs to be in a concentration 10 times greater than acridine in order decrease the acridine's corrosion inhibition. Further study on competitive adsorption is needed.

Model validation with crude oil

Using the constants calibrated for each chemical class in Table 7 and Equation 43, it is possible to calculate the corrosion inhibition of one crude oil knowing its composition. One crude oil was chosen to test the model. Table 11 shows the crude oil's origin and properties.

Table 11. *Crude oil tested. Chemical composition and corrosion inhibition*

Origin	North sea
API	37.7
Atomic oxygen	0.0449 wt.%
Atomic sulfur	0.160667 wt.%
Atomic mercaptans sulfur	0.000197 wt.%
Atomic total nitrogen	483.66 ppm wt
Atomic basic nitrogen	154.15 ppm wt
Asphaltene	Unknown
Corrosion inhibitor	Type unknown, present in very low amount
Measured corrosion inhibition	70%
Calculated corrosion inhibition	61%

The inhibition of corrosion calculated using Equation 43 for the oxygen class is 61%, the sulfur class is 5% and finally the nitrogen class is 54%. In consequence, using the second assumption (the corrosion inhibition is equal to the maximum corrosion inhibition calculated for each chemical class) the corrosion inhibition should be 61%. However, the corrosion inhibition measured is 70%. The error between the measurement and the model is acceptable. It is possible that a competitive adsorption model would improve Equation 43 and generate more accurate corrosion inhibition predictions.

Discussion

Corrosion inhibition due to the adsorption process of surface active compounds naturally present in crude oil is not a new subject of study. Hackerman published a list of papers on

the subject more than 50 years ago⁶⁸⁻⁷³. He found that polar organic compounds such as carboxylic acids, sulfur and nitrogen containing compounds can adsorb onto a steel surface and inhibit corrosion by “increasing the true ohmic resistance” and “interfering with anodic and cathodic chemical processes”¹⁷. The results found in this report are in agreement with these earlier studies.

Srhiri⁷⁴, in his study of corrosion inhibition by nitrogen containing compounds, found similar results as the one found in this dissertation. Interestingly, the shape of EIS experiments shows the same two time constants as for the acridine results presented in this chapter. This is an indication that the corrosion mechanisms are the same. The inhibition of the pyrroles studied was however higher than the one recorded here. According to Srhiri “the presence of a heteroatom in an organic compound with unsaturated bond causes the adsorption process on the metal surface”, this was found in this research also.

Snyder⁵⁷ published a detailed study of oxygen and nitrogen containing compounds naturally present in crude oil and explained that even if they are present in very small amount their effect on corrosion is major. These results are also in agreement with the results presented here.

However, in the previous research discussed above, the inhibition is calculated for one chemical only. Efir^{15,24,53}, Hernandez *et al.*^{25,27} and Durnie^{13,67} tried to extend the common knowledge (that surface active compounds can adsorb and inhibit corrosion) by making prediction of corrosion rates in real conditions.

Efir^{15,24,53} explained that “metal organic compound, nitrogen, sulfur and oxygen containing compounds” have a direct effect on corrosion. He gave a simple relationship between corrosion rate and the concentration of nitrogen / sulfur containing compounds in the crude oil, Equation 44.

$$CR = 0.0015 * (\%wtN * \%wtS)^{-1.1}$$

Equation 44

The development of this equation comes from the desire to find a simple solution from the study of real crude oils. However, as shown in this chapter the relation between crude oil corrosion inhibition and crude oil composition is not that simple, because even within the same chemical class, different chemicals behave differently.

Vera and Hernandez²⁵ tried the same approach. They used SARA analysis and corrosion experiments from a large quantity of Venezuelan crude oils to find a relationship between crude oil corrosion inhibition and crude oil composition. The first crude model²⁵ stated the effect of resins on corrosion is stronger than the effect of aromatics, which is also stronger than the effect of saturates. The model was improved a year later²⁶ and published as two similar equations (Equation 45), one for asphaltenic crude oils and one for paraffinic crude oils:

$$\begin{cases} IC_{asphaltenic} = 0.48 + 0.00444 \cdot (\% crude oil) + 0.00488 \cdot (resine + aspahltene) + 0.0436 \cdot (sulfur) \\ IC_{paraffinic} = -0.23 + 0.0026 \cdot (\% crude oil) + 0.0576 \cdot (resine) + 0.000844 \cdot (nitrogen) - 0.333(asphaltene) \end{cases}$$

Equation 45

They improved the statistical analysis, and used an artificial neural network to create a more complex mathematical model²⁷. This model is able to predict the corrosion inhibition for Venezuelan crude oils. However, this model cannot predict with accuracy the corrosion inhibition for fields that have not yet been tested. However, few experiments are sufficient to train the artificial neural network. This is a powerful solution to predict the inhibition of corrosion, but because of the nature of the input (SARA analysis), it is not possible to extract physical knowledge from it.

Durnie^{13,67} used a very different approach. He studied a large array of chemical compounds, and predicted the corrosion inhibition properties of these compounds using quantum molecular parameters. Interestingly, he found that adsorption isotherms such as

Tempkin or Langmuir are suited to describe the adsorption of corrosion inhibitors. Thus, they were good predictors of the corrosion rate.

Conclusion

The prediction made by the corrosion inhibition model (Equation 43) compared to the experimental results from Ayello and Ajmera's experiments for the crude oil chemistry and Li's experiments for the corrosion inhibitors is represented in *Figure 55*. This model calculates an approximation of the corrosion inhibition due to the adsorption of chemical compounds present in crude oil onto the metal surface. This model proved to be quite accurate for the only crude oil tested. More experiments are needed to validate the model. In order to calculate the real corrosion rate of a steel pipeline under oil-water flow, a good understanding of the flow pattern is needed. This is discussed in Chapter 4.

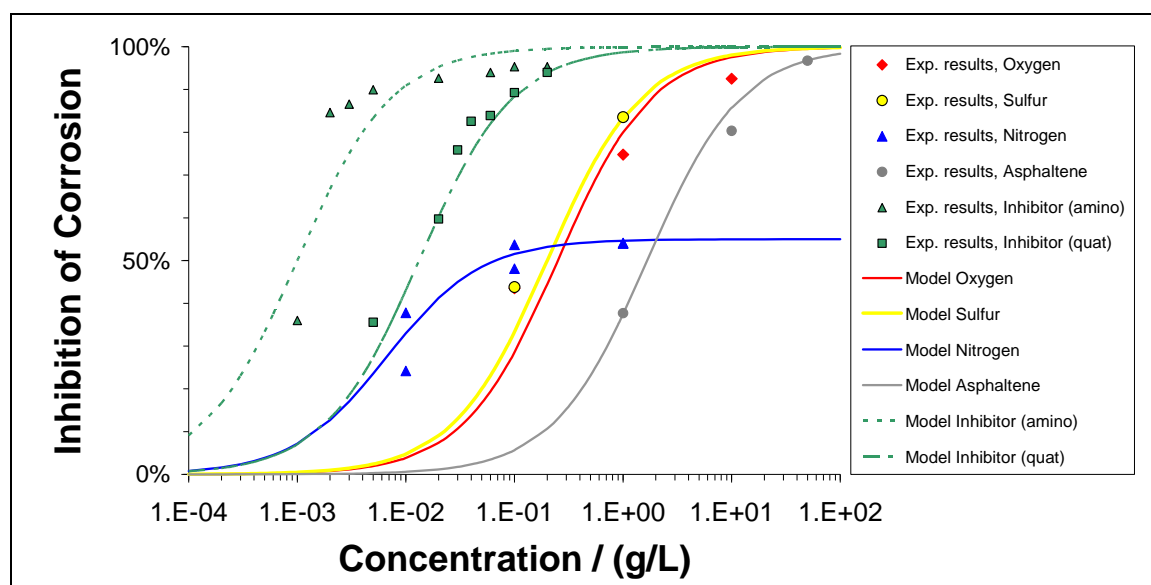


Figure 55. Comparison between inhibitions of corrosion calculated and measured for oxygen, sulfur, nitrogen containing compounds, asphaltenes and corrosion inhibitors.

CHAPTER 4 CRUDE OIL CHEMISTRY EFFECTS ON PHASE WETTING

Introduction

The previous section has shown that some of crude oil's naturally occurring surface active compounds have a great impact on corrosion. However, crude oil's naturally occurring surface active compounds impact corrosion in an additional manner, by changing the steel's wettability properties. Knowing which phase wets the pipe (oil or water) is fundamental for prediction of corrosion rates. While corrosion can be high when water wets the pipe, corrosion is slow or even non-existent when the pipe is wet by oil.

To understand which phase wets the pipe, it is important to understand two phenomena. First we need to understand flow patterns to know where the water and oil phases are in the pipe. If turbulence of the flow is intense and water content is low, then water is entrained. Thus, water is pushed away from the pipe wall. There is no corrosion in such conditions. This is the focus of part 1 of the study presented below. However, if the turbulence is low and the water is settled on the bottom of the pipe, steel wettability becomes the most important parameter. In such conditions, hydrophilic steel will corrode while hydrophobic steel will corrode less. Steel wettability is the focus of part 2. Finally, part 3 present the results obtained in dynamic conditions where there is a synergy between flow pattern and steel wettability.

Part 1 - Study of flow pattern

Introduction

The wetting of the internal surface of the pipe depends on what happens both at the steel surface and in the bulk (flow effect). If the turbulence of the oil phase is strong enough to break the water phase into droplets and entrain them in the flow, the water droplets theoretically never touch the pipe wall. This condition can be predicted by a combined set

of three equations (Equation 35) called the water wetting model. When the condition described by Equation 35 is satisfied, the model predicts that the water phase flows as droplets in a continuous oil phase. The pipe is therefore free from corrosion.

$$2.22 \cdot D \cdot \left(\frac{\rho_o u_o^2 D}{\sigma} \right)^{-0.6} \left(\frac{\varepsilon_w}{\varepsilon_o} \right)^{0.6} \left(\frac{\rho_m}{\rho_o} \cdot \frac{1}{\varepsilon_o} \cdot f \right)^{-0.4} < \min \left\{ \begin{array}{l} \frac{3}{8} \cdot \frac{\rho_o}{\Delta \rho} \cdot \frac{f \cdot u_m^2}{g \cdot \cos \beta} \\ 0.632 \cdot \sqrt{\frac{\sigma}{(\rho_w - \rho_o) \cdot \cos \beta' \cdot g}} \end{array} \right\}$$

Equation 35

The prediction of the model depends on hydrodynamic parameters such as oil velocity u_o , water velocity u_w , water cut ε_w , density of the oil ρ_o , inclination β and size D of the pipe and also on the oil-water interfacial tension σ . The crude oil chemistry does not have a direct effect on hydrodynamic parameters but it can change the oil-water interfacial tension. Polar compounds have a hydrophilic head attached to a hydrophobic tail as shown on Figure 56. The head tends to be in the aqueous phase while the tail resides in the oil phase. The accumulation of such polar compounds at the oil-water interface decreases the oil-water interfacial tension⁷⁵.

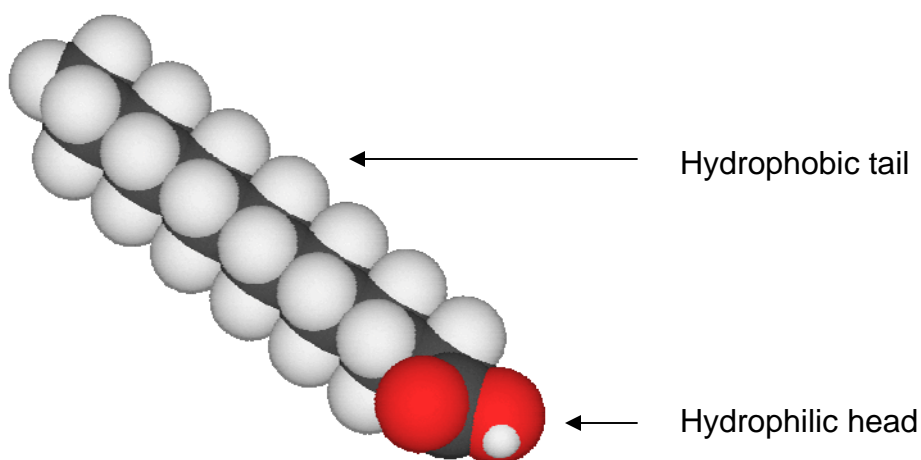


Figure 56. Representation of a polar molecule with a hydrophilic head group and hydrophobic tail, C14 chain organic acid: myristic acid.

The oil-water interfacial tension is a key parameter in the breaking process of the water phase into entrained droplets by the turbulence of the oil phase. Strong oil-water interfacial tension makes it more difficult for the turbulence to break the water phase into droplets. Therefore, it is easier to obtain a stratified flow, which can be corrosive since water is then in direct contact with the pipe wall.

The hydrophilic head of the polar molecule is attracted by the water phase, while the hydrophobic tail has affinity for the oil phase. Consequently, the concentration of polar compounds is at its maximum at the oil-water interface and the interfacial tension decreases. The effect of this decrease of interfacial tension (as shown by the water wetting model) is good from a corrosion point of view: the water phase becomes easier to entrain.

Experimental technique: Tensiometer

To determine the effect of surface active compounds on the flow pattern and consequently on corrosion, interfacial oil-water tension was measured with a platinum ring tensiometer showed in *Figure 57*. Surface active compounds were added to 1 L of model oil. The oil and water were mixed together in a beaker for 1 hour and then left to settle overnight to equilibrate prior to testing.



Figure 57. Platinum ring tensiometer used in these experiments.

Table 12. *Oil-water interfacial tension testing*

Oil phase	Model Oil + polar compound
Water phase	Water + 1 wt.% sodium chloride, pH 5.0
Water cut	20 %
Temperature	25 °C
Pressure	0.13 MPa

Experimental results

Table 13 shows the results obtained with the tensiometer. All chemicals were added to the oil phase, except acetic acid, which was added to the water phase because of the low solubility of acetic acid as a monomer in model oil.

Table 13. Evolution of the oil-water interfacial tension function of the polar compound added to the oil phase (exception: acetic acid)

CHEMICAL CLASS	CHEMICAL COMPOUND	CONCENTRATION	OIL-WATER INTERFCIAL TENSION / dyne-cm ⁻¹		
			Mean	Min	Max
BASE LINE	Model Oil	Pure model oil	38	37	40
AROMATICS	Naphthalene	40 wt. %	40	38	41
OXYGEN COMPOUNDS	Acetic Acid (added to the water phase)	10 ppm	30	29	31
		100 ppm	30	29	31
		1000 ppm	30	29	31
	Myristic Acid	0.1 wt. %	28	27	29
		1 wt. %	24	24	25
	TCI	0.1 wt. %	27	27	28
1 wt. %		18	17	20	
SULFUR COMPOUNDS	Dibenzothiophene	0.1 wt. %	34	34	35
		1 wt. %	30	29	31
	Dioctyl sulfide	0.1 wt. %	36	35	37
		1 wt. %	31	29	32
	Tetradecanethiol	0.1 wt. %	36	34	38
		1 wt. %	35	33	37
NITROGEN COMPOUNDS	Carbazole	0.1 wt. %	39	38	40
		1 wt. %	39	37	40
	Acridine	0.1 wt. %	40	38	41
		1 wt. %	39	38	40

It is interesting to notice from the results presented above that all polar compounds decrease the oil-water interfacial tension. If carbazole and acridine slightly increase the oil-water interfacial tension, it is because they were tested in model oil with 40 wt.% tetrahydronaphthalene. As explained in the previous chapter, this was done because of poor solubility properties. The highest oil-water interfacial tension change is measured for long chain organic acids. 0.1 wt.% and 1 wt.% of myristic acid decreases the oil-water interfacial tension by 26% and 37% respectively. TCI is able to decrease the oil-water interfacial tension even more, 0.1 wt.% and 1 wt.% of TCI decrease the oil-water interfacial tension by 29% and 53% respectively. Such decreases in the oil-water interfacial tension are significant. However, a large change in the oil-water interfacial tension is necessary to “improve” the flow pattern as the Figure below shows. *Figure 58* was calculated using the water wetting model (Equation 35) and the value of the oil with TCI-water interfacial tension measured.

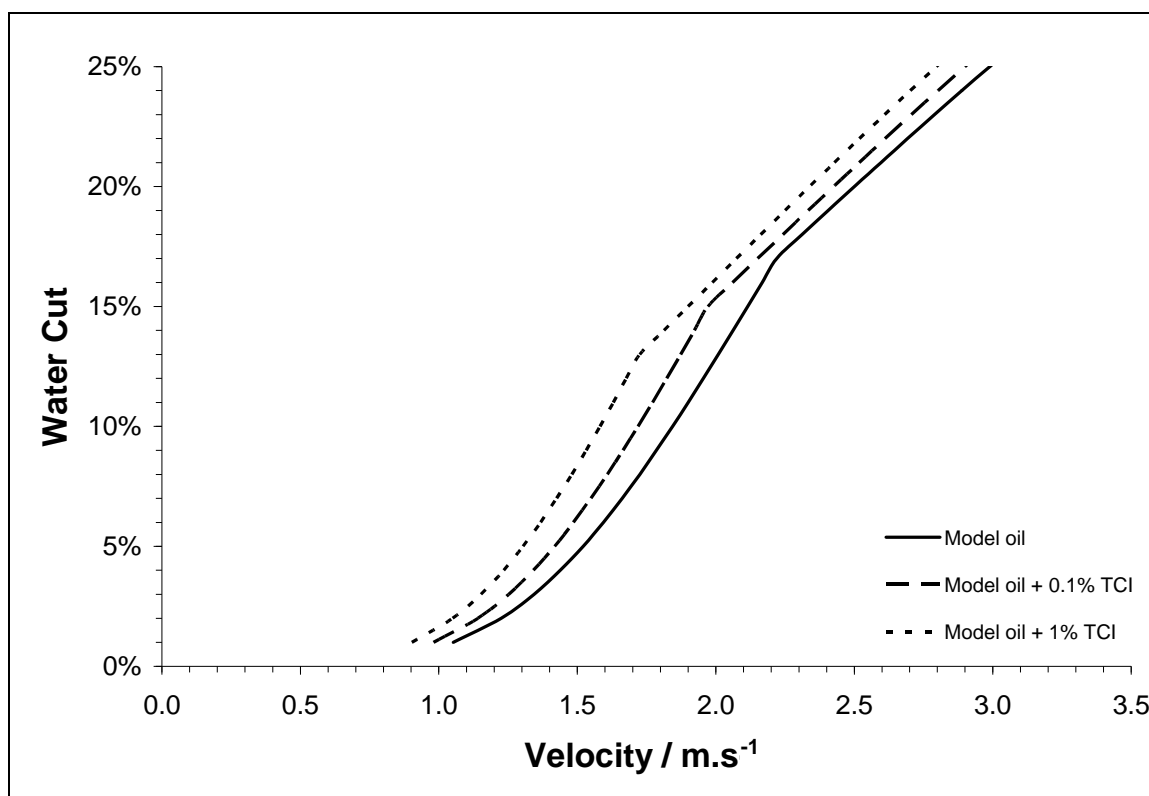


Figure 58. Evolution of the transition line calculated using the water wetting model for three concentrations of TCI added to model oil (0 wt.%, 0.1 wt.% and 1 wt.%).

Discussion

The effect of polar compounds on the oil-water interfacial tension has been studied in the past⁷⁶⁻⁷⁸. However, the relationship between oil-water interfacial tension and phase wetting is a new connection. Studies on crude oil-water interfacial tension are usually connected to reservoir studies on oil recovery and emulsification not corrosion in oil-water flow.

Varadaraj *et al.* concluded in his study of emulsification that naphthenic acids having a molecular weight in the range of 250-425 g·mol⁻¹ are the principal contributors on the oil-water interfacial tension effects⁷⁶. In consequence, a higher impact on the oil-water interfacial drop can be expected than the effect measured on myristic acid and TCI. Adamson used Gibbs sorption equation⁷⁷ (Equation 46) to calculate the decrease of the oil-water interfacial tension $d(\sigma_{o/w})$ as a function of the log of the concentration of naphthenic acids C_{naph} .

$$d(\sigma_{o/w}) = -2.303 \cdot \Gamma \cdot RT \cdot d \log(C_{naph}) \quad \text{Equation 46}$$

Where Γ is the surface excess of naphthenic acids, R is the universal gas constant (8.314 J·mol⁻¹·K⁻¹) and T is the temperature in Kelvin. Moreover, he concluded that the heteroatom such as oxygen and nitrogen on large asphaltene macromolecules have an effect on the oil-water interfacial tension. Asphaltenes were not a part of the test matrix in this research, more experiments should be done to study the effect of asphaltenes on oil-water interfacial tension. It would be useful to test the effect of asphaltenes on the oil-water interfacial tension in order to predict more accurately the effect of crude oil's polar compounds on multiphase flow.

The same approach as Varadaraj was used by Lord⁷⁸. In his experiments pH had a great effect on the oil-water interfacial tension. All the measurements done in this research are

done at pH 5.0. It would be useful to test the effect of myristic acid at pH 3.0, 4.0, and 6.0 to predict more accurately the effect of organic acid on multiphase flow.

Finally, all the experiments presented above give equilibrium values of the oil-water interfacial tension. Xu, in his study of dynamic interfacial tension, proved that dynamic interfacial tension may differ from interfacial tension by “more than a factor of 10”⁷⁹. He introduced a new method called “drop volume” to measure dynamic oil-water interfacial tensions.

Conclusion

Experiments showed that, if the compound tested, the only ones that had a strong effect on the oil-water interfacial tension are naphthenic acids. However, these changes translate into relatively small changes in the predicted flow pattern. Larger naphthenic acid molecules and asphaltenes should be tested in the future to see if the effect found is larger than the one presented here, otherwise the effect of crude oil’s chemicals on flow regime as related to water wetting should be considered as a second order effect. The next section of this study will focus on the other aspect of phase wetting: what happens at the metal surface, *i.e.* the steel wettability.

Part 2 - Study of steel wettability

Introduction

The first effect of oil chemicals on wettability was related to the flow pattern. The second effect described here is related to steel wettability. This part focuses on what happens on the metal surface. Knowing which phase is more attracted to the steel surface is important in order to predict wetting properties and corrosion rates accurately. The adsorption at the metal surface of hydrophobic chemicals can change steel surface properties. Steel is hydrophilic in nature, but could become hydrophobic. This situation is best described in terms of Young’s equation:

$$\psi = -\sigma_{o/w} \cos \theta = \sigma_{s/o} - \sigma_{s/w} \quad \text{Equation 47}$$

The contact angle of a water droplet on a steel surface immersed in oil is a representation of the interaction of the interfacial forces steel-oil ($\sigma_{s/o}$) and steel-water ($\sigma_{s/w}$). If the contact angle is larger than 90° the affinity of the steel for water ($\sigma_{s/w}$) is stronger than the affinity of the steel for oil ($\sigma_{s/o}$) and *vice versa*.

Therefore, the measurement of the contact angle of a water droplet on a steel surface immersed in oil tainted with chemical compounds will show the effect of these chemical compounds on the steel wettability.

Experimental technique: Static contact angle measurement

The wettability test procedure is as follows. One percent by weight of surface active compound is added to 1 L of model oil. The oil phase (model oil, 800 mL) and water phase (200 mL) are mixed together in a beaker for 1 hour, then left to settle overnight to equilibrate. A flat carbon steel coupon is cleaned with acetone and polished sequentially with 400 and 600 grit sandpaper, then further cleaned with isopropanol in an ultrasonic bath for 2 minutes. The coupon is then dried and immersed in the model oil in the setup shown in *Figure 59*. A droplet of water is then added on the top of the coupon. A video recording of the evolution of the droplet at the metal surface is taken over 10 minutes, allowing for the measurement of the water droplet-steel surface's contact angle as a function of time.

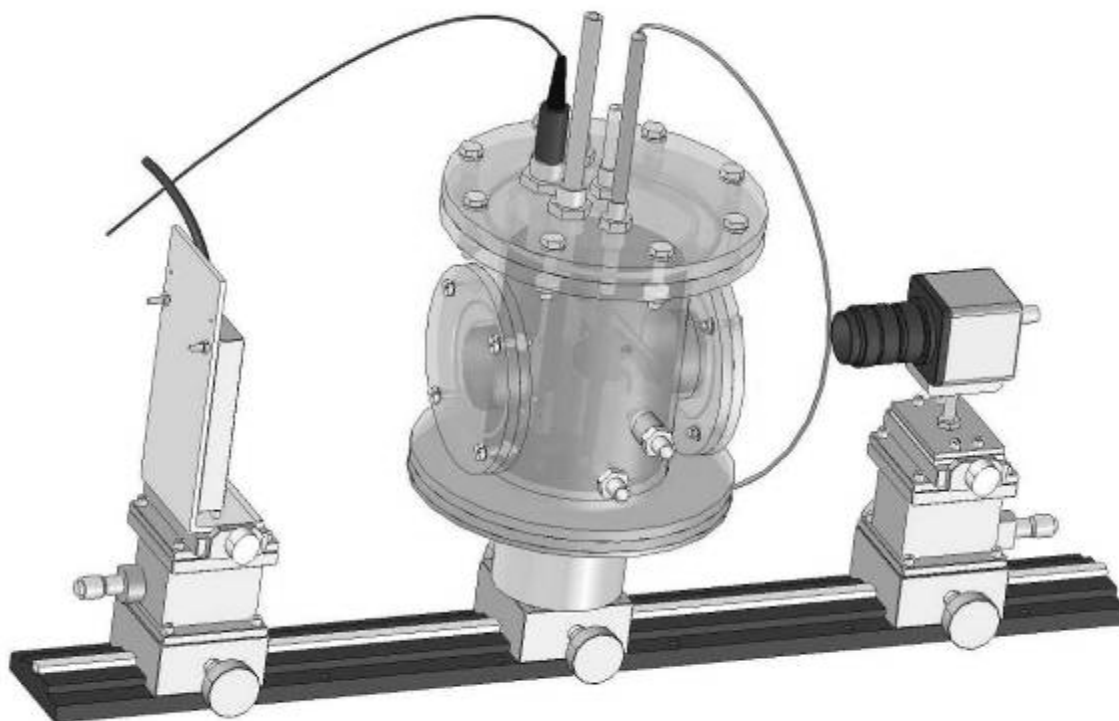


Figure 59. Drawing of the contact angle measurement setup⁸⁰, the cell is made of acrylic to allow the camera on the right to video.

As the roughness of the metal surface is important in contact angle study, a picture of the metal surface is shown in *Figure 60*. The picture⁸⁰ was taken with an infinite focus microscope, and gives the roughness of the sample about: 1.1 μm .



Figure 60. 3D picture of the metal surface after polishing with 600 grit sandpaper, roughness: 1.1 μm .

Table 14. *Static contact angle measurements test matrix*

Oil phase	Model Oil + polar compound
Water phase	Water + 1 wt.% sodium chloride pH 5.0
Water cut	20%
Temperature	25°C
Pressure	0.13 MPa

Experimental results

The baseline experiment was done with model oil and a pure water droplet: When a spherical water droplet touches a flat steel surface the water-steel contact angle is 180°. Interfacial forces act and the water droplet spreads across the steel surface displacing the oil. Therefore the contact angle decreases as a function of time. *Figure 61* shows the evolution of a water droplet in model oil during the first 10 minutes. The final water-steel contact angle is 58°.

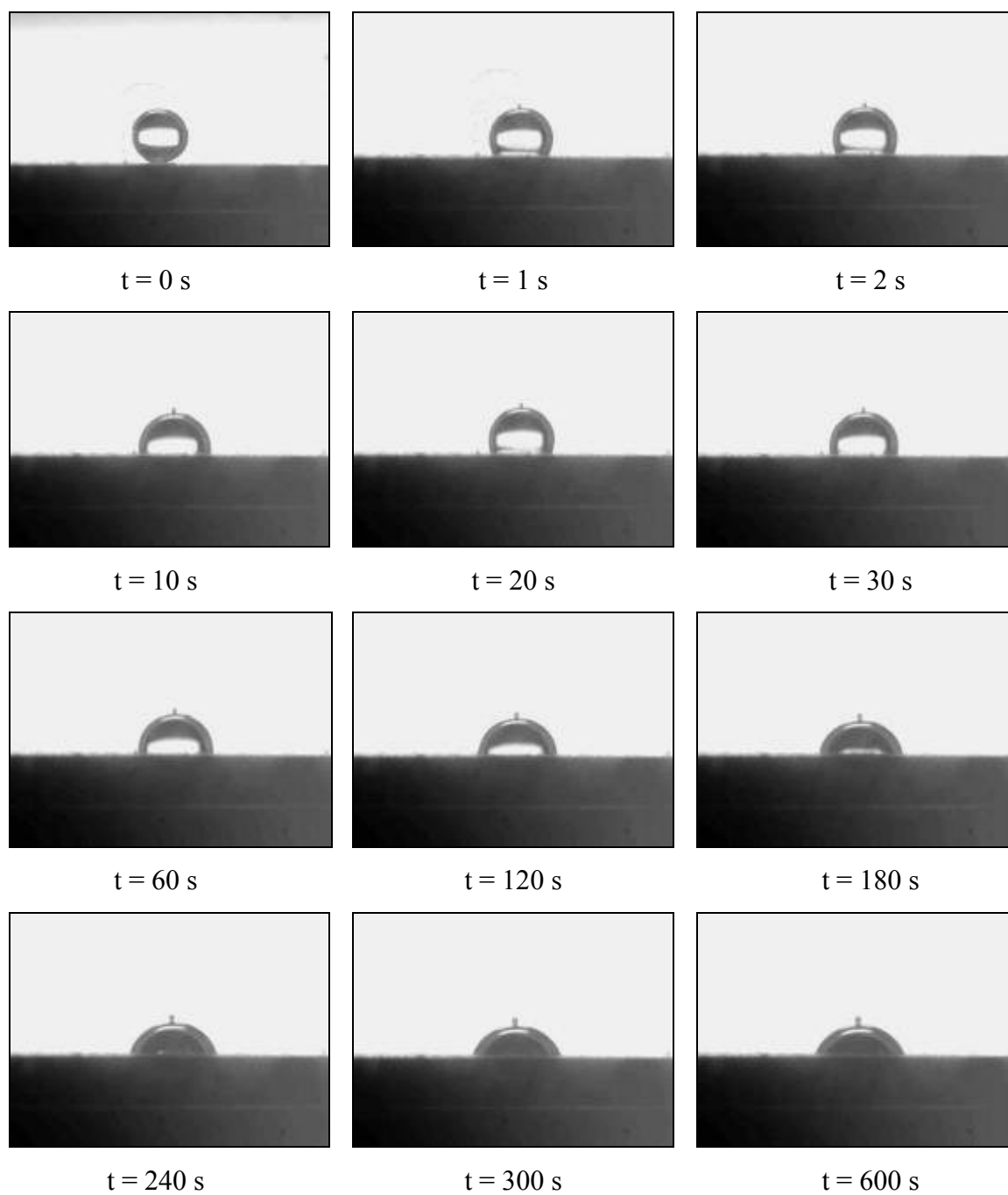


Figure 61. Evolution of a water droplet in model oil during the first 10 minutes as the contact angle evolves from 180° to 58° .

The same experiment was repeated with surface active compounds added to the oil phase. Heuristically, the chemicals that are able to have an effect on corrosion would be expected to have a similar effect on the steel wettability. Table 15 shows the water-steel contact angle after 5 minutes and after 2 hours for the chemicals used in this study (as in the case of the inhibition testing, the nitrogen compounds were tested in the modified model oil that contained 40 wt.% tetrahydronaphthalene in LVT-200).

Table 15. *Contact angle measurements*

CHEMICAL CLASS	CHEMICAL COMPOUND	Concentration added to the oil phase	Contact angle after 5 min	Contact angle after 10 min
BASE LINE	Model Oil	Pure	58°	58°
AROMATICS	Naphthalene	40 wt.%	130°	60°
OXYGEN COMPOUNDS	Acetic Acid (added to the water phase)	10 ppm	54°	53°
		100 ppm	62°	60°
		1000 ppm	60°	60°
	Myristic Acid	0.1 wt.%	180°	180°
		1 wt.%	180°	180°
	TCI	0.1 wt.%	176°	176°
		1 wt.%	180°	180°
	SULFUR COMPOUNDS	Dibenzothio- phene	0.1 wt.%	52°
1 wt.%			48°	48°
Dioctyl sulfide		0.1 wt.%	55°	56°
		1 wt.%	97°	84°
Tetradecane- thiol		0.1 wt.%	79°	72°
		1 wt.%	104°	95°
NITROGEN COMPOUNDS	Carbazole	0.1 wt.%	130°	78°
		1 wt.%	100°	90°
	Acridine	0.01 wt.%	127°	75°
		0.1 wt.%	135°	97°

For more clarity, the results shown in Table 15 are plotted on *Figure 62* and *Figure 63*.

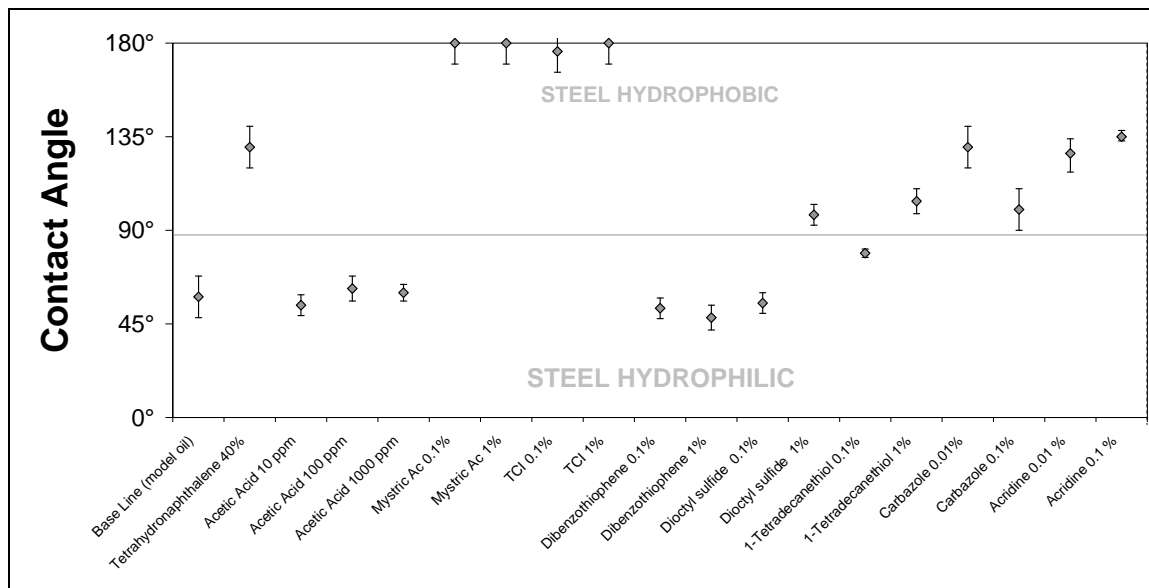


Figure 62. Water-Steel contact angle after 5 minutes. Organic acids have the strongest effect on steel wettability.

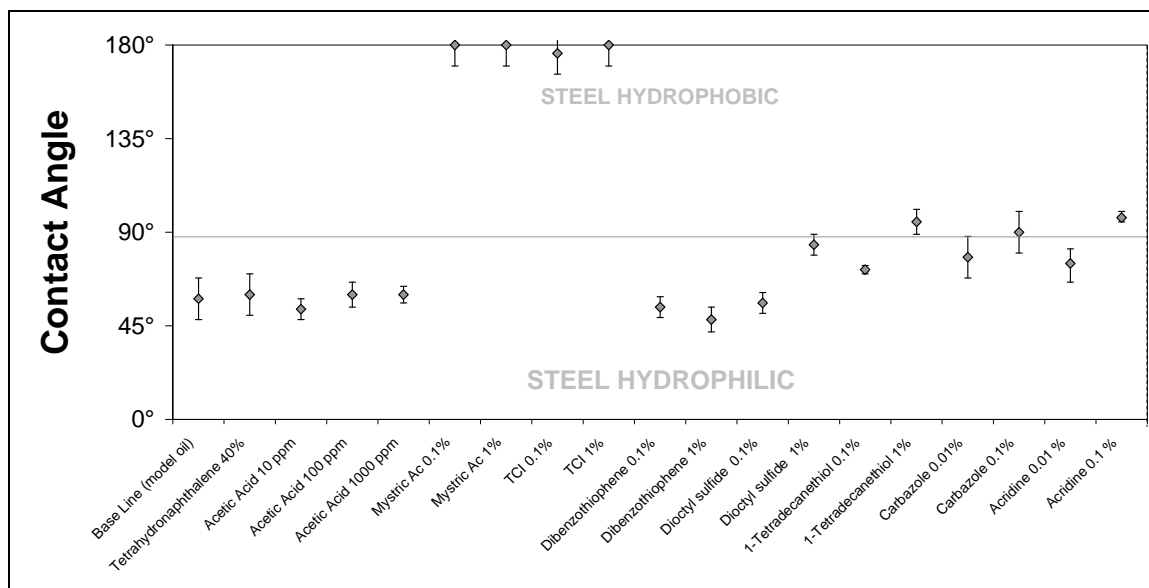


Figure 63. Water-Steel contact angle after 120 minutes. Organic acid effect on steel wettability is not time dependent.

Aromatic compounds

The contact angle water-steel remained at 180° (steel hydrophobic) for more than 30 seconds then started to decrease. It reached 130° after 5 minutes and then a stable value of about 60° in less than 2 hours (the steel surface becoming hydrophilic under 90°). Even though the final contact angle is the same as the one obtained with model oil, the time needed to reach the final value is much longer. In this experiment, it seems that the aromatics are adsorbed onto the metal surface and the water phase slowly displaces the adsorbed oil phase. This explains why no effects related to aromatics were found in the corrosion measurements: in the corrosion measurements, steel was pre-wetted with water. In such conditions, aromatics can not displace the water layer. In the wettability experiments, steel is pre-wetted with model oil. In such conditions, it takes time for the water phase to replace the aromatics adsorbed onto the metal surface. It should be noticed that aromatics adsorb onto iron using π -interactions, which are very weak.

In consequence, the oil layer is displaced more rapidly when the oil is free of aromatics. Even though the final value of the contact angle is the same, the effect of aromatics must not be neglected, particularly in intermittent oil-water flow. When a water droplet touches the pipe wall, this droplet either wets the pipe or rebounds from it. Without compounds added to the model oil the water immediately wets steel, while when aromatics are added to the oil phase water droplets can bounce off the surface without wetting it. This effect can strongly limit the corrosiveness of dispersed oil-water flow.

Oxygen containing compounds

Low molecular weight organic acids do not have an effect on steel wettability. However, the strongest effect is found with the high molecular weight organic acids. While steel is naturally hydrophilic, once it is wet with model oil and myristic acid or naphthenic acids, steel becomes completely hydrophobic. Even after a long period of time, the water droplet touching the steel surface never wetted it. The contact angle never decreased below 180°.

The effect of naphthenic acids on wettability is even stronger than the effect of aromatics. It is possible to conclude that if a pipe wall is pre-wetted with oil containing naphthenic acids, dispersed water droplets in the oil flow are not going to be corrosive as they cannot easily wet the pipe wall.

Sulfur containing compounds

The effect on wettability is weaker than for the organic acids. Dibenzothiophene and dioctyl sulfide do not change the steel wettability. Even tetradecanethiol, which is a good corrosion inhibitor, is only able to change the contact angle from 58° to 95°. Although it is a significant change in the wettability of the steel, this change of contact angle is not sufficient to affect the wettability and reduce corrosion significantly on its own. Once a water droplet wets the pipe, corrosion happens irrespectively of the water-steel contact angle.

Nitrogen containing compounds

Nitrogen containing compounds were tested using the modified model oil with 40 wt.% tetrahydronaphthalene. No significant effect on the steel wettability is found for the nitrogen containing compounds. It is possible that the strong effect of the oil aromaticity (tetrahydronaphthalene) is masking the effect of the nitrogen containing compounds.

Discussion

Hoeiland *et al.*⁸¹ and Kowalewski *et al.*¹⁹ in their respective studies of wettability alteration found similar results as the one shown above. Dubey and Doe⁸² found similar results in their tests of real crude oils. Even though the research focuses on reservoir recovery, and therefore on silica as a surface, this confirms that polar compounds are effective in changing surface wettability properties.

However, Anderson⁸³ studied the effect of polar compounds on reservoir wettability and concluded that “wettability alteration is determined by the interaction of the oil constituent, the mineral surface and the brine chemistry, including ionic composition and pH”. Yang *et al.*⁸⁴ and Drummond and Israelchvili²⁹ showed evolution of silica wettability as a function of pH and salt concentration. Since the experiments presented above have been done at 1 wt.% NaCl and pH 5.0 only, it would be interesting to repeat some of these experiments with different salt concentrations and pH.

Conclusion

The study of steel wettability demonstrated very interesting results. Some of the surface active compounds tested such as long-chain carboxylic acids were able to significantly alter steel wettability. Interestingly, the change of wettability recorded was always in the favorable direction (from a corrosion point of view) because steel changed from hydrophilic towards hydrophobic. In the case of organic acids, hydrophilic steel became completely hydrophobic. The next part of this study will focus on the synergy between flow pattern and steel wettability, when both effects happen simultaneously in a pipe.

Part 3 – Study of the synergy between steel wettability and flow pattern

Introduction

In oil-water flow, the phase that is wetting the pipe wall depends on steel wettability as well as on the flow pattern. The steel wettability under flowing conditions is a complex issue to solve and no mechanistic model encompassing both aspects of the problem had been developed. Experiments were designed to address this problem. The most accurate experimental setup used to study wettability under dynamic conditions would be one which is as close as possible to actual field conditions. Therefore a large flow loop has been developed at the ICMT at Ohio University to perform this task. However, large scale experiments are expensive and time consuming, as a consequence, a small scale setup was developed and tested first, and then the promising data were used to optimize the test matrix for the flow loop experiments.

Experimental technique

Small scale: Doughnut cell

Dynamic phase wetting experiments were conducted in an apparatus designed by Li⁶⁶. The apparatus is represented on *Figure 64* and *Figure 65*. It has a circular channel flow. The effect of one surface active compound on phase wetting in flowing conditions can be observed using visual observation and conductivity probes. About 160 conductivity probes are set flush on the bottom of the channel. One probe is shown in *Figure 66*.

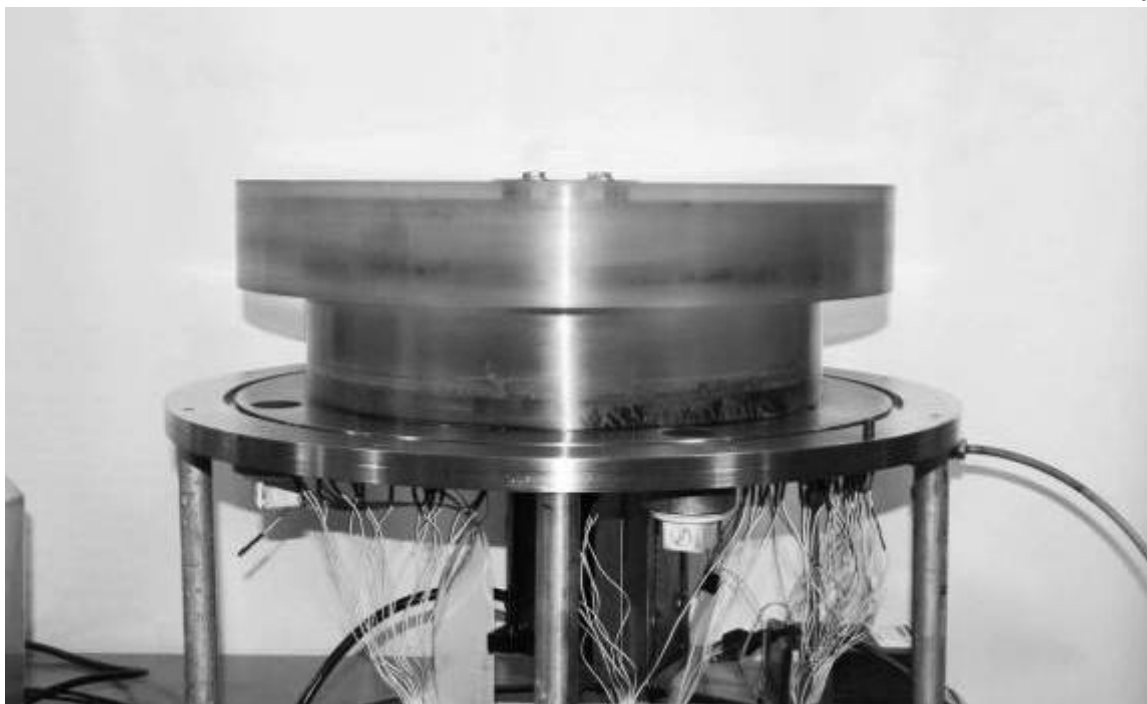


Figure 64. Phase wetting experiment apparatus called the 'doughnut cell'.

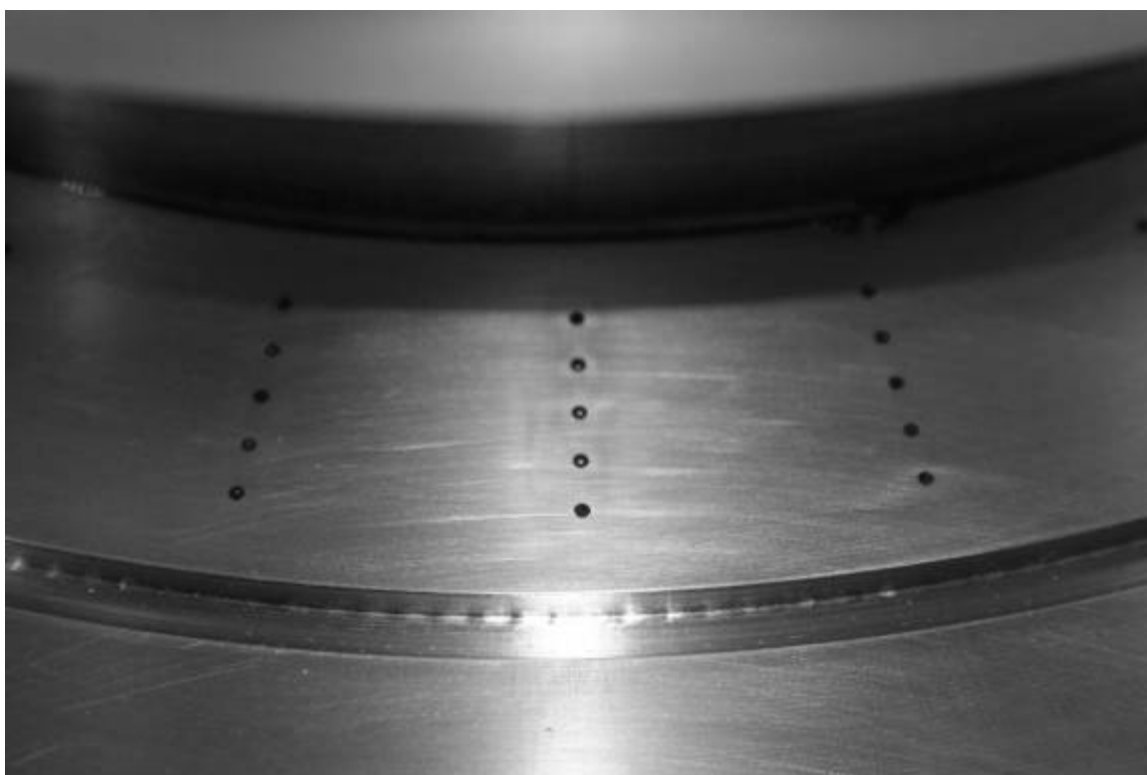


Figure 65. The bottom of the doughnut cell shows conductivity probes.



Figure 66. One conductivity probe, 160 conductivity probes are used in the doughnut cell.

Table 16. Doughnut cell test matrix

Oil phase	Model Oil + polar compound
Water phase	Water + 1 wt.% sodium chloride pH 5.0
Superficial water velocity	0.5 to 1.5 m·s ⁻¹
Water cut	2 to 20 %
Doughnut diameter	50 cm
Chancel size	3 cm wide 8 cm high
Inclination	Horizontal
Temperature	25°C
Pressure	0.13 MPa

Large scale: Flow loop

Experiments were also conducted in a 60 m long; 10 cm (4 inch) diameter fully inclinable flow loop. The flow loop is specially designed for phase wetting determination in 2 phase or 3 phase flow. *Figure 67* shows the schematic of the flow loop, and *Figure 68* and *Figure 69* show pictures of the flow loop in the horizontal and 15° position respectively.

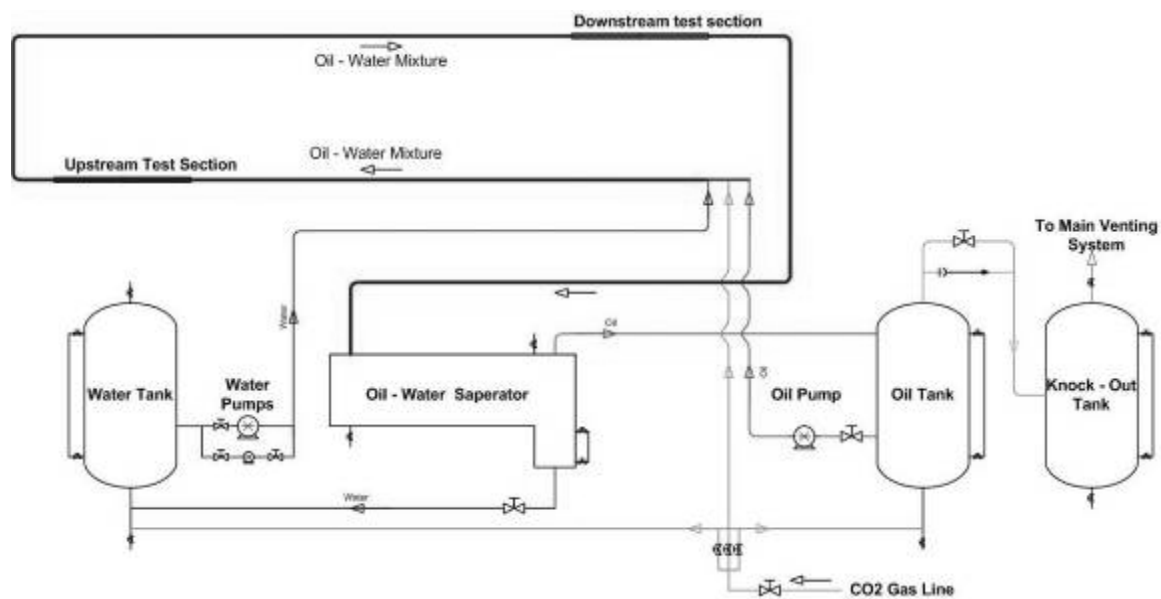


Figure 67. Schematic of the flow loop.



Figure 68. Picture of the flow loop in horizontal position.



Figure 69. Picture of the flow loop in 15° position.

Oil is stored in a 1.2 m³ stainless steel tank and pumped by a positive displacement pump equipped with a variable speed motor. The oil velocity is precisely controlled in a range of 0.5 - 3 ms⁻¹. Water is stored separately from the oil in another 1.2 m³ stainless steel tank. 1 wt.% sodium chloride is added to the water phase in order to increase the conductivity of the water. Two positive displacement pumps enabling both low and high flow rates are used to pump the water through the system. The oil-water mixture is created in a static T-mixer, then flows into a 3 m flexible hose, and into a 14 m straight stainless steel pipe where the flow pattern develops and stabilizes. The mixture then flows through a 2 m long “upstream” test section and a 2 m long transparent pipe, which allows flow visualization. After flowing through two consecutive 90° bends, the mixture goes into a 14 m straight stainless steel pipe where the downstream flow pattern develops and is fully established. The stainless steel pipe section is followed by another 2 m long mild steel “downstream” test section and 2 m long transparent pipe, before entering an oil-water separator. The separator is a cylinder made of carbon steel (0.8 m internal diameter, 4.8 m long). The internal surface of the separator is carefully coated with corrosion resistant epoxy. Separation efficiency was checked during each test, and was close to 100%. Therefore the separated oil goes into the oil tank and the water flows into the water tank. A good separation is needed to control the oil/water ratio of the flow.

It should be noted that in order to minimize the effect of oxygen on corrosion measurements, the system is deoxygenated before each experiment using pure carbon dioxide. The final oxygen concentration is lower than 25 ppb. Also, particular attention was given to the materials used in the flow loop. The flow loop (except the 2 test sections) is free from corrosion, by using non-corrosive materials such as stainless steel, epoxy, or plastic.

The test section is a 2 m long carbon steel pipe spool followed by a 2 m long acrylic pipe. During the experiments the inner wall of the test section corrodes, which leads to an increase of Fe²⁺ ion concentration by CO₂ corrosion. The general corrosion rate is measured by following the increase of Fe²⁺ ion concentration. Five rows of wall

conductance probes, four high frequency impedance probes, one wall sampling port, and an electrical-resistance (ER) probe are installed on the test section as shown in *Figure 70*.

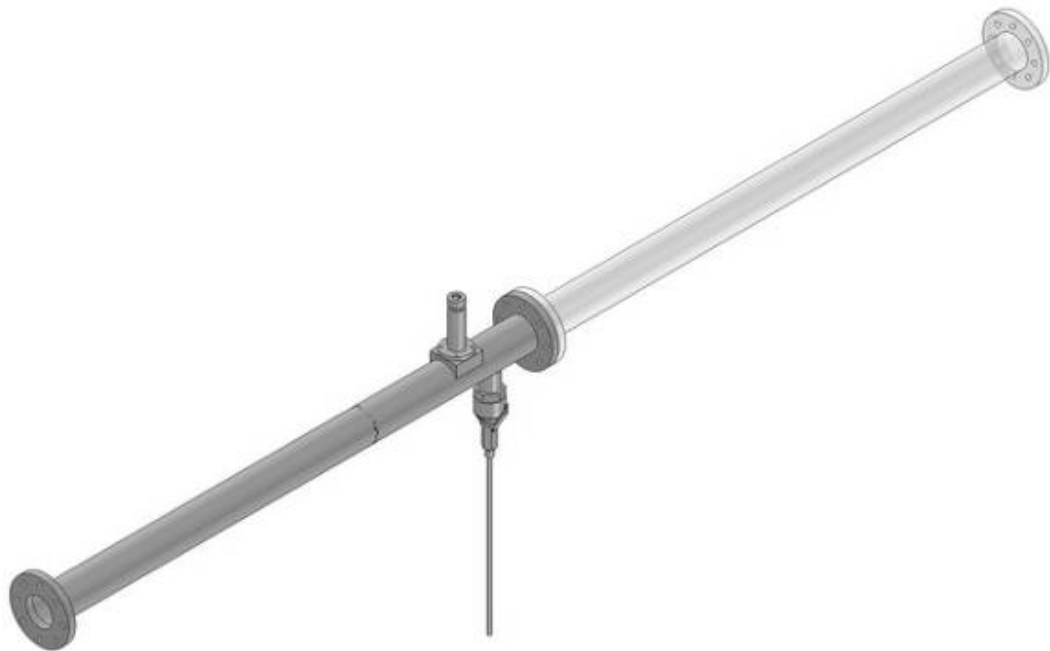


Figure 70. Representation of the test section.

Five rows of conductance probe elements, with a total of 180, form the wall conductance probe. It is used to determine the phase wetting along the circumference of the pipe internal wall. Each probe is flush mounted on the pipe wall. A staggered configuration of wall conductance probes is used to minimize the effect of a particular liquid phase “snaking” around the isolated pinheads leading to erroneous readings. In addition, this special configuration is very useful to determine the phase wetting at the flowing conditions where small droplets randomly impinge the pipe wall surface.

A wall sampling port is used to measure the water/oil ratio close to the pipe surface by extracting the fluid from the bottom of the pipe. It is used to confirm the results of the wall conductance probe. Particular attention was made to avoid erroneous readings by too slow or too fast suction.

An ER probe is used to determine the corrosion rate and, indirectly, the phase wetting condition. The ER probe is mounted on the bottom of the pipe. Corrosion measurements were used to confirm the results obtained by the wall sampling and wall conductance probes.

Finally, the test section is followed by a 2 m long transparent PVC pipe, which allows the visualization of the multiphase flow. Fluorescein sodium salt (10 ppm) is added to the water phase in order to increase the color difference between oil and water. Water appears green under UV light, while oil stays the same dark color. A sample picture is shown in *Figure 71*. Visual observation and recording was conducted only for the “clear” model oil. With real crude oils, flow pattern visual observation is impossible. The overlapping of these four different techniques allows a high degree of confidence in the results described below.

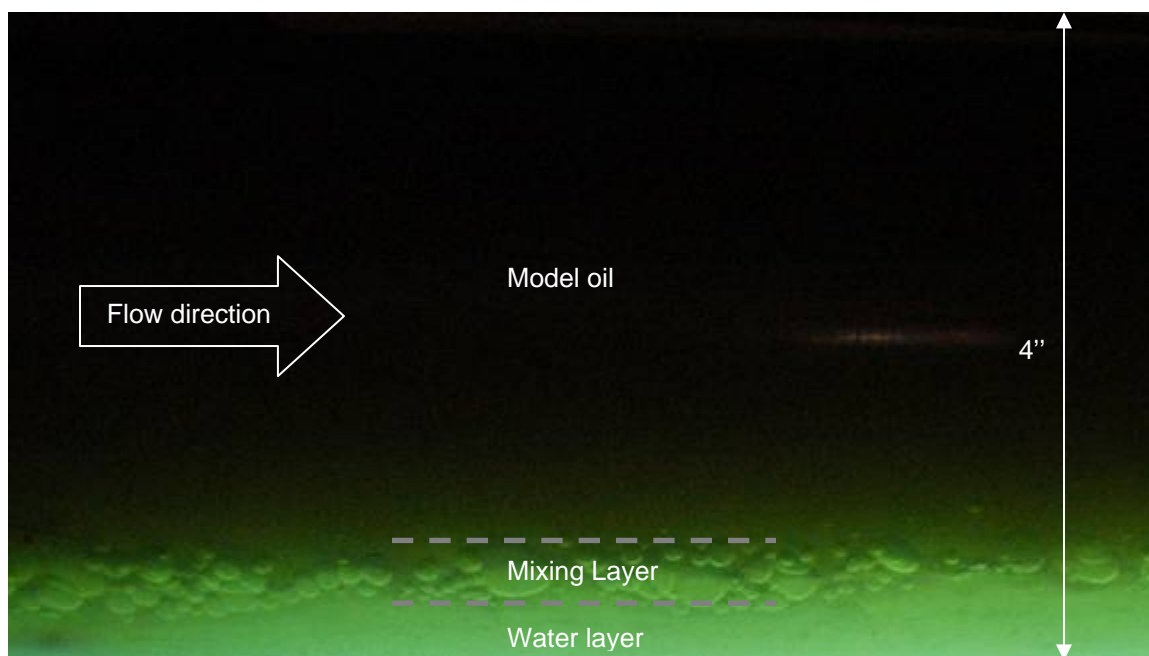


Figure 71. Example of flow visualization picture, water appears green under UV light, oil is black.

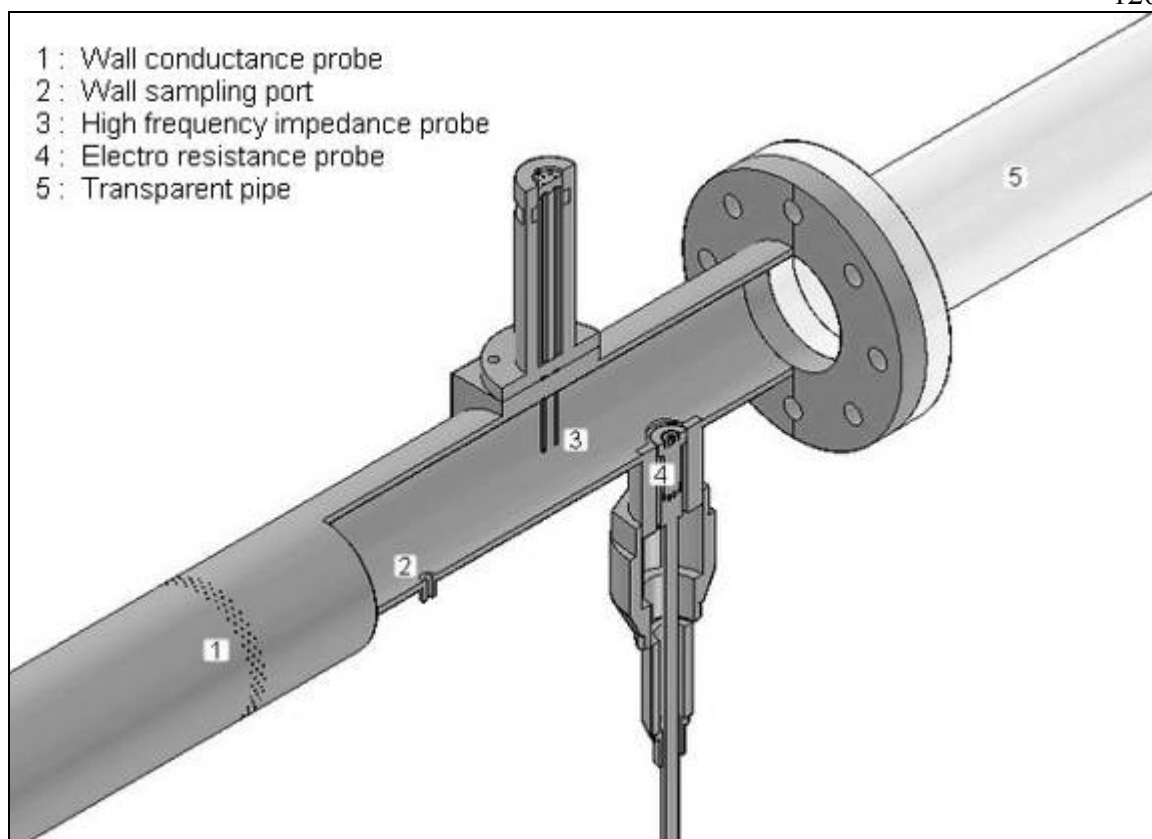


Figure 72. Representation of the instrumentation of the test section.

Experimental results

Small scale results

Model oil and model compound

It was found during previous experiments on the static contact angle that myristic acid has a strong effect on steel wettability. It was reported that steel wet by model oil (LVT-200) is hydrophilic; whereas steel wet by model oil with only 1 percent of myristic acid is completely hydrophobic. However these tests were performed in static conditions. *Figure 73* shows the results obtained testing model oil in dynamic conditions in the doughnut cell. *Figure 74* to *Figure 76* show the results obtained testing myristic acid under the same conditions.

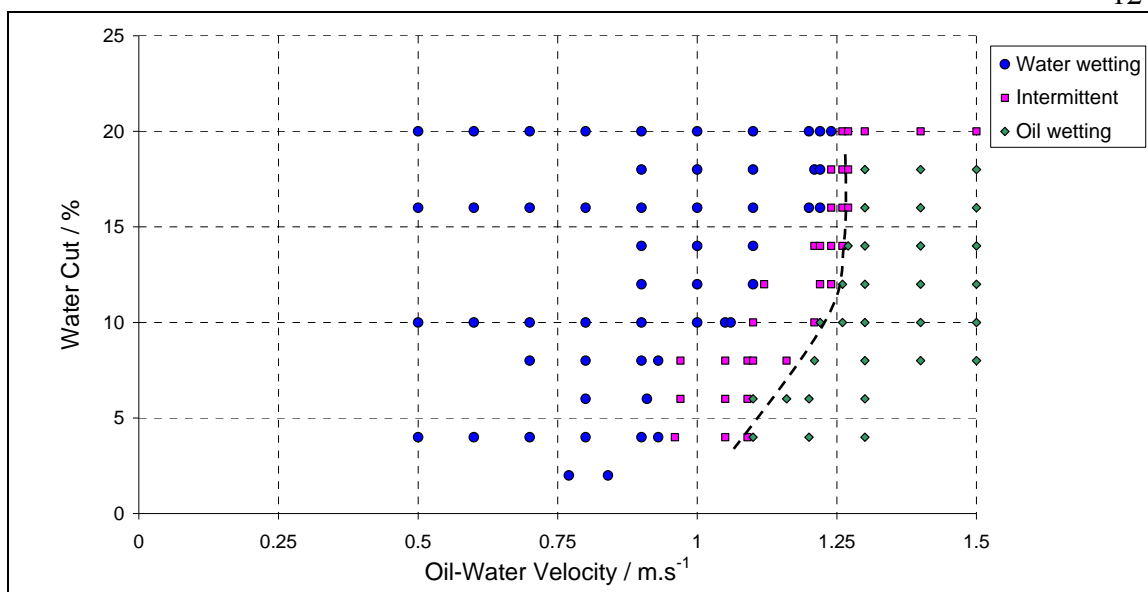


Figure 73. Phase wetting map obtained in a doughnut cell with pure model oil. No chemicals are added to the oil phase. Points are measurements, line is just an indicator separating oil and water wetting regions.

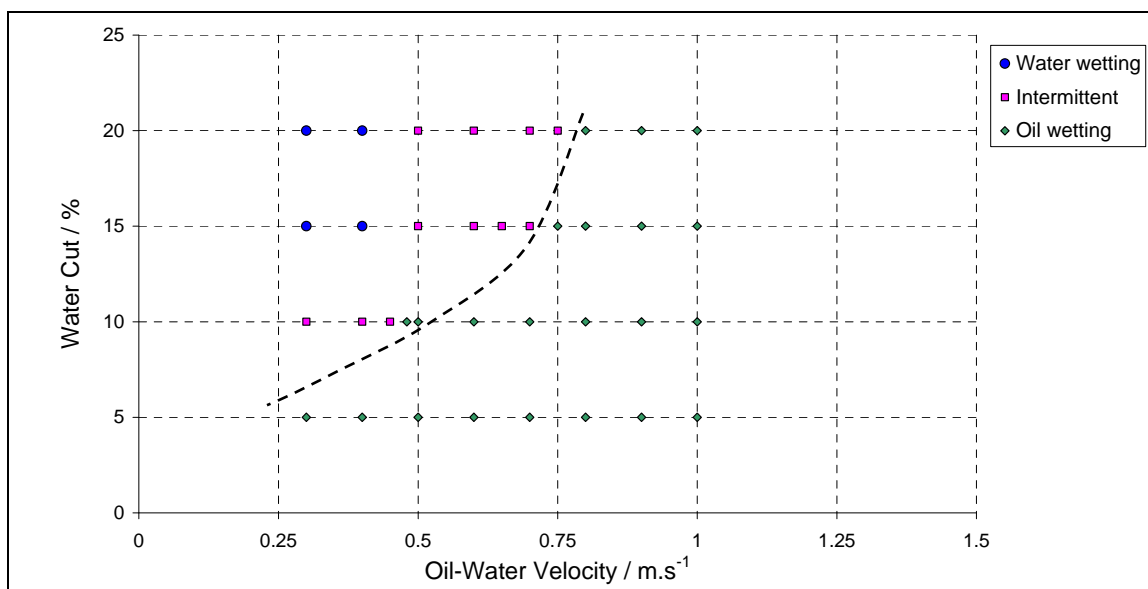


Figure 74. Phase wetting map obtained in a doughnut cell with 0.01 wt.% myristic acid added to the oil phase. Points are measurements, line is just an indicator separating oil and water wetting regions.

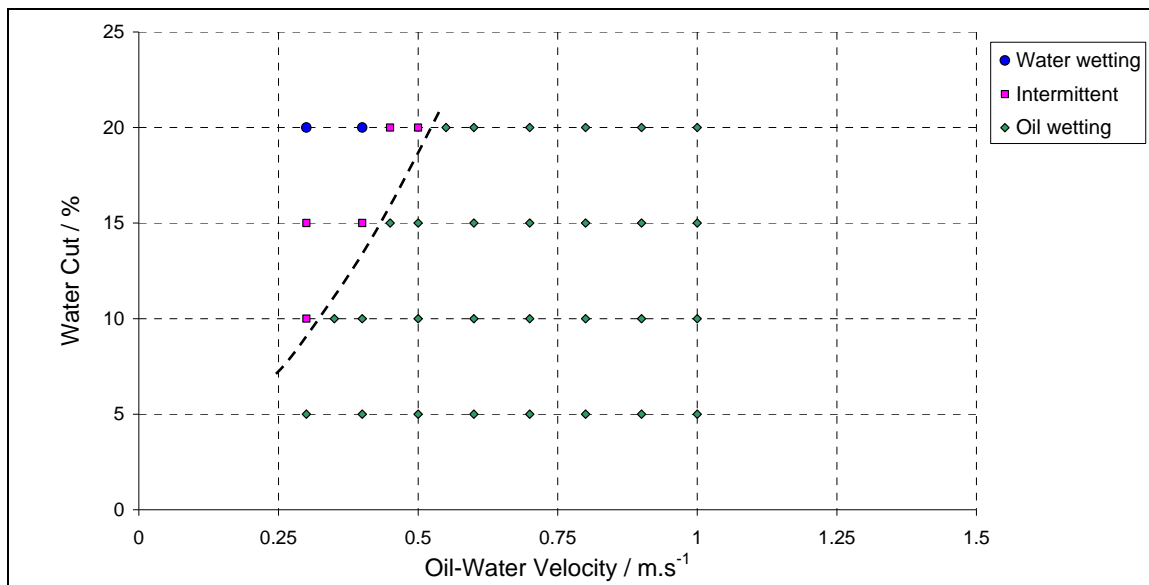


Figure 75. Phase wetting map obtained in a doughnut cell with 0.05 wt.% myristic acid added to the oil phase. Points are measurements, line is just an indicator separating oil and water wetting regions.

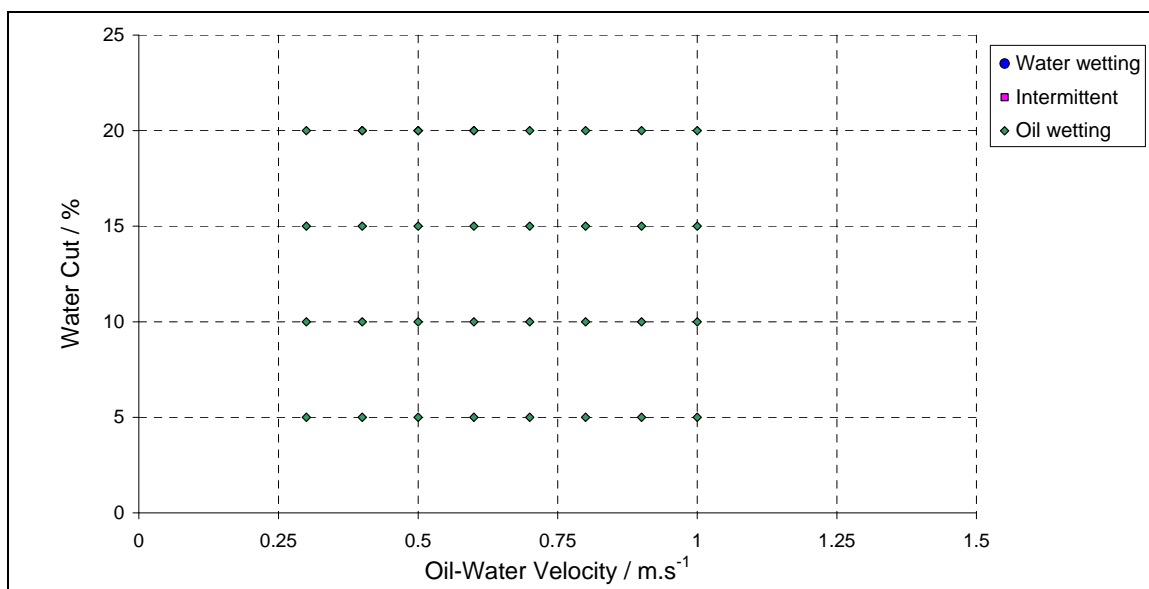


Figure 76. Phase wetting map obtained in a doughnut cell with 0.1 wt.% myristic acid added to the oil phase.

The effect of myristic acid on steel wetting in flowing conditions is as profound as it was in static conditions. Even for very low concentrations of myristic acid, the transition line between “oil wetting” to “intermittent wetting”, where water begins to wet the steel, is shifted to low oil-water velocities. It should be noted that myristic acid does not change the oil-water interfacial tension enough to change the flow pattern, therefore at low velocities water is still on the bottom of the pipe, but a layer of adsorbed oil makes a barrier between the steel and the water layer.

In the same way as in the test with myristic acid, crude oils have been tested in the doughnut cell by Li⁶⁶. Results are shown in *Figure 77*.

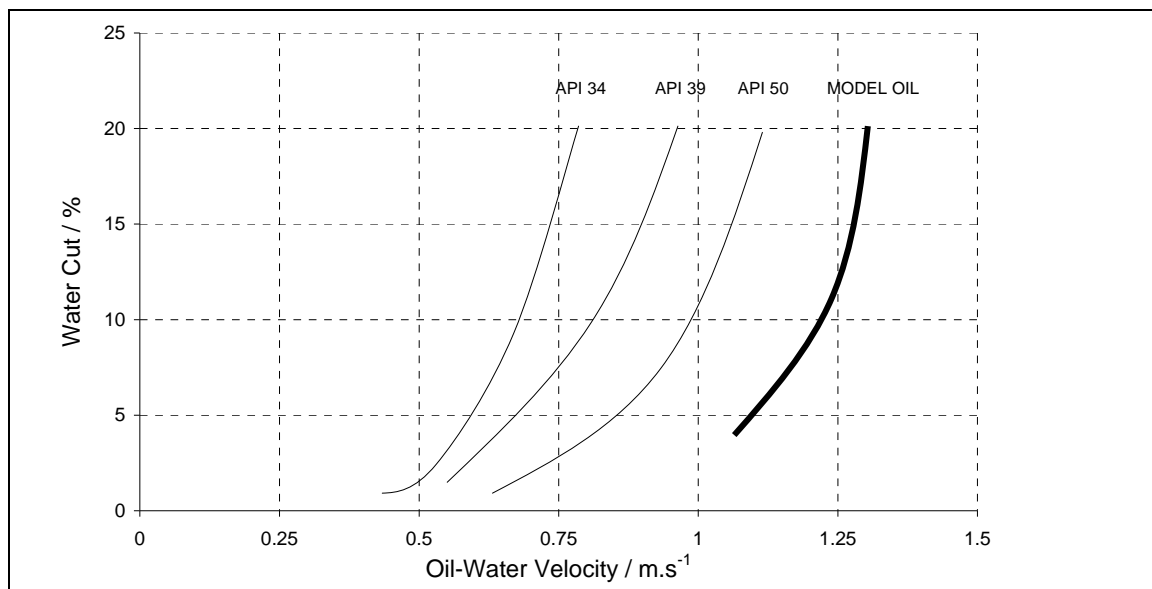


Figure 77. Phase wetting map of Middle Eastern crude oils API 50 to 34. Experiment done by Li⁶⁶.

The naphthenic acid and aromatic concentration of these crude oils from the Middle East are unknown (Saudi crude oils have typically very low TAN number). It is therefore impossible to compare these results with results found with crude oils from a different location.

It is still possible to compare the effect of density on the transition line oil wetting to intermittent wetting because these crude oils should have similar chemical properties since they come from the same field.

Interestingly, increase in crude oil density (API decreases) induced in the results a shift of the transition line to lower oil-water velocity. This means that for the same water cut, the minimum flow velocity needed to entrain the water phase is slower. Also, the “trend” of the transition line is the same, showing that the mechanism of water entrainment has not been changed between crude oils. The trend is also similar to the transition line obtained during the model oil tests, pointing to the same conclusion. These results can be explained by the following. Density increases come from the fact that the concentration of large molecules, such as aromatics and heavy molecular weight naphthenic acids, increase too. According to the results found in part 2, these molecules can coat the surface and change the steel surface from hydrophilic to hydrophobic. It is normal then, that the transition line is shifted to lower oil-water velocities. If steel is hydrophilic, as soon as the first water droplet drops out of the flow, water will wet the pipe. However in these conditions, when the steel is hydrophobic, the first water droplet touching the steel surface will be wiped away by the flow, before interfacial forces bond water to the pipe surface.

These tests were then repeated in a large flow loop in order to determine precisely the minimum velocity needed to disperse and entrain the water phase in the oil flow. Accuracy is needed to operate oil-water two phase flow (with Middle Eastern crude oils) under free corrosion conditions. Another oil was tested, with an API 37. The crude oil was from North Sea and the composition is presented in Table 17.

Table 17. *Composition of the crude oil from the North Sea tested in the doughnut cell*

Chemical class	Concentration	Unit
Aromatic	26.5	wt.%
Organic oxygen	0.045	wt.%
Sulfur	0.21	wt.%
Mercaptan sulfur	0.0001	wt.%
Total nitrogen	440	ppm wt.
Basic nitrogen	152	ppm wt.
Asphaltenes	<0.1	wt.%

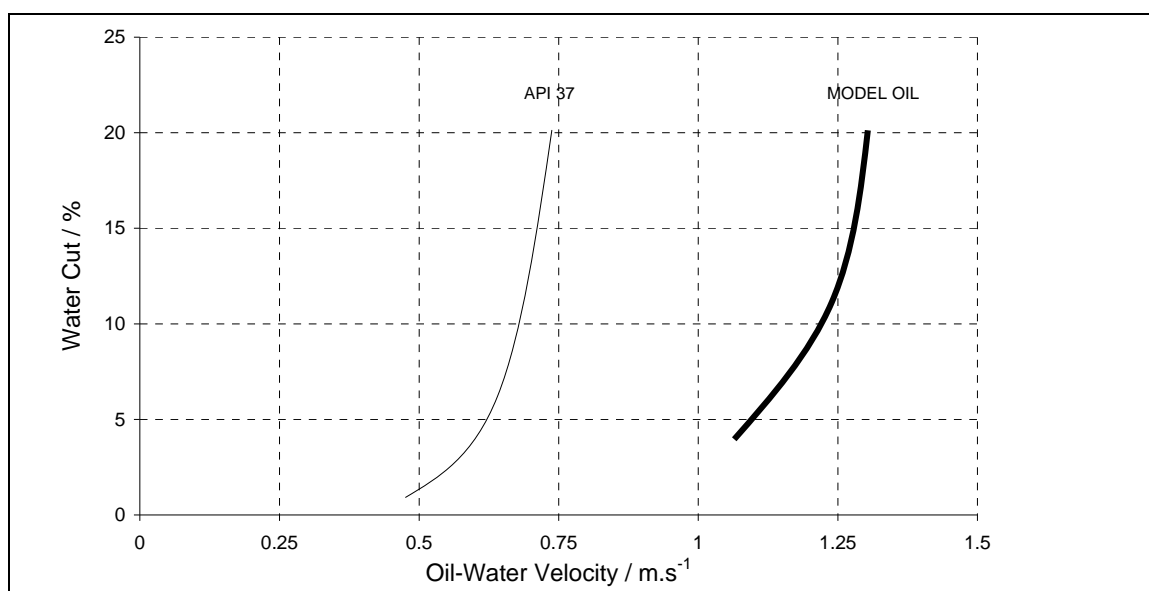


Figure 78. Phase wetting map comparison between model oil and crude oil API37, doughnut cell experimental results. Experiment done by Li⁶⁶.

As expected, the effect of the crude oil from the North Sea is similar to the effect found during the previous experiments on Middle Eastern crude oils. The transition line from oil wetting to intermittent wetting is shifted to lower flow velocities about 0.5 to 0.75 m·s⁻¹.

These results are compared in *Figure 79* with the results obtained with myristic acid. 0.045 wt.% of organic oxygen is equivalent of 0.32 wt.% of myristic acid, if all the oxygen in the crude was made out of myristic acid.

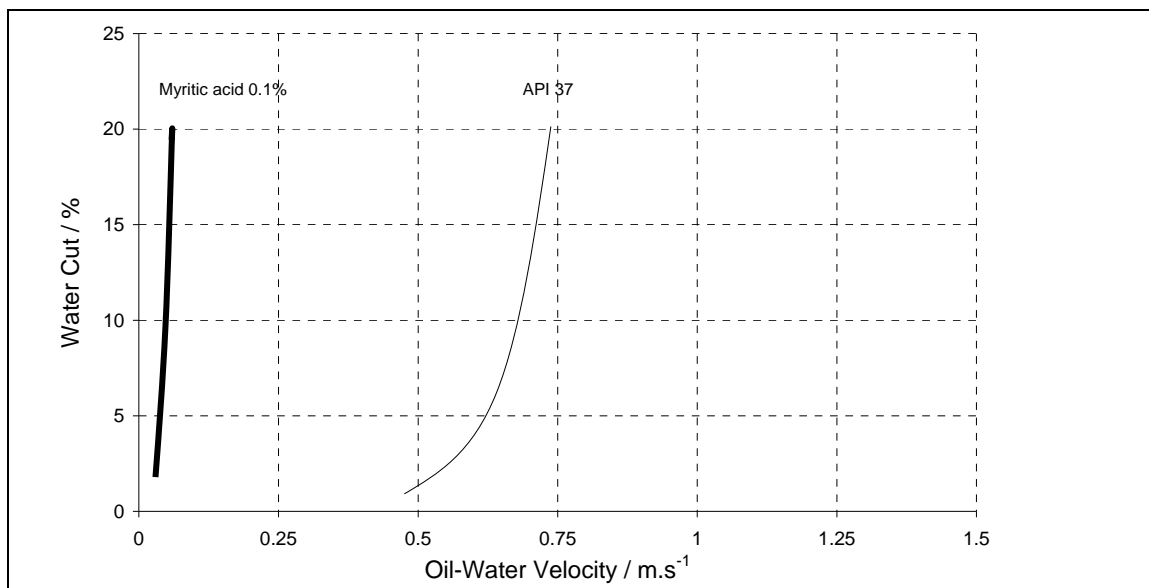


Figure 79. Phase wetting map comparison between model oil mixed with myristic acid and crude oil API37, similar organic acid concentration.

The highest concentration of myristic acid tested is 0.1 wt.%. This concentration gives an approximate transition line under $0.1 \text{ m}\cdot\text{s}^{-1}$. However, a higher concentration of naphthenic acid in the crude oil test does not produce such a high effect on phase wetting. The transition line, as stated above, is in between 0.5 to $0.75 \text{ m}\cdot\text{s}^{-1}$. The difference between the two is explained by the fact that myristic acid is a model compound, having a long carbon chain composed of 14 atoms of carbon. This allows the organization of the molecules upward on the metal surface. Such “organized” arrangements create a perfect oil layer that water droplets can penetrate. However, in real crude oils the arrangement of the molecule is not organized. This creates openings in the oil layer adsorbed onto the metal surface allowing water to wet the steel.

*Large scale results**Model oil tests*

Phase wetting determination and recording of the flow were carried out next in a large flow loop. The main test parameters are shown in Table 18.

Table 18. *Test matrix: model oil test in large flow loop*

Oil phase	Model Oil
Water phase	Water + 1 wt.% sodium chloride + 10ppm fluorescein
Superficial water velocity	0.5 to 3.0 m·s ⁻¹
Water cut	0 to 20 %
Pipe diameter	10.2 cm (4 inch)
Pipe inclination	Horizontal (0°)
Temperature	25°C
Pressure	0.13 MPa

A model oil phase wetting map is determined based on the overlapping information from wall conductance probes, wall sampling port, corrosion monitoring (Fe²⁺ monitoring, ER probe), and flow visualization. The phase wetting found is shown in *Figure 80*. This map shows the wetting state as a function of the oil-water mixture velocity and water cut. Three wetting regimes were found: water wetting, intermittent wetting, and oil wetting. Four flow patterns were observed: stratified flow, stratified flows with mixing layer; semi dispersed flows and fully dispersed flow.

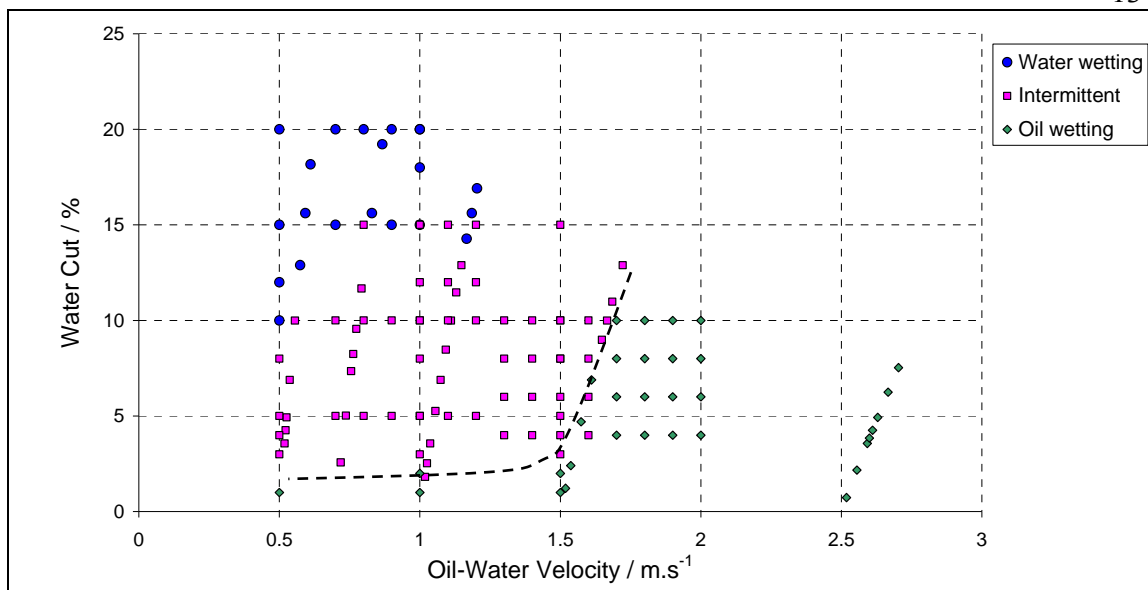


Figure 80. Model oil phase wetting map measured in large flow loop in horizontal position. Points are measurements, line is just an indicator separating oil and water wetting regions.

Mixture velocity = 0.5 m.s⁻¹: at low velocity, stratified flow prevails.

At water cut lower than 10%, water flows as droplets as it is shown in Figure 81 and Figure 82. The droplets average diameter is 10 mm. Interaction between droplets is very weak at these conditions. The droplets wet the pipe periodically. Therefore the wall conductance probe detects an intermittent oil-water wetting condition. Stratified flow was found for high water cut. As the water volume fraction increases, the coalescence between droplets increases. At around 10 to 15% water cut, all the individual droplets had disappeared to become a single layer of water, flowing at the bottom of the pipe. A water cut of 10 % is insufficient to form a continuous water layer on the bottom of the pipe. In such conditions the wall conductance probe detects intermittent oil-water wetting. An increase in the water cut up to 15 % creates a clear stratified flow, with a fully continuous water layer on the bottom. The oil-water interface becomes relatively smooth. In such conditions the wall conductance probe detects water wetting.

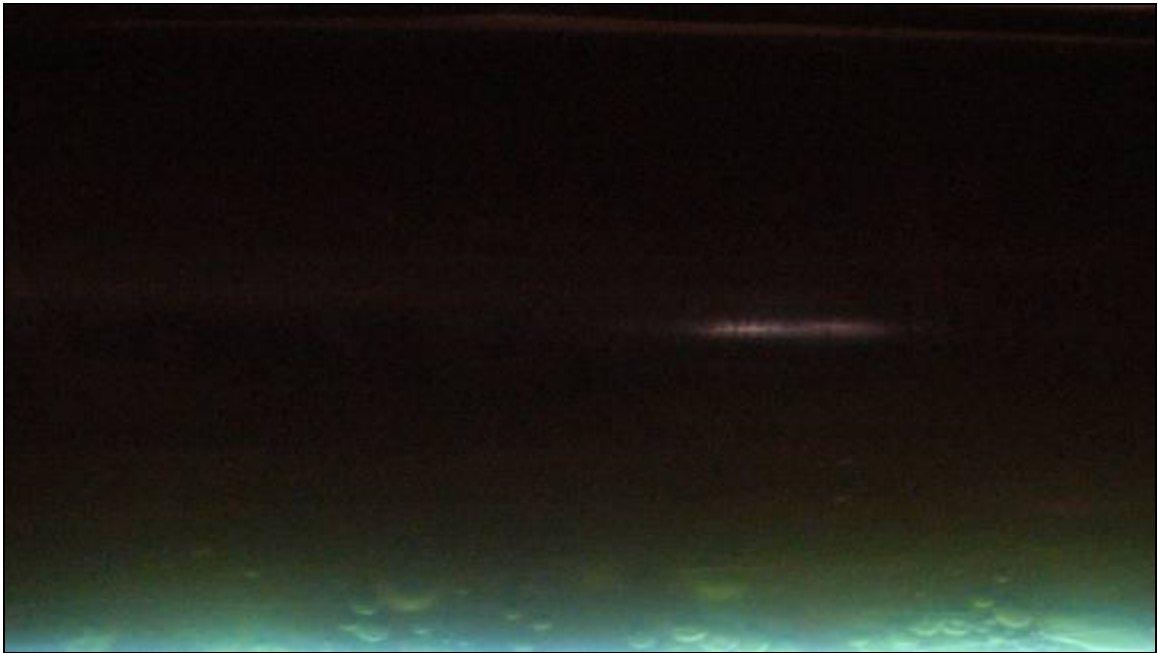


Figure 81. Picture of the flow in 4 inch pipe, oil-water mixture velocity $0.5 \text{ m}\cdot\text{s}^{-1}$, water cut 5%.



Figure 82. Picture of the flow in 4 inch pipe, oil-water mixture velocity $0.5 \text{ m}\cdot\text{s}^{-1}$, water cut 10%.

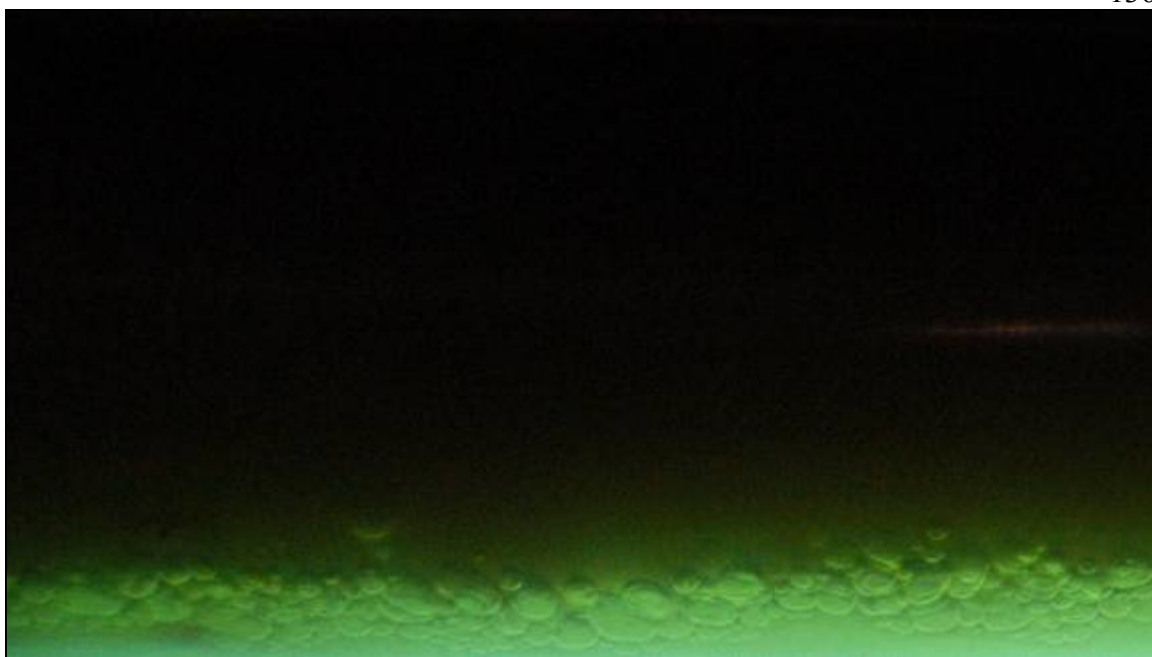


Figure 83. Picture of the flow in 4 inch pipe, oil-water mixture velocity $0.5 \text{ m}\cdot\text{s}^{-1}$, water cut 15%.

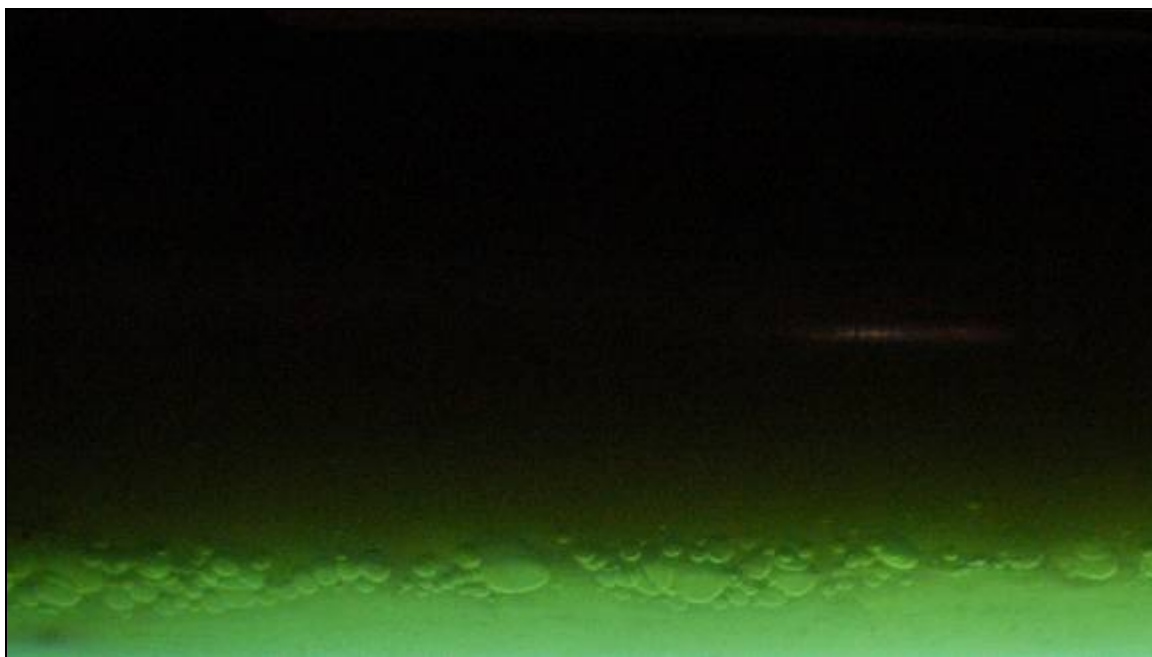


Figure 84. Picture of the flow in 4 inch pipe, oil-water mixture velocity $0.5 \text{ m}\cdot\text{s}^{-1}$, water cut 20%.

Mixture velocity = 1 m·s⁻¹: stratified flow with mixing layer prevails.

At 1 m·s⁻¹ the flow turbulence increases the rate of breakup, consequently the size of the water droplets decreases to 5 mm average. For water cuts lower than 7 %, the small water droplets are dragged into the oil phase and the big droplets wet the bottom of the pipe. According to the wall conductance probe this is an intermittent oil-water wetting condition. Increasing the water cut up to 10% creates a continuous water layer, but the turbulence disrupts the oil-water interface. Some water is then dragged into the oil phase; the flow becomes stratified with a mixing layer. This means the flow has enough energy to break the oil-water interface but not enough to maintain the water droplets in the flow. Unexpectedly, the water layer is not continuous. The wall conductance probe detects intermittent oil-water wetting conditions. The increases of the water cut, more than 15%, creates a thick water layer at the bottom of the pipe. For such water cuts the wall conductance probe detects water wetting.



Figure 85. Picture of the flow in 4 inch pipe, oil-water mixture velocity 1 m·s⁻¹, water cut 5%.



Figure 86. Picture of the flow in 4 inch pipe, oil-water mixture velocity $1 \text{ m}\cdot\text{s}^{-1}$, water cut 10%.



Figure 87. Picture of the flow in 4 inch pipe, oil-water mixture velocity $1 \text{ m}\cdot\text{s}^{-1}$, water cut 15%.

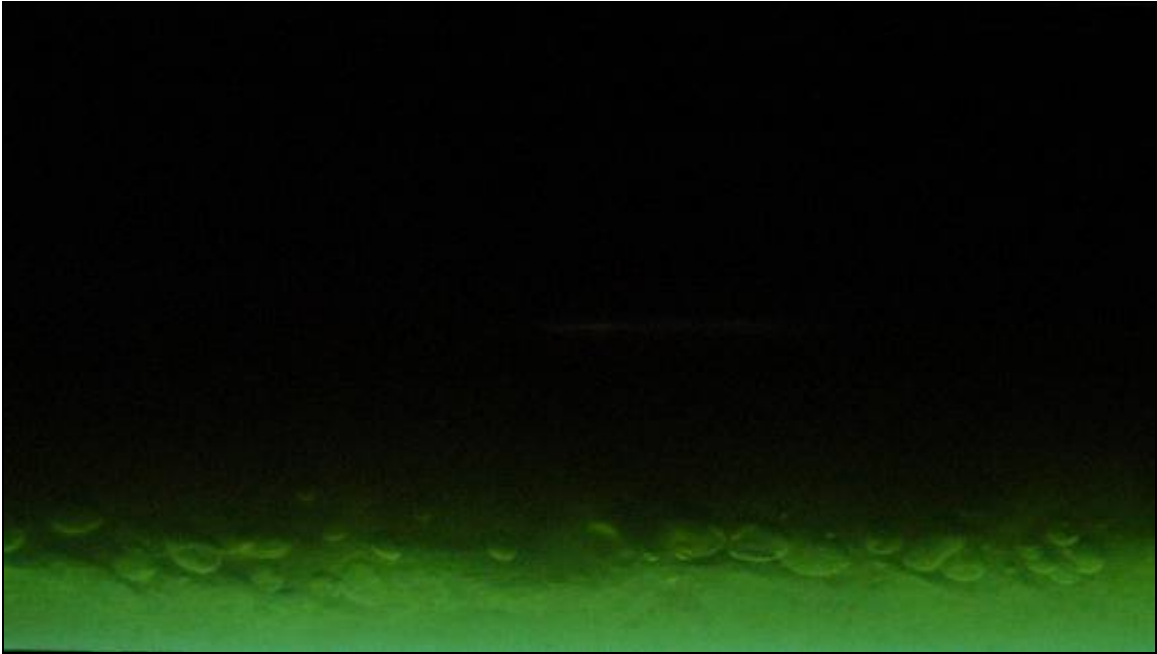


Figure 88. Picture of the flow in 4 inch pipe, oil-water mixture velocity $1 \text{ m}\cdot\text{s}^{-1}$, water cut 20%.

Mixture velocity $> 1.5 \text{ m}\cdot\text{s}^{-1}$: dispersed flow prevails.

The $1.5 \text{ m}\cdot\text{s}^{-1}$ is a critical velocity for this model oil-water horizontal flow. Only dispersed flow and semi-dispersed flow were found for such velocities; this was the case for any water cut in the range of 0 – 20%. The turbulence created small water droplets. These water droplets are dragged by the flow into the oil phase. However, the distribution of water is not uniform; there is more water at the bottom of the pipe than at the top: it is a semi-dispersed flow. According to the wall conductance probe, this is an oil wetting condition. For higher velocity, more than $2.5 \text{ m}\cdot\text{s}^{-1}$, the water is uniformly distributed in the pipe cross section. The oil flow has enough energy to break the oil-water interface and enough turbulence to sustain the water droplet in the flow; it is a fully dispersed flow. From a corrosion point of view, it is a good situation; the water is kept off the walls of the pipe. Oil wets the entire pipe wall section therefore the pipe is free from corrosion. There is agreement with the corrosion measurement results. Oil wetting is detected by the wall conductance probe.



Figure 89. Picture of the flow in 4 inch pipe, oil-water mixture velocity $1.5 \text{ m}\cdot\text{s}^{-1}$, water cut 5%.



Figure 90. Picture of the flow in 4 inch pipe, oil-water mixture velocity $1.5 \text{ m}\cdot\text{s}^{-1}$, water cut 10%.



Figure 91. Picture of the flow in 4 inch pipe, oil-water mixture velocity $1.5 \text{ m}\cdot\text{s}^{-1}$, water cut 15%.

During the tests with the model oil, four different flow regimes were found: stratified flow, stratified flow with mixing layer, semi dispersed flow and fully dispersed flow. *Figure 92* is a representation of the flow pattern observation during the model oil-water flow experiments.

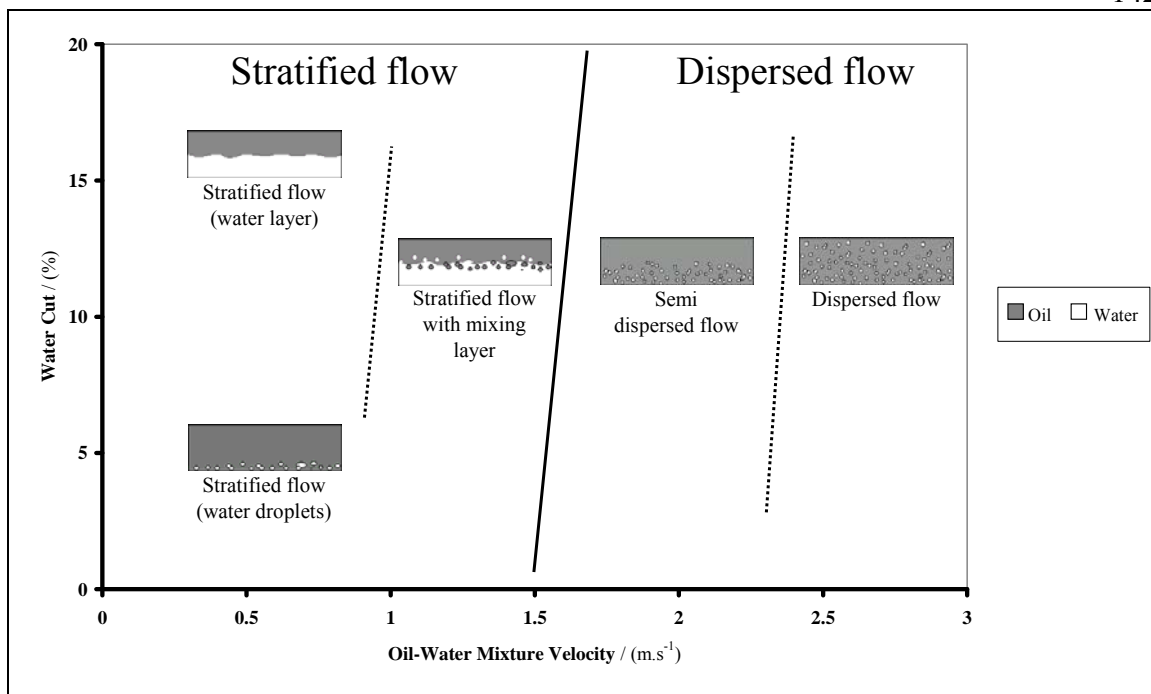


Figure 92. Flow pattern map with model oil, horizontal flow through a 4" pipe.

Stratified flow: water flows on the bottom of the pipe; consequently, the water wets the pipe.

Stratified flow was found for low velocity ($<1 \text{ m}\cdot\text{s}^{-1}$) at any water cut used (0 – 20%). Water wetting was found only for water cuts higher than 15% whereas intermittent oil-water wetting was found for lower water cuts. This can be explained by the rate of water droplet coalescence. At low water cuts, the water droplets are dispersed on the bottom of the pipe and randomly wet the pipe; it is an intermittent oil-water wetting situation. As the water cut increases, the rate of coalescence between water droplets increases too. Around 15% water cut, there is enough water to create a continuous water layer. The water wets the bottom of the pipe continuously, leading to a steady water wetting condition.

Stratified flow with mixing layer: water flows on the bottom of the pipe; consequently, the water wets the pipe.

In the range of 0 to 15% water cuts and 1 to 1.5 m·s⁻¹ velocities, only intermittent oil-water wetting was found. The water layer formed is not continuous, therefore allowing the oil to wet the bottom of the pipe for short periods of time. At 1 m·s⁻¹ mixture velocity the water pump could not deliver more than 15% of the total flow rate, but presumably for higher water cuts a continuous water layer would be formed.

Semi-dispersed flow: Water droplets are flowing in the oil phase and oil wets the whole pipe wall.

Semi-dispersed flow was found for high velocity, more than 1.5 m·s⁻¹. At such velocities the turbulence breaks the oil-water interface. Consequently, water flows as small droplets entrained by the oil phase. However, if the distribution of water is not uniform, more water droplets can be seen in the bottom portion of the pipe. Oil wets all the pipe sections, this is an oil wetting situation.

Dispersed flow: Water droplets are dispersed in the oil flow and oil wets the whole pipe wall.

At oil-water mixture velocities higher than 2.5 m·s⁻¹, the water droplets are small and their distribution in the pipe cross section is apparently uniform. It appears that all the water phase is fully entrained by the flowing oil phase, which is an oil wetting situation.

It should be noticed that there is a perfect overlapping of the boundaries between stratified flow and dispersed flow in *Figure 92*; and the limit between intermittent wetting and oil wetting in *Figure 80*. This suggests that the flow pattern is the major effect on which phase, either oil or water, wets the pipe for model oil.

Tests with myristic acid in model oil

It was found earlier that long chain organic acids such as myristic acid are able to change the affinity of the steel for water. It is therefore interesting to test model oil containing myristic acid in the flow loop and compare the results with the model oil tests.

Table 19. *Test matrix: myristic acid tests in large flow loop*

Oil phase	Model Oil + myristic acid
Water phase	Water + 1 wt.% sodium chloride
Superficial water velocity	0.5 to 3.0 m·s ⁻¹
Water cut	0 to 20 %
Pipe diameter	10.2 cm (4 inch)
Pipe inclination	Horizontal (0°)
Temperature	25°C
Pressure	0.13 MPa

As for the model oil tests, a phase wetting map was determined based using the wall conductance probe. However, as it will be explained, there is an interesting disagreement between the flow visualization and the wall conductance probes.

Figure 93 to *Figure 95* show the phase wetting map when respectively 0.01 wt.%, 0.05 wt.%, and 0.08 wt.% of myristic acid is added to the oil phase.

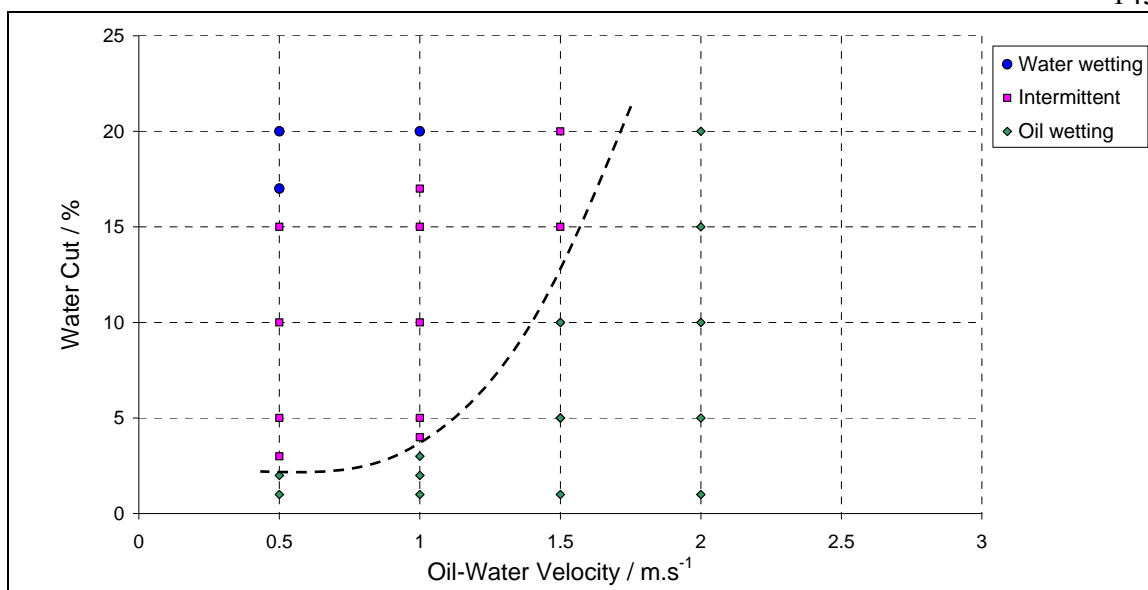


Figure 93. Phase wetting map measured in a large flow loop (4" ID, horizontal flow), with 0.01 wt.% myristic acid added to the model oil. Points are measurements, line is just an indicator separating oil and water wetting regions.

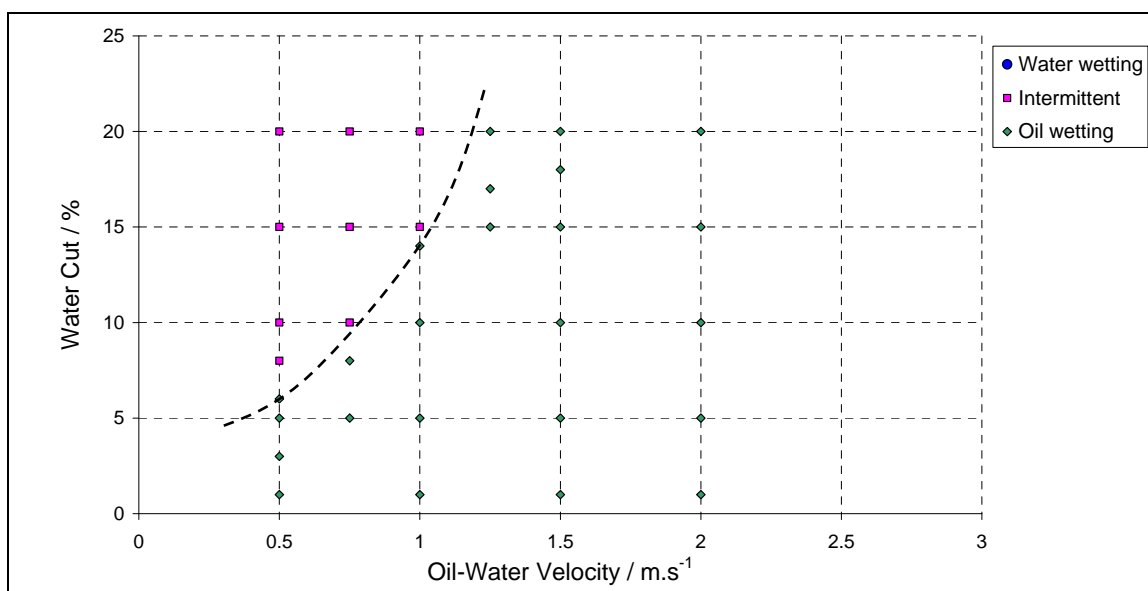


Figure 94. Phase wetting map measured in a large flow loop (4" ID, horizontal flow), with 0.05 wt.% myristic acid added to the model oil. Points are measurements, line is just an indicator separating oil and water wetting regions.

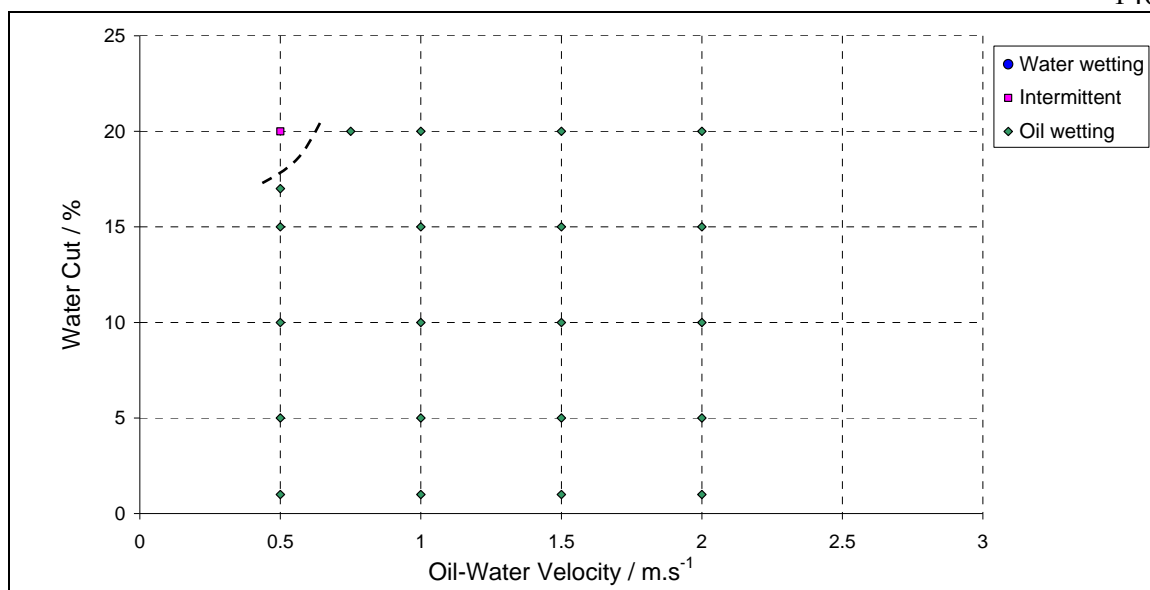


Figure 95. Phase wetting map measured in a large flow loop (4" ID, horizontal flow), with 0.08 wt.% myristic acid added to the model oil. Points are measurements, line is just an indicator separating oil and water wetting regions.

From these graphs one can see that the myristic acid effect is large. *Figure 93* to *Figure 95* show that the myristic acid is able to alter steel wettability, and that this change is proportional to myristic acid concentration. The “movement” of the critical transition line, between oil wetting and intermittent wetting (no corrosion and corrosion situation), is summed up in *Figure 96*.

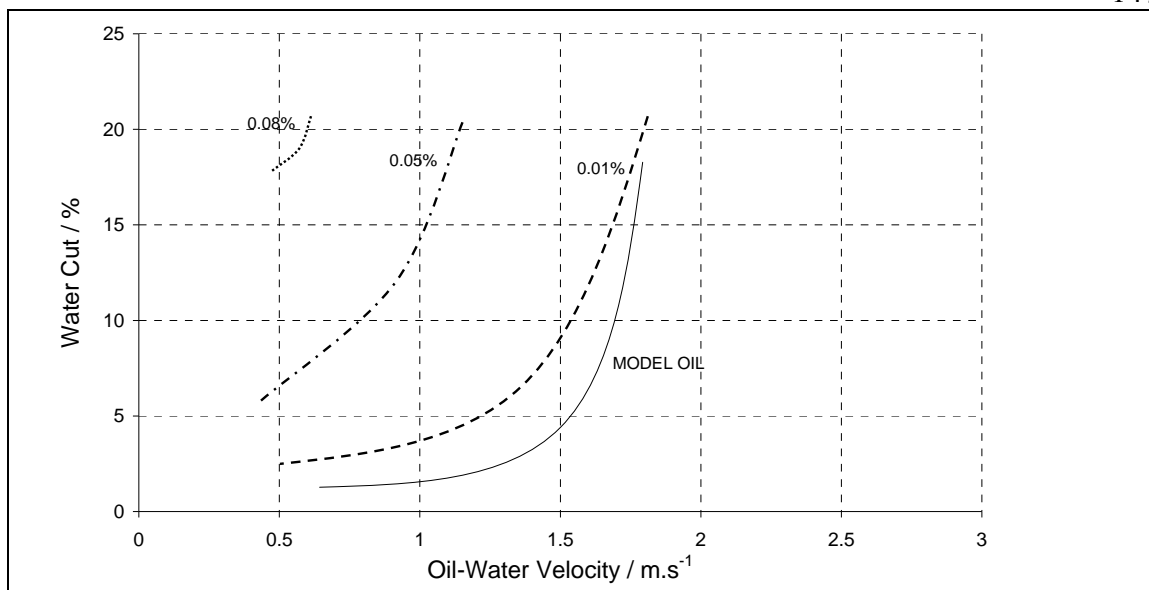


Figure 96. Evolution of the transition line oil wetting to intermittent wetting as a function of the quantity of myristic acid added to the oil phase.

As expected from the results presented in Part 1, myristic acid has no significant effect on the flow pattern. The three maps recorded during myristic acid experiments have the same appearance as the flow pattern maps recorded for pure model oil and shown on *Figure 92*. As a consequence, the flow pattern appears then not to be in agreement with the phase wetting maps recorded with myristic acid.

It is interesting to notice that in the case of model oil there is a perfect overlapping of the phase wetting map and the flow pattern map while for myristic acid this appears not to be the case. These results suggest that when steel is hydrophilic (as in tests with model oil), the flow pattern determines which phase wets the pipe. If the steel is hydrophobic (model oil with myristic acid tests) the phase wetting map is determined by a combination of flow pattern and steel's affinity for water. As the steel becomes more hydrophobic, the flow has less of an effect on which phase wets the pipe.

Crude oils test

Five crude oils from the Middle East were tested in the large scale flow loop as part of the water wetting project for Saudi Aramco. The results are shown below.

Middle Eastern crude oil API 50

Figure 97 shows the phase wetting map for Middle Eastern crude oil API 50 in horizontal flow.

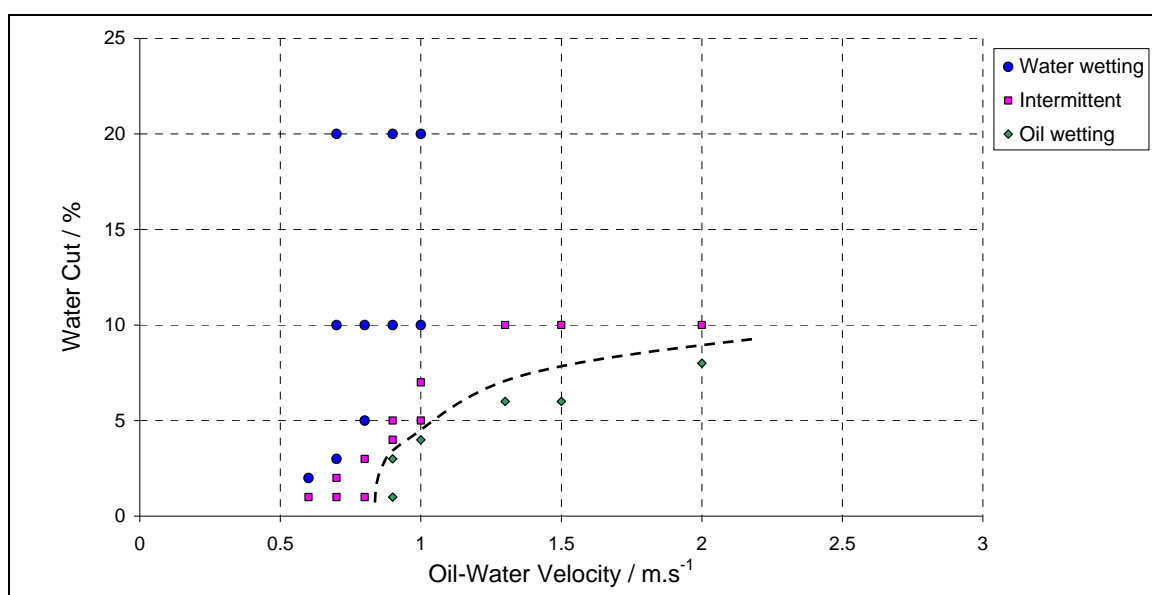


Figure 97. Flow loop experiment, phase wetting map of Middle Eastern oil API 50. Points are measurements, line is just an indicator separating oil and water wetting regions.

From the phase wetting map above, it is clear that water wetting prevails when water cut is high. At a lower water cuts and oil-water mixture velocity around $1 \text{ m}\cdot\text{s}^{-1}$, stable oil wetting occurs at. For, water cuts lower than 5% stable oil wetting occurs at even lower velocities.

The results from fluid sampling suggested that a pure water layer is formed on the bottom of the pipe in the water wetting regime. Moreover, corrosion measurements using Fe^{2+} monitoring under the following conditions: flow velocity $0.7 \text{ m}\cdot\text{s}^{-1}$ and water cut 15%

showed an increase in Fe^{2+} concentration. These results further confirm that under water wetting conditions, a continuous water layer will corrode the bottom of the pipe.

Middle Eastern crude oil API 40:

Figure 98 shows the phase wetting map for Middle Eastern crude oil API 40 in horizontal flow.

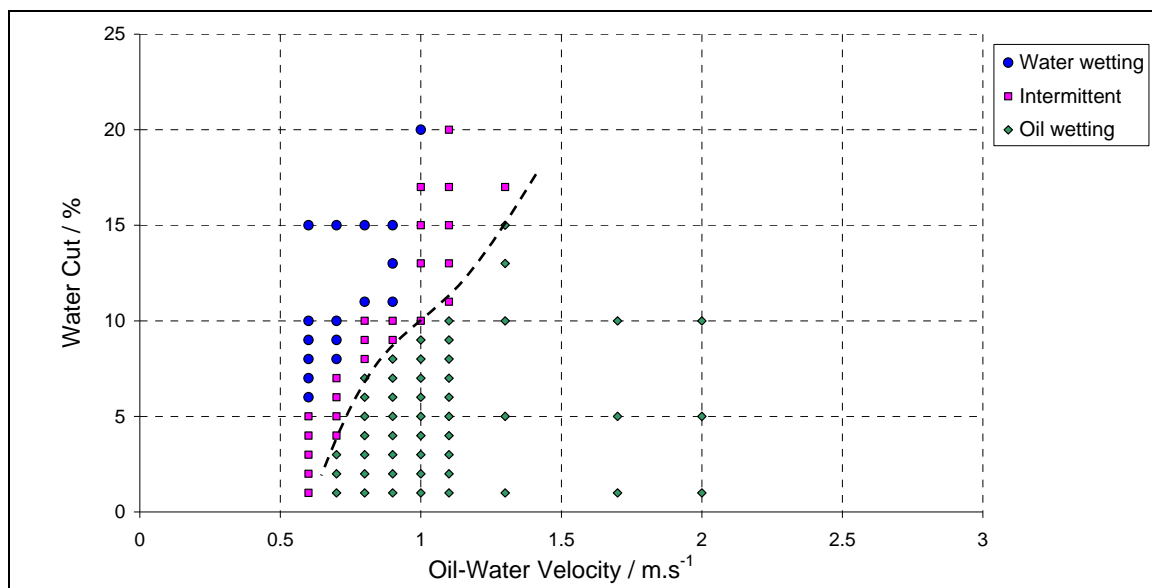


Figure 98. Flow loop experiment, phase wetting map of Middle Eastern oil API 40. Points are measurements, line is just an indicator separating oil and water wetting regions.

The phase wetting map above shows that oil wetting prevails at velocities higher than $1 \text{ m}\cdot\text{s}^{-1}$ and water wetting prevails at water cuts higher than 20%. At 5% water cut, the transition from oil wetting to intermittent wetting is found at $0.75 \text{ m}\cdot\text{s}^{-1}$. At 10% water cut, a first transition from water wetting to intermittent oil-water wetting was found at $0.75 \text{ m}\cdot\text{s}^{-1}$ and a second transition from intermittent to oil wetting was found at $1 \text{ m}\cdot\text{s}^{-1}$. At 15% water cut, the transition from water wetting to intermittent wetting was found at $1 \text{ m}\cdot\text{s}^{-1}$ and the next transition to oil wetting at $1.3 \text{ m}\cdot\text{s}^{-1}$. At higher water cuts, more than 17%, no oil wetting was found.

Fluid sampling at the wall was used at a velocity of $0.6 \text{ m}\cdot\text{s}^{-1}$ and water cut of 5%, the sample recovered was about 90% water and 10% oil. For the same velocity, a small increase in water cut to 10% produced a sample of pure water. The results from the wall conductance probes further confirm the results obtained from the conductance probes

A test was performed with Fe^{2+} monitoring. At $0.9 \text{ m}\cdot\text{s}^{-1}$ 4% water cut the Fe^{2+} concentration did not increase. This confirms that the pipe is free from corrosion and therefore wet by oil. A small increase in the water cut gave different results. At $0.9 \text{ m}\cdot\text{s}^{-1}$ 8% water cut the Fe^{2+} concentration increases by 0.2 ppm in 30 min and at $0.9 \text{ m}\cdot\text{s}^{-1}$ 12% water cut the Fe^{2+} concentration increases by 0.4 ppm in 30 min. The increase of Fe^{2+} concentration can be converted into a corrosion rate.

The corrosion rate was 0 mm/yr at $0.9 \text{ m}\cdot\text{s}^{-1}$ and 4% water cut. The corrosion rate increases from 1.8 mm/yr. at $0.9 \text{ m}\cdot\text{s}^{-1}$ and 8% water cut to 3.9 mm/yr at $0.9 \text{ m}\cdot\text{s}^{-1}$ and 12% water cut. This experiment shows that the corrosion rate under water wetting conditions is almost double the corrosion rate under intermittent oil-water wetting condition.

Middle Eastern crude oil API 34:

Figure 99 shows the phase wetting map for Middle Eastern crude oil API 34 in horizontal flow.

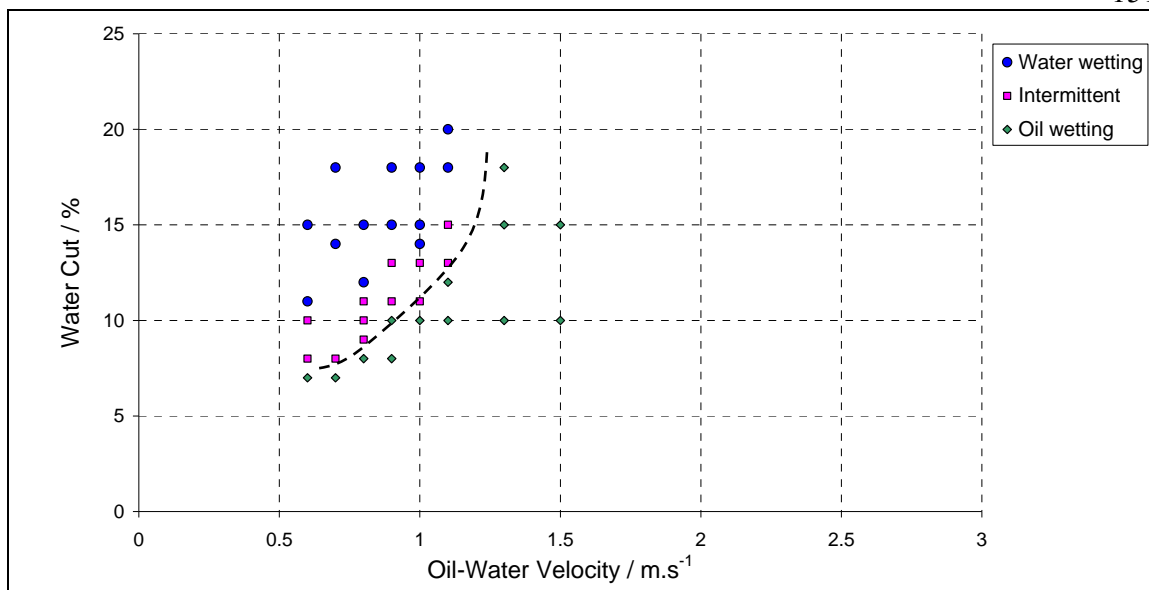


Figure 99. Flow loop experiment, phase wetting map of Middle Eastern oil API 34. Points are measurements, line is just an indicator separating oil and water wetting regions.

The phase wetting map above shows clearly that (as for crude oil API 50 and API 40) water wetting prevails at high water cuts and low velocities. However, the oil wetting area is found for higher water cuts, at $0.6 \text{ m}\cdot\text{s}^{-1}$ the transition from oil wetting to intermittent wetting is found at 7% water cut. For comparison, no oil wetting was found at $0.6 \text{ m}\cdot\text{s}^{-1}$ for crude oil API 50 and API 40.

Fluid sampling gave mixed results. At a velocity of $0.6 \text{ m}\cdot\text{s}^{-1}$ and water cut of 7%, the fluid recovered was 10% water and 90% oil. This is typical of intermittent wetting conditions. The rest of the fluid sampling proved to be in agreement with the phase wetting map. Two explanations are possible for the disagreement at low velocity between fluid samplings and the wall conductivity probes. Either this Middle Eastern oil API 34 has a different chemistry compared to the other Middle Eastern oils, thus changing its wetting properties or there were false readings made with the conductivity probes.

Corrosion measurement using Fe^{2+} concentration seems to support the idea that Middle Eastern oil API 34 is different from the other two oils. Fe^{2+} concentration monitoring was

Fluid samplings confirm these results. Tests with fluid samples recovered at a flow velocity set at $0.6 \text{ m}\cdot\text{s}^{-1}$ and water cut of 2% had 1% water and 99% oil, confirming a stable oil wetting condition. After increasing the water cut to 5% fluid samples recovered had an average of 50% water and 50% oil confirming an intermittent oil-water wetting condition. Increasing the water cut to 15% at the same low velocity fluid samples increased from 50% to 99% water, which is consistent with the water wetting recorded by the conductivity probes in such conditions.

It should be noted that during the corrosion test (Fe^{2+} concentration monitoring) a stable emulsion formation started. Pictures of the emulsion were taken, showing the nature of the emulsion: water in oil. A composite of the images taken is shown in *Figure 101*. Once the emulsion above was formed the conductivity probes detect only oil, even at very high water cuts and low velocity.

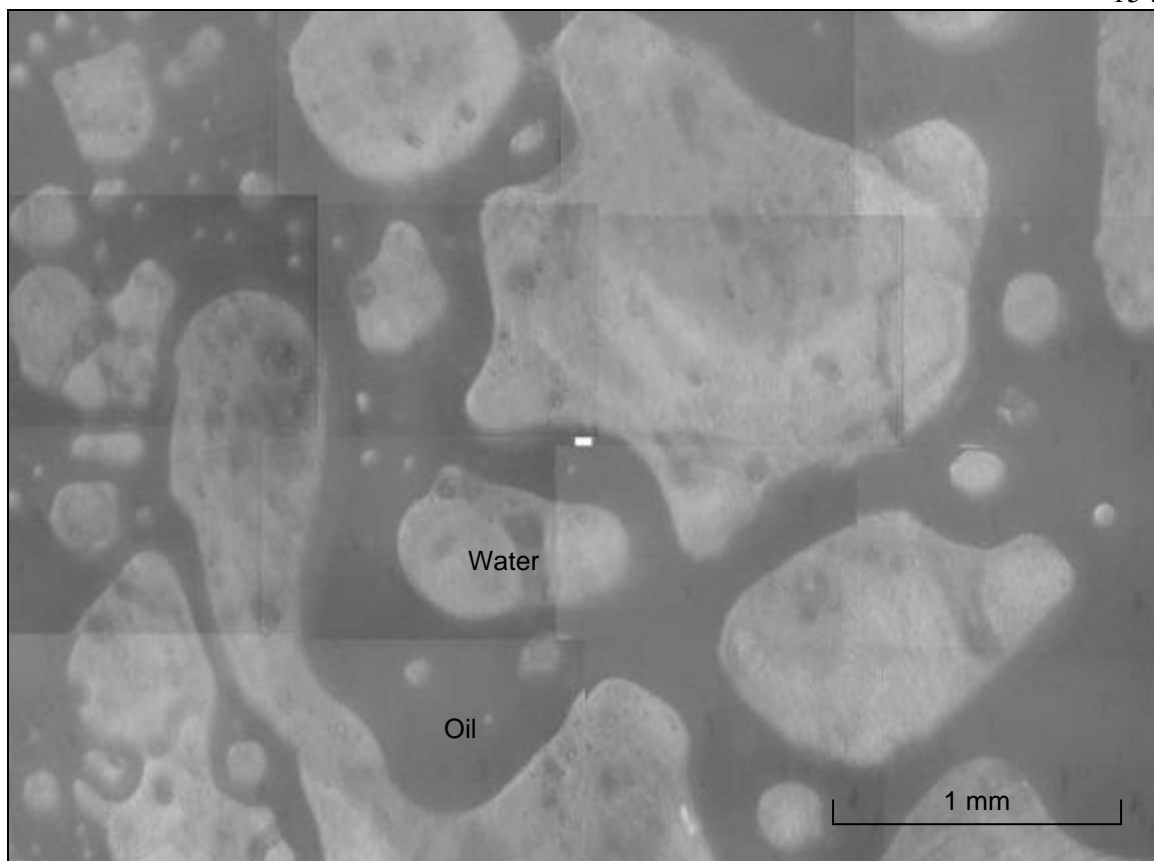


Figure 101. Composite of 16 pictures taken with a microscope of the water in oil emulsion.

Middle Eastern crude oil API 27:

Figure 102 shows the phase wetting map for Middle Eastern crude oil API 27 in horizontal flow. This oil is the heaviest Middle Eastern oil tested.

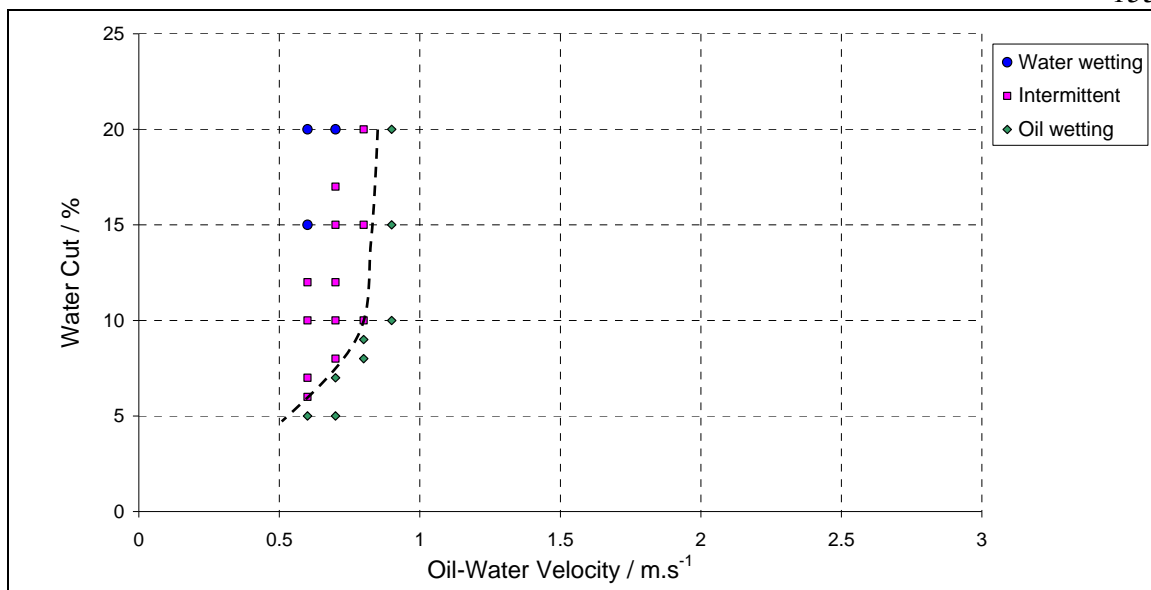


Figure 102. Flow loop experiment, phase wetting map of Middle Eastern oil API 27. Points are measurements, line is just an indicator separating oil and water wetting regions.

The water wetting area on the phase wetting map was reduced further, and oil wetting prevails at velocities higher than $0.8 \text{ m}\cdot\text{s}^{-1}$. The transition line from oil wetting to intermittent wetting has the same trend as the other Middle Eastern oils: API 50, 40, 30. It should be noted that such heavy oil is known to produce water-in-oil emulsions. Once the emulsion formed, wall conductance probes indicated oil wetting.

Fluid sampling has been performed to confirm the results found with the phase wetting map. At a velocity of $0.6 \text{ m}\cdot\text{s}^{-1}$ and 5% water cut, fluid recovered from the bottom of the pipe had 10% water and 90% oil. Increasing the water cut to 10% the fluid recovered had 70% water 30% oil. Increasing further in the water cut up to 15 % and the fluid recovered had 95% water 5% oil. All fluid sampling results are consistent with the phase wetting map obtained from the conductivity probes.

Summary of work with crude oils

The phase wetting maps for all the Middle Eastern crude oils presented above in *Figure 97* to *Figure 102* show very different transition lines oil wetting to intermittent wetting. These are summarized *Figure 103* which shows the superposition of the transition line for all the Middle Eastern crude oils.

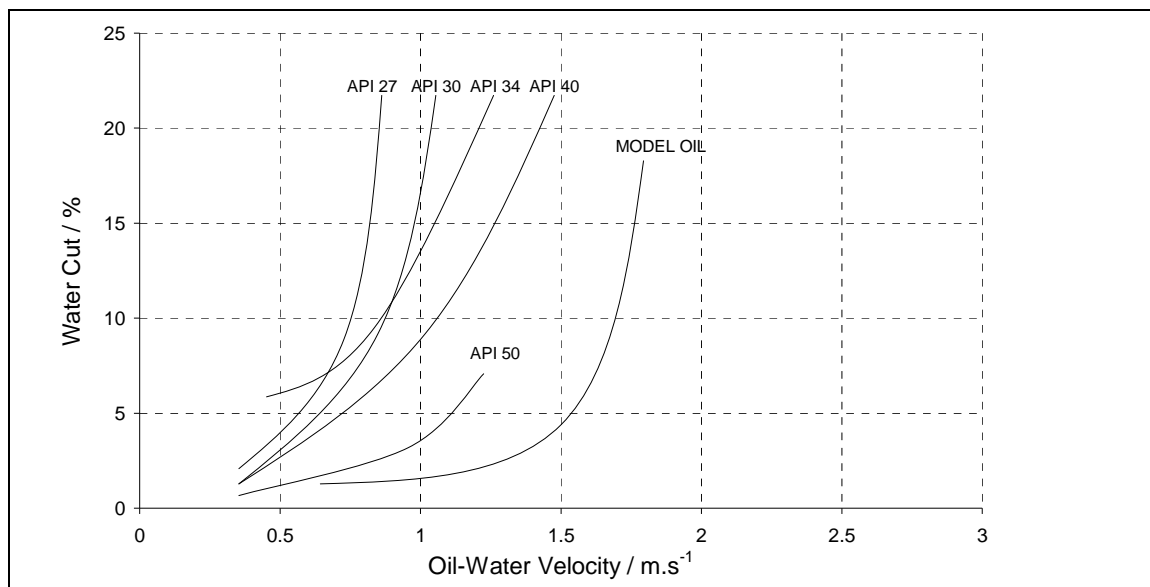


Figure 103. Phase wetting maps of Middle Eastern crude oils API 27 to 50.

The model oil has an API very close to Middle Eastern oil API 40. If the physical properties of the oil, such as density and viscosity, were the main parameters influencing phase wetting, the two transition lines should be identical. However, at 5% water cut the transition from oil wetting to intermittent wetting is found at a velocity of $0.6 \text{ m}\cdot\text{s}^{-1}$ for the crude oil while the same transition is found above $1.5 \text{ m}\cdot\text{s}^{-1}$ for the model oil. At 10% water cut, the transition line is found at $1.1 \text{ m}\cdot\text{s}^{-1}$ for the crude oil and $1.7 \text{ m}\cdot\text{s}^{-1}$ for the model oil. These results confirm the effect from crude oil chemistry on phase wetting under dynamic conditions.

Also, *Figure 103* shows that heavy oils entrain more easily the water phase than lighter crude oils. At 5 % water cut the transition line oil wetting to intermittent wetting is at $0.6 \text{ m}\cdot\text{s}^{-1}$ for API 27 oil and $1.1 \text{ m}\cdot\text{s}^{-1}$ for API 50 oil. At 10% water cut the transition

shifted to $0.75 \text{ m}\cdot\text{s}^{-1}$ for API 27 oil and $1.4 \text{ m}\cdot\text{s}^{-1}$ for API 50 oil. These results are consistent with the Middle Eastern phase wetting maps obtained in small scale experiments. The same conclusion is achieved: as the density increases (API decreases) the concentration of large molecules such as aromatics and naphthenic acids increase, too. This change in the crude oil chemistry has a direct effect on the wettability of the pipe and therefore on the phase wetting map.

Phase wetting prediction

Introduction

Flow velocity and water cut are the main parameters in the water wetting model (Equation 35) to predict which phase wets the pipe. If the condition in Equation 35 is satisfied, the flowing oil phase entrains the water phase. This flowing condition is called oil wetting because the water phase is dispersed in the oil phase and oil wets the pipe. On the contrary, when the condition in Equation 35 is not satisfied water can drop out of the oil flow and either intermittently wet the bottom of the pipe (intermittent wetting), or permanently wet the bottom of the pipe (water wetting) and a continuous water layer is formed.

Interestingly, when the oil flow does not have enough turbulence to sustain water droplets in the flow, another phenomenon influences which phase wets the pipe; it is steel surface wettability. Hydrophilic steel pipes will be more easily wet by water than hydrophobic steel pipes under the same flow conditions.

Model prediction for hydrophilic steel

If the steel surface is hydrophilic, water wetting conditions appear when a water droplet approaches and then wets the steel surface. For this reason, the large scale experiments performed with hydrophilic conditions seen with model oil are in good agreement with the prediction made by the water wetting model (Equation 35) which accounts solely for

the breakup/coalescence of water droplets. Both experimental results and water wetting model prediction are plotted in *Figure 104*.

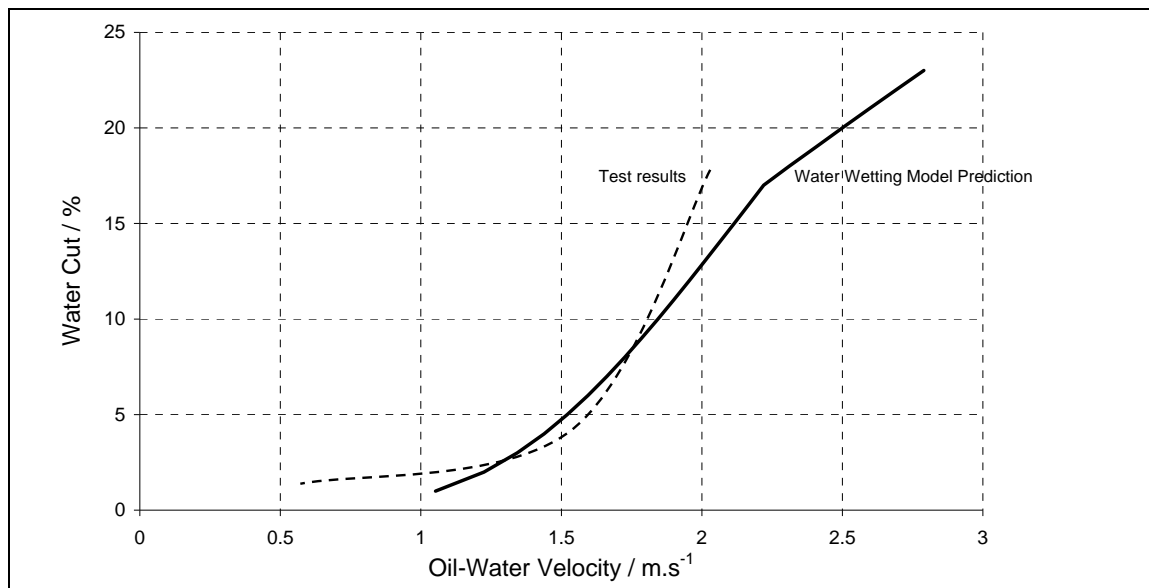


Figure 104. Comparison: transition line oil wetting to intermittent wetting function for the model oil (dashed line) with water wetting model's prediction (solid line).

Though the overall model prediction of the water wetting model is good when the pipe surface is hydrophilic, the prediction of the droplet size (Equation 23) is only approximate. *Figure 105* shows the prediction of droplet size calculated with Equation 23 and the size measurement of real droplet from pictures of the flow (*Figure 81* to *Figure 91*). The droplet size predicted by the model is in agreement with the experimental results at $0.5 \text{ m}\cdot\text{s}^{-1}$ from 3 to 5% water cut. Below 3% water cut the prediction is smaller than the real size of the droplets and above 5% the prediction is larger than the real size of the water droplets. For a velocity of $0.75 \text{ m}\cdot\text{s}^{-1}$ the model prediction is in agreement with the experimental data from 3 to 8% water cut. And at $1 \text{ m}\cdot\text{s}^{-1}$ the model is also in agreement with the experimental data from 3 to 8% water cut.

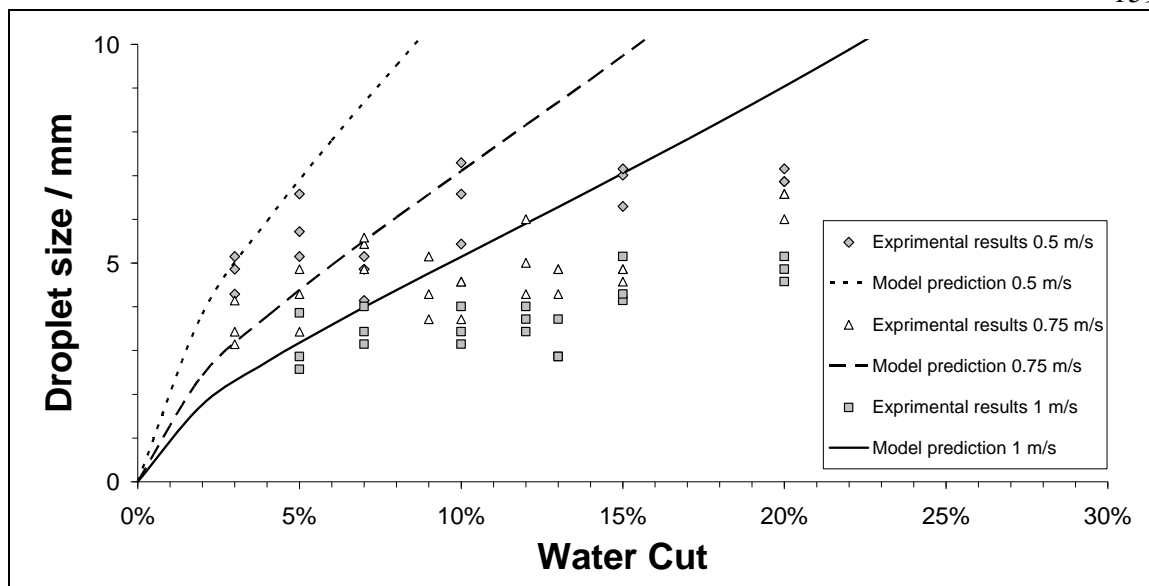


Figure 105. Comparison: size of water droplet measured experimentally and prediction of the water wetting model oil (Equation 21).

Model prediction for hydrophobic steel

When the steel surface is hydrophobic, phase wetting prediction is more complex than when the steel is hydrophilic. Phase wetting in the case of hydrophilic steel depends solely on one phenomena: hydrodynamic forces affecting the droplet breakup/coalescence in the bulk. When the hydrodynamic forces allow the water to approach the pipe wall, water readily wets the hydrophilic steel surface. This has been covered by the water wetting model (Equation 23).

In contrast, phase wetting with hydrophobic steel depends on hydrodynamic forces as well as interfacial forces such as surface tensions (steel-water, steel oil and oil-water). For this reason the water wetting model fails to predict phase wetting for model oil containing myristic acid. Figure 106 shows the comparison between the transition lines (oil wetting to intermittent wetting) for the experimental results obtained with myristic acid (Figure 93 to Figure 95) and the prediction.

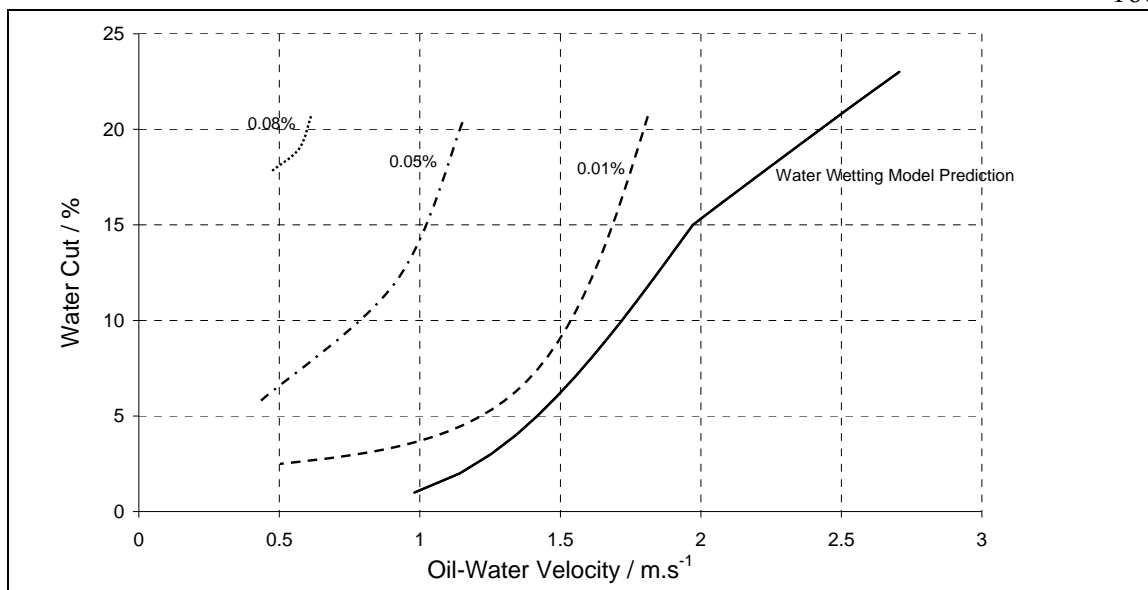


Figure 106. Comparison of transition lines for oil wetting to intermittent wetting as a function of the concentration of myristic acid including the water wetting model prediction.

In order to compensate for the effect of surface forces on phase wetting in the current water wetting model, a simple mechanistic model has been developed to predict the transition line from oil wetting to intermittent wetting.

First, the velocity transition from oil wetting conditions to water wetting conditions for one known water cut is named T_{WC} . Then, in the same way as the inhibition of corrosion was introduced in the previous chapter, an inhibition of wettability (IW) is created. The inhibition of wettability (Equation 49) induced by one surface active compound is defined as the ratio of the value of the transition oil wetting to intermittent wetting with chemicals adsorbed onto the metal surface (steel hydrophobic) divided by the value of the same transition when no chemicals are adsorbed (steel hydrophilic).

For one water cut, and one chemical compound,

$$IW_{\%} = \left(1 - \frac{T_{WC \text{ with chemical}}}{T_{WC \text{ with no chemical}}} \right) \cdot 100$$

Equation 48

First, if IW can be calculated for every water cut tested by experiments, all the values calculated should be equal, as only one value can be explained by an adsorption model.

Second, such a model is based on the assumption that the inhibition of wettability is proportional to the amount of surface active chemicals adsorbed onto the metal surface. It was proved in the previous chapter that crude oil's surface active compounds adsorb onto the metal surface as a function of their concentration. Also, experiments proved that some surface active compounds are able to “coat” the metal surface and create a hydrophobic surface. Assuming that the creation of this hydrophobic surface is proportional to the concentration of surface active compounds, it is possible to introduce a new equation predicting a boundary between oil wetting to intermittent wetting as a function of the concentration of surface active compounds. *Figure 107* shows the transition line between oil wetting to intermittent wetting if the value of the transition line is multiplied by $(1 - IW)$.

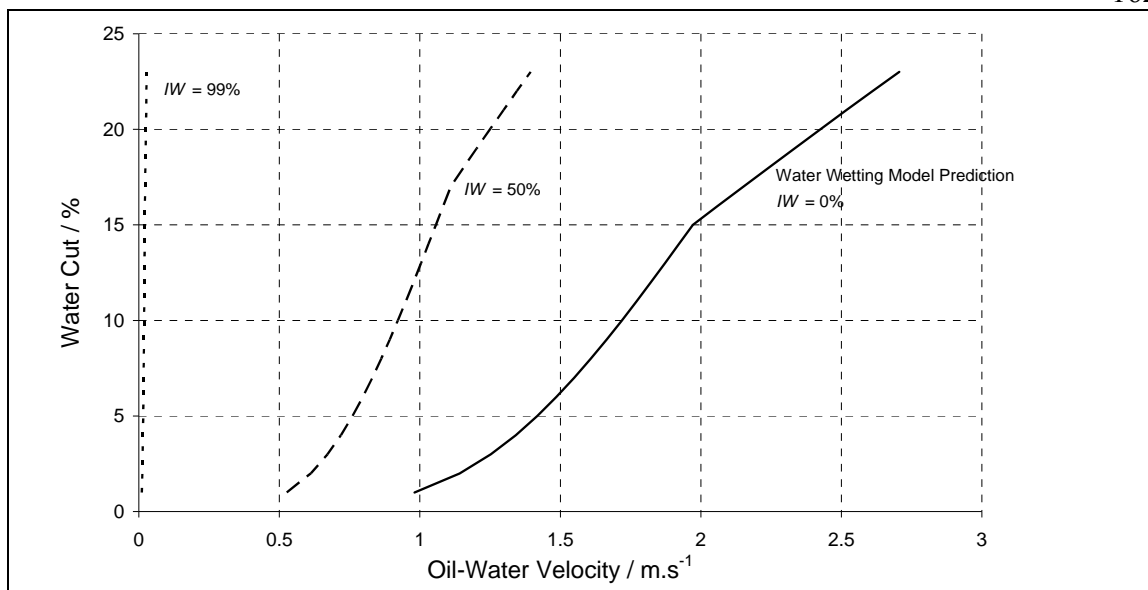


Figure 107. Evolution of the transition line oil wetting to intermittent wetting as a function of the inhibition of wettability (IW).

$IW = 0$ If the steel is hydrophilic, the only forces that affect phase wetting are hydrodynamic forces. When the water drop-out occurs, water wetting is observed.

$IW = 1$ If the steel is completely hydrophobic, the transition line is a vertical line on the Y axis. As a consequence, the steel can not be wet by water under any condition (stagnant or dynamic). $IW = 1$ implies that hydrodynamic forces have no effect on the phase wetting. Such results were found during the test of myristic acid effect on steel wettability (Table 15). A picture of a water droplet in model oil containing 1% myristic acid on a steel surface under stagnant conditions is shown in Figure 108. The contact angle of such a water droplet is 180° ; there is no direct contact between the water phase and the steel surface. If $IW = 1$, water wetting can not happen even for very low velocities. Of course $IW = 1$ is an ideal case from a corrosion point of view, and should not be assumed to occur in the field.

$0 < IW < 1$ The natural hydrophilic nature of the steel surface has been altered by the adsorption of surface active compounds. Wettability of the steel has also been altered as a function of the type and amount of surface active compounds adsorbed onto the steel

surface. This is a real case scenario where phase wetting depends on the synergy between hydrodynamic forces and steel wettability.

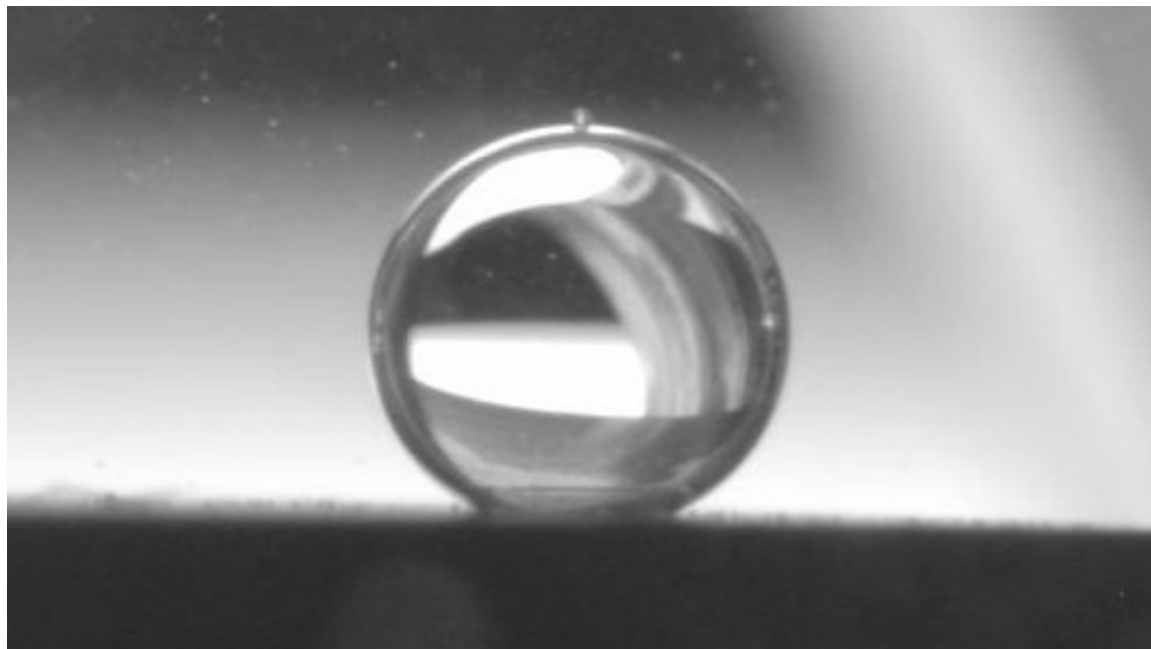


Figure 108. Picture of a water droplet (1 wt.% NaCl, pH 5.0) immersed in model oil mixed with 1 wt.% myristic acid on a steel surface. The water droplet is gently moving on a slightly inclined steel surface, the water droplet does not wet the steel surface.

Model calibration

The large scale experiments can be used to calibrate the model. Two chemical classes of surface active compounds were found to have an effect on steel wettability, high molecular weight organic acids and aromatics. Myristic acid (representing naphthenic acids) was tested on a large scale in the flow loop. These results can be used to calibrate the model. The comparison between experimentation and modeling results are shown on *Figure 109*.

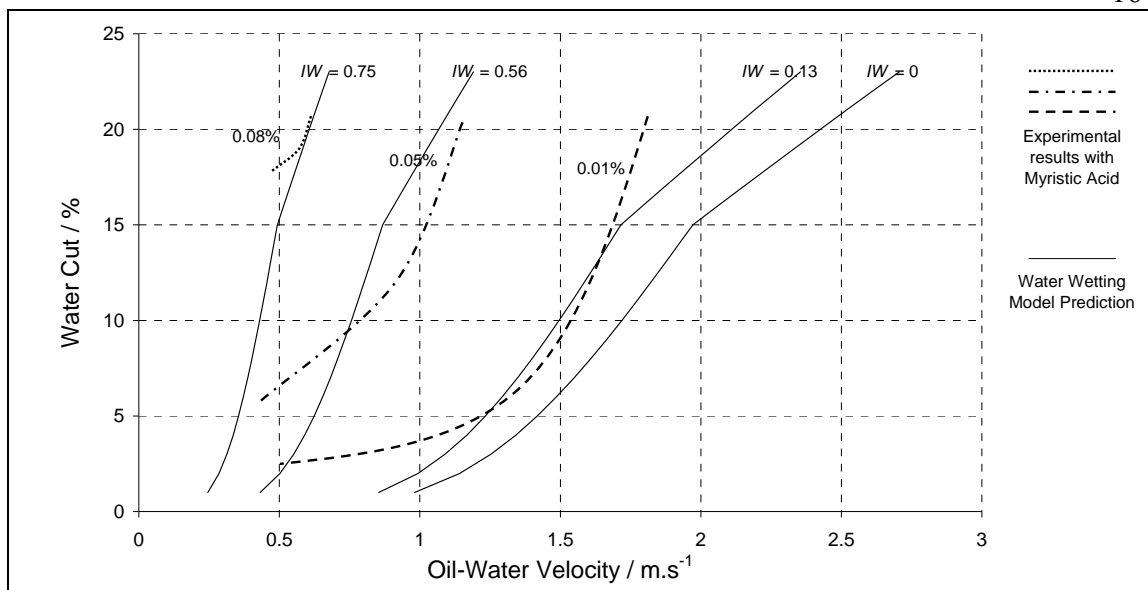


Figure 109. Comparison between large scale tests (with myristic acid) and modified water wetting model (values of IW are empirical).

Using the myristic acid results on Figure 109 and Equation 49, the prediction of wettability alteration from naphthenic acids can be predicted, using the same mathematical model as for the inhibition of corrosion.

$$IW_{\%} = 1 \cdot \frac{225 \cdot [O_{naph}]}{1 + 225 \cdot [O_{naph}]} \quad \text{Equation 49}$$

Where $[O_{naph}]$ represents the oxygen concentration in the model oil.

Equation 49 predicts that if the oxygen concentration in naphthenic acid, $[O_{naph}]$ is equal to zero, the change in wettability is equal to zero. However, if $[O_{naph}] = 0.018$ wt.% the alteration of wettability calculated by the equation equals 80%, if $[O_{naph}] = 0.040$ wt.% the alteration of wettability calculated by the equation equals 90%. Figure 110 shows the comparison of the prediction made by Equation 49 and the results found in Figure 109.

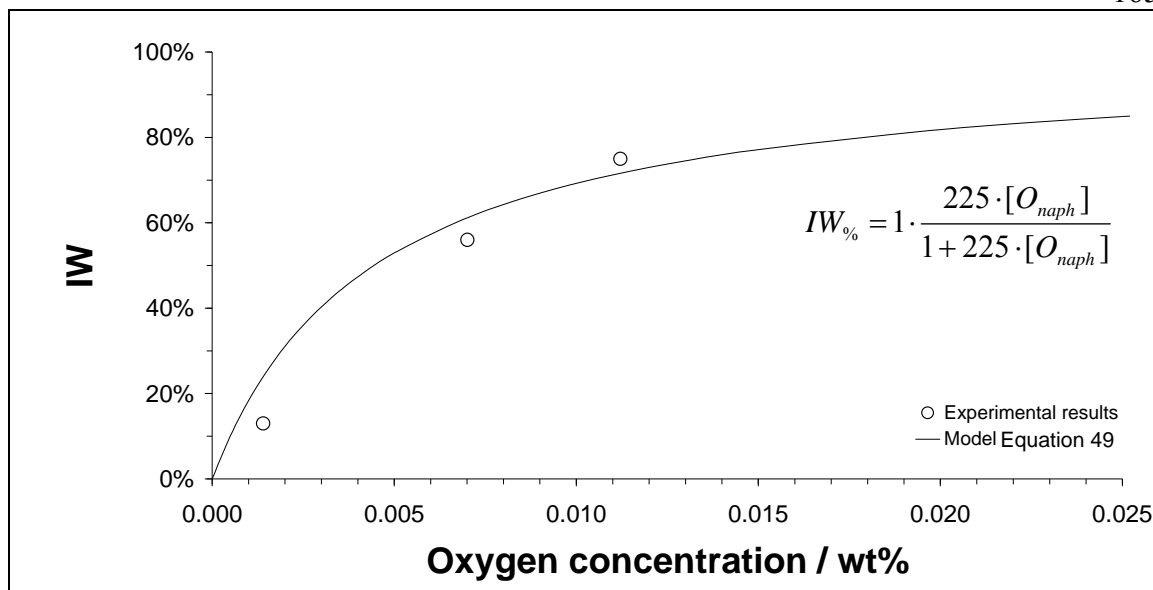


Figure 110. Comparison of the wettability alteration (IW), experimental results vs. the prediction made by Equation 49.

Large scale experiments with myristic acid were used to calibrate the inhibition of wettability model for naphthenic acids. The same experiments can be done with tetrahydronaphthalene in order to predict the effect of aromatics on the inhibition of wettability.

The results of the large scale experiments (Figure 97 to Figure 102) are compared with the water wetting model, and the inhibition of wettability model in Figure 111 to Figure 115.

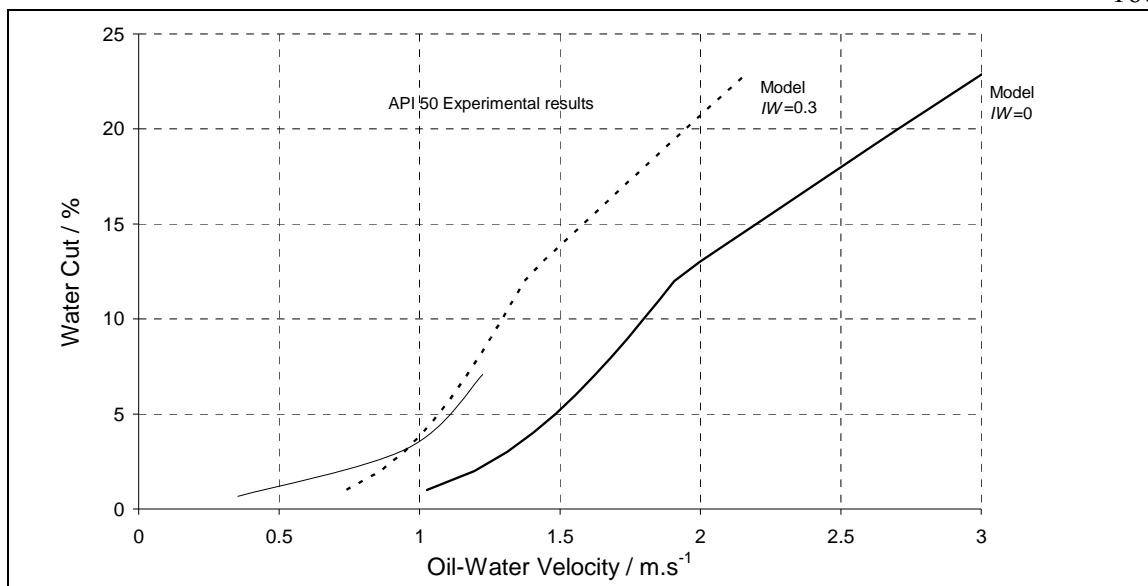


Figure 111. Large scale experiment results with Middle Eastern oil API 50 from Figure 97 and the prediction from the water wetting model ($IW = 0$) and the prediction from the corrected water wetting model with $IW = 0.3$.

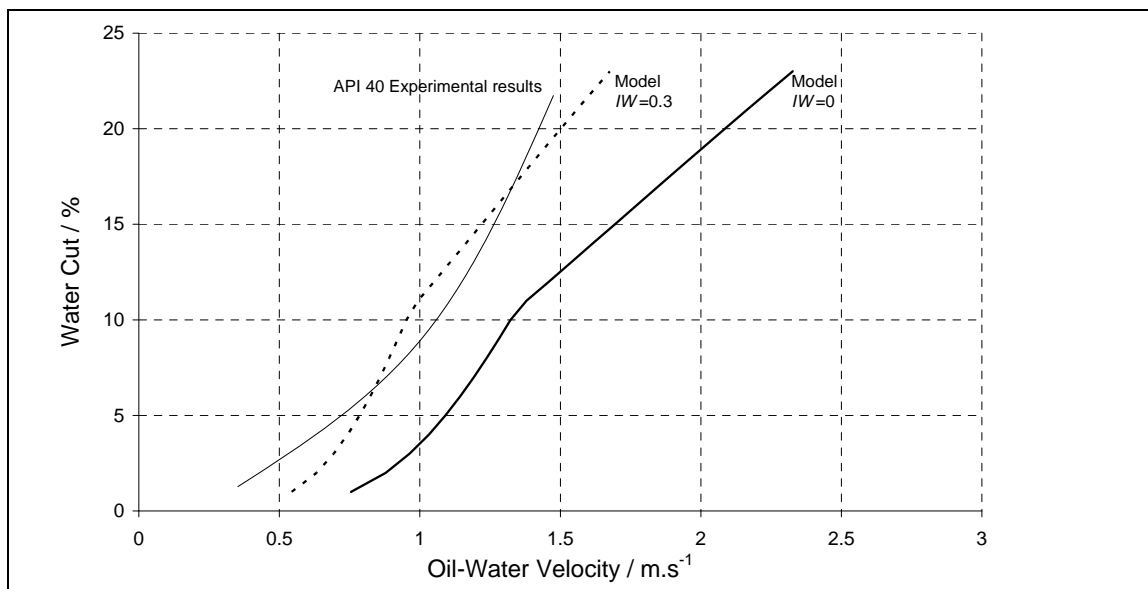


Figure 112. Large scale experiment results with Middle Eastern oil API 40 from Figure 98 and the prediction from the water wetting model ($IW = 0$) and the prediction from the corrected water wetting model with $IW = 0.3$.

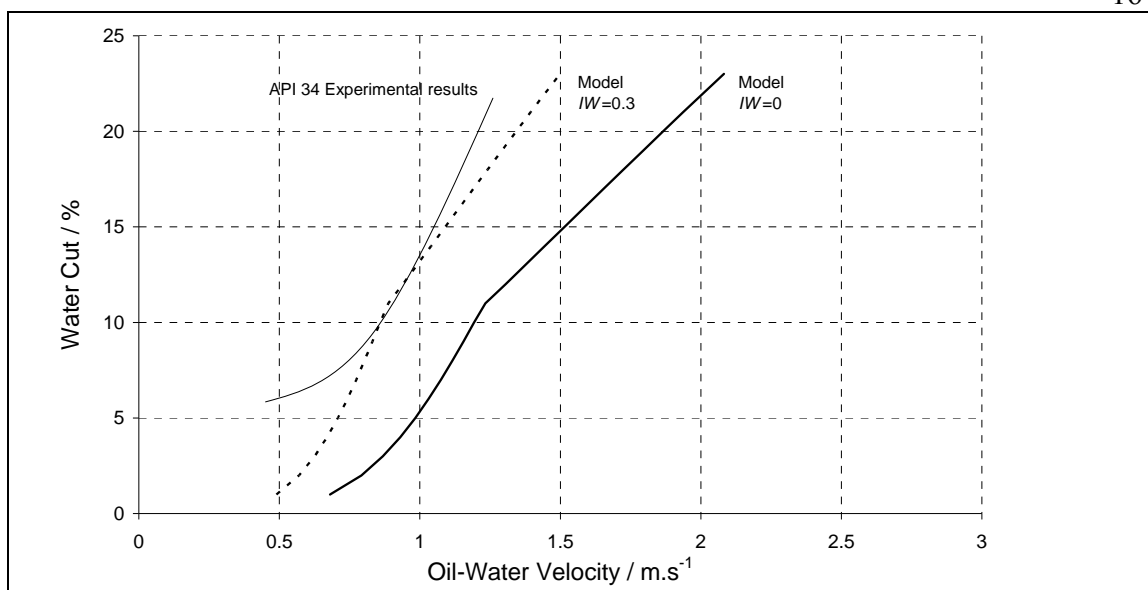


Figure 113. Large scale experiment results with Middle Eastern oil API 34 from Figure 99 and the prediction from the water wetting model ($IW = 0$) and the prediction from the corrected water wetting model with $IW = 0.3$.

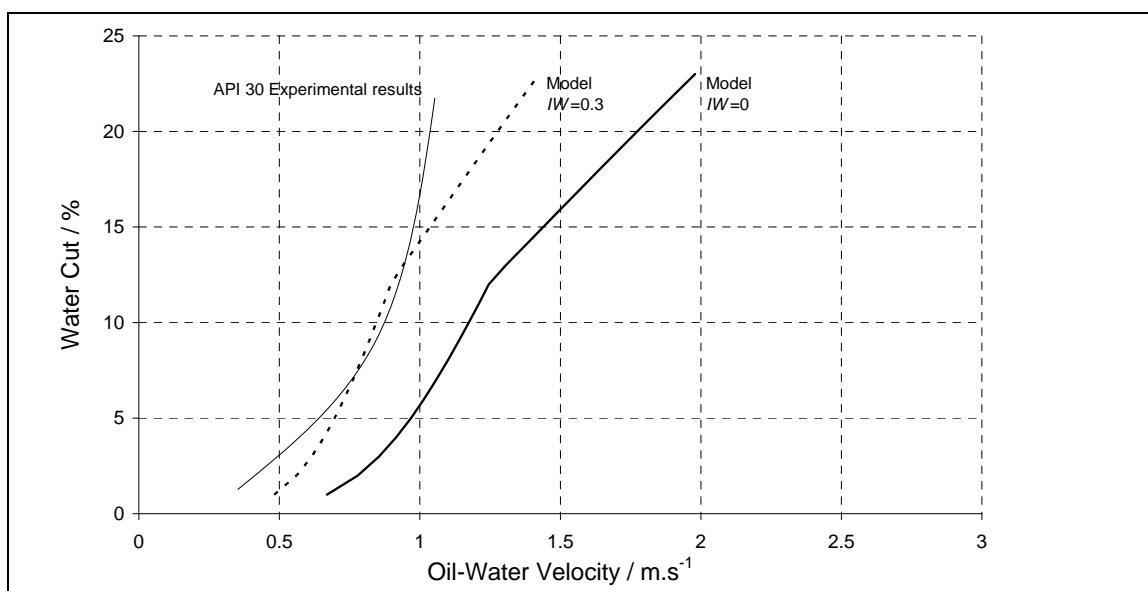


Figure 114. Large scale experiment results with Middle Eastern oil API 30 from Figure 100 and the prediction from the water wetting model ($IW = 0$) and the prediction from the corrected water wetting model with $IW = 0.3$.

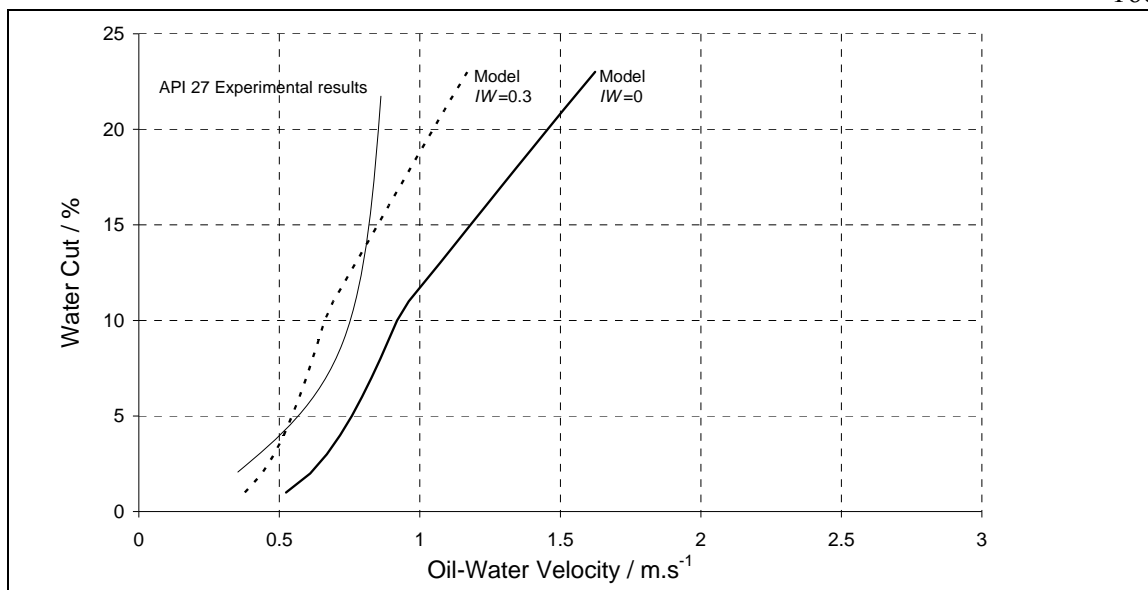


Figure 115. Large scale experiment results with Middle Eastern oil API 27 from Figure 102 and the prediction from the water wetting model ($IW = 0$) and the prediction from the corrected water wetting model with $IW = 0.3$.

Figure 111 to Figure 115 show the comparison of the water wetting model (Equation 35) prediction and the experimental results of the corresponding Middle Eastern crude oil. All these figures confirm that the water wetting model is insufficient to predict the phase wetting with these crude oils. However, these figures also show the corrected water wetting model of hydrophobic steel surfaces using the inhibition of wettability. The Figures show that the same value of IW (0.3) is needed in order to correct for the water wetting model. If the physics used in the inhibition model is right, all five crude oils should have the same inhibition of wettability properties, since all five crude oils need the same value of IW to correct the water wetting model.

The inhibition of wettability can be measured from contact angle measurement. It is impossible to measure the contact angle of a water droplet in crude oil since it is impossible to see a water droplet in black crude oil. However, the effect of wettability alteration can be seen by using clear model oil after the steel has been pre-wetted with crude oil.

A steel coupon is prepared according to the same procedure as the test in Part 2. The steel coupon is first immersed in a crude oil for 1 hour (to let surface active compound adsorb onto the metal surface). The excess crude oil is mechanically removed using absorbent paper, and the coupon is immersed in clear model oil. A water droplet is placed onto the metal surface following the same procedure as explained in Part 2. Contact angle measurements taken after 10 minutes are shown in Table 20.

Table 20. *Contact angle measurement: water droplet in model oil (the steel is previously wetted by crude oil) with the empirical value of IW*

Oils pre-wetting the metal surface	Contact angle	Nature of steel surface	IW
Model oil	60°	Hydrophilic	0
Middle Eastern oil API 50	161°	Hydrophobic	0.3
Middle Eastern oil API 40	159°	Hydrophobic	0.3
Middle Eastern oil API 34	165°	Hydrophobic	0.3
Middle Eastern oil API 30	164°	Hydrophobic	0.3
Middle Eastern oil API 27	162°	Hydrophobic	0.3

The results in the Table above show that crude oil can change the steel wettability greatly by adsorption of surface active compounds onto the metal surface. Also, the alteration of wettability remained after immersion of the steel coupon in model oil. More importantly, only one value of IW is found for all the Middle Eastern oils. The table above shows that all Middle Eastern oils change steel wettability to the same magnitude.

Summary of the prediction

The first two parts of this chapter proved that surface active compounds naturally present in crude oil can significantly decrease both the oil-water interfacial tension and the water-steel interfacial tension. Both effects are beneficial from a corrosion point of view. The oil-water interfacial tension change was in the beneficial direction, but only slightly improved the flow pattern (from a wetting perspective), the water-steel interfacial tension's decrease was more significant and improved the steel wettability properties. Additionally, the study of the synergy between the two effects (both on a small scale and a large scale) showed that crude oil's naturally occurring surface active compounds can significantly decrease the corrosiveness of oil-water flows.

The synergy between effects (corrosion inhibition / wettability) should be considered with care. For example, myristic acid was found to be only a moderate corrosion inhibitor as shown in the previous chapter. However, the same molecule can reduce the corrosion rate to zero, not by conventional corrosion inhibition, but by changing the steel wettability, thus "pushing" water droplets away from the surface. Therefore, the choice of a high molecular weight naphthenic acid would be good for inhibition of corrosion in a pipeline carrying crude oils with small amounts of water.

CHAPTER 5 CONCLUSION

Achievements

The comprehensive study of crude oil chemistry effects on corrosion inhibition and phase wetting in oil-water flow was designed to test two main hypotheses:

Hypothesis 1 - Corrosion inhibition is induced by the accumulation of surface active compounds from the crude oil at the metal surface.

The experimental study proved that the adsorption of some surface active compounds onto the metal surface directly from the oil phase is able to inhibit iron dissolution, confirming Hypothesis 1. The experimental results were used to calibrate a mechanistic model of corrosion inhibition (Equation 43) based on the concentration of the organic species present in crude oil. It was found that in a crude oil, only a small fraction of organic species present have a direct effect on corrosion: for oxygen containing compounds only the high molecular weight organic acids, for sulfur containing compounds only the mercaptans and for nitrogen containing compounds only the basic nitrogen class. Even in these classes, not all sub-classes have an effect on corrosion. In the end, only a small percentage of the crude oil's complex chemistry controls its inhibitive properties.

Hypothesis 2 – The phase wetting of a steel pipe changes due to a synergy between the alteration of the steel wettability (by accumulation of surface active compounds at the metal surface) and modification of the flow pattern (by accumulation of surface active compounds at the oil-water interface).

The experimental study showed that phase wetting changes primarily due to the adsorption of surface active compounds onto the metal surface. On the other hand, the

change of flow pattern expected due to accumulation of surface active compounds at the oil-water interface is only a second-order effect.

As for the inhibition of corrosion, a mechanistic model of the change of wettability based on the crude oil's chemistry was created and calibrated using experimental results. It was found that the effect of the crude oil chemistry on steel wettability is produced by only two classes of compounds (aromatics and organic acids) while the other chemical classes tested have very little effect on steel wettability. It is now possible to calculate the flow pattern in a pipeline comingling oil and water using the water wetting model (Equation 35). And, in the case where it is predicted that the water will settle on the bottom of the pipe, it is also possible to determine whether the water is going to wet the steel surface or not using the wetting model (Equation 49).

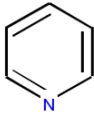
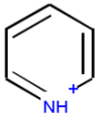
Recommendations for future work

Crude oil chemistry: This study focused on crude oil's surface active compounds. The surface active compounds are the chemicals most likely to adsorb onto the metal surface. However, crude oil has chemicals likely to change corrosion not only by adsorption of a thin film of organic species but also by deposition of a thick film of large molecules such as paraffins or asphaltenes. The effect of these large molecules needs to be studied for a complete understanding of the crude oil chemistry effect on corrosion and phase wetting in oil-water flow.

pH effect: Proton concentration is known to be a very important issue in a corrosion studies. The pH greatly influences proton reduction and therefore corrosion rates. Moreover, pH influences the solubility of surface active compounds such as carboxylic acids and pyridine. Carboxylic acids and pyridine normally adsorb onto the metal surface. Therefore, the protective layer might be formed or dissolved solely by changing the pH

as it is shown in Table 21. Further tests should be run at different pH, adjusting the pH by adding sodium bicarbonate or hydrochloric acid.

Table 21. *pH effect on carboxylic acid and pyridine*

Properties	Oil soluble	Water soluble	pKa
Carboxylic acid	R-COOH	R-COO ⁻	4 ~ 5 depending on R
Pyridine			5.6

Temperature: Temperature has an effect on the solubility of crude oil's chemicals in oil and water. In this study temperature was controlled and fixed at 25°C. More tests are needed to understand the effect of temperature on corrosion inhibition as well as on the steel wettability.

BIBLIOGRAPHY

1. Ayello, F., Robbins, W., Richter, S., & Nešić, S., (2008). Crude Oil Chemistry Effects on Inhibition of Corrosion and Phase Wetting. Paper presented at the 17th *International Corrosion Congress*, Las Vegas, NV, paper #3149.
2. Ayello, F., Li, C., Tang, X., & Nešić, S., (2008) Determination of phase wetting in oil-water pipe flow. Paper presented at *NACE CORROSION/08*, New Orleans, LA, paper #08566.
3. Tang, X., Ayello, F., Li, C., Nešić, S., & Cai, J., (2007). Effect of oil type on phase wetting transition in oil-water flows. Paper presented at *NACE CORROSION/07*, Nashville, TN, paper #07170.
4. Tang, X.; Ayello, F.; Li, C.; Cai, J., & Nešić, S., (2006). Water wetting and corrosion in horizontal and inclined flow of oil - water mixture. Paper presented at the *11th Middle East conference*, Manama Bahrain, SAUDI ARABIA, paper #06290.
5. Li, C.; Tang, X.; Ayello, F.; Cai, J., & Nešić S., (2006). Experimental Study on Water Wetting and CO₂ Corrosion in Oil-Water Two-Phase Flow. Paper presented at *NACE CORROSION/06*, San Diego, CA, paper #06595.
6. Cai, J.; Nešić, S.; Li, C.; Tang, X., & Ayello, F., (2005). Experimental Studies of Water Wetting in Large Diameter Horizontal Oil-Water Pipe Flows. Paper presented at *Society of Petroleum Engineers Annual Conference*, Dallas TX, paper #95512.
7. Campbell, R., (2006). Interview-BP faulty in Alaska's biggest oil spill. <http://www.reuters.com>, retrieved on November 10, 2007.
8. Choy, M., (2008). Alaska probes oil spill at Conoco's Alpine field. <http://www.reuters.com>, retrieved on December 08, 2008.
9. Wicks, M., & Fraser, J.P., (1975). Entrainment of water by flowing oil. *Materials performance*, 9-12.

10. Smith, L.M., Simon Thomas, M.J.J., & De Waard, C., (1987). Controlling factors in the rate of CO₂ corrosion. Paper presented at *NACE CORROSION/87*, Brighton, UK, paper #26.
11. De Waard, C., & Lotz, U., (1993). Prediction of CO₂ corrosion of carbon steel. Paper presented at *NACE CORROSION/93*, Houston, TX, paper #69.
12. Adams, C.D., Garber, J.D., Garber, F.H., & Singh C., (1993). Verification of computer model tubing life predictions by field data". Paper presented at *NACE CORROSION/93*, Houston, TX, paper #82.
13. Durnie, W.H., De Marco, R., Kinsella, B.J., & Jefferson, A., (1998). Predicting the performance of oil field corrosion inhibitors from their molecular properties. Paper presented at the *Corrosion and Prevention Conference*, Hobart, Australia, 187-192.
14. Durnie, W.H., De Marco, R., Kinsella, B.J., & Jefferson, A., (2003). In situ study of the adsorption of inhibitors of carbon dioxide corrosion. *Surface and interface analysis*, 35, 536-543.
15. Efir, K.D., (2004). *Corrosion tests and standards* (350-358). West Conshohocken: ASTM International.
16. Cook, E.L., & Hackerman, N., (1951). Adsorption of polar organic compounds on steel. *The Journal of physical and colloid chemistry*, 55(4), 549-557.
17. Hackerman, N., & Makrides, A.C., (1954). Action of polar organic inhibitor. *Industrial and engineering chemistry*, 46(3), 523-527.
18. Ragil, K., Bonn, D., Broseta, D., Indekeu, J., Kalaydjian, F., & Meunier, J., (1998). The wetting behavior of alkanes on water. *Journal of Petroleum Science & Engineering*, 20, 177-183.
19. Kowalewski, E., Holt, T., & Torsaeter, O., (2002). Wettability alterations due to an oil soluble additive. *Journal of Petroleum Science & Engineering*, 33, 19-28.
20. Nešić, S., Cai, J., & Kun-Lin, J.L., (2005). A multiphase flow and internal corrosion prediction model for mild steel pipeline. Paper presented *NACE CORROSION/05*, Dallas, TX, paper #05556.

21. Rudin, J., & Wasan, D.T., (1992). Mechanisms for lowering the interfacial tension in alkali/acidic oil systems – 1. Experimental studies. *Colloids and surfaces*, 68, 67-79.
22. Rudin, J., & Wasan, D.T., (1992). Mechanisms for lowering the interfacial tension in alkali/acidic oil systems – 2. Theoretical studies. *Colloids and surfaces*, 68, 81-94.
23. Kokal, S., (2002). Crude-oil emulsions: a state-of-the-art review. Paper presented at the *SPE annual technical conference and exhibition*, San Antonio, TX, paper #77497.
24. Efir, K.D., (2006). Oil characteristics, water/oil wetting and flow influence on the metal loss corrosion. PART 2: Chemistry, wettability and experimental evaluation. Paper presented *NACE CORROSION/06*, San Diego, CA, paper #06114.
25. Mendez, C., Duplat, S., Hernandez, S.E., & Vera, J.R., (2001). On the mechanism of corrosion inhibition by crude oil”; Paper presented *NACE CORROSION/01*, Houston, TX, paper #01030.
26. Hernandez, S.E., Duplat, S., Vera, J.R., & Baron, E., (2002). A statistical approach for analyzing the inhibiting effect of different types of crude oil in CO₂ corrosion of carbon steel. Paper presented *NACE CORROSION/02*, Houston, TX, paper #02293.
27. Hernandez, S.E., Nešić, S., Weckman, G., & Ghai, V., (2005). Use of artificial networks for predicting crude oil effect on CO₂ corrosion of carbon steels. Paper presented *NACE CORROSION/05*, Dallas, TX, paper #05554.
28. Bertrand, E., Bonn, D., Broseta, D., Dobbs, H., Indekeu, J.O., Meunier, J., Ragil, K., & Shahidzadeh, N., (2002). Wetting of alkanes on water. *Journal of Petroleum Science & Engineering*, 33, 217-222.
29. Drummond, C., & Israelchvili, C., (2003). Fundamental studies of crude oil-surface water interaction and its relationship to reservoir wettability. *Journal of Petroleum Science & Engineering*, 45, 61-81.

30. Jones, D.A., (1991). *Principles and prevention of corrosion*. New York: Macmillan Publishing Company.
31. De Waard, C., Lotz, U., & Milliams, D.E., (1991). Predictive model for CO₂ corrosion engineering in wet natural gas pipeline. *Corrosion*, 47, 750-764 .
32. Gray, L.G.S., Anderson, B.G., Danysh, M.J., & Tremaine, P.G., (1989). Mechanism of Carbon Steel Corrosion in Brines Containing Dissolved Carbon Dioxide at pH 4. Paper presented *NACE CORROSION/89*, Houston, TX, paper #464 .
33. Stern, M., (1955). The Electrochemical Behavior, Including Hydrogen Overvoltage, of Iron in Acid Environments. *Journal of the Electrochemical Society*, 102(11), 609-616.
34. Nešić, S., Postlethwaite, J., & Olsen, S., (1996). An Electrochemical Model for Prediction of Corrosion of Mild Steel in Aqueous Carbon Dioxide Solutions. *Corrosion*, 52, 280.
35. Hinze, J.O., (1955). Fundamentals of the hydrodynamic mechanism of splitting in dispersion process. *A.I.Ch.E. Journal*, 1(3), 289-295.
36. Taitel, Y., & Dukler A.E., (1976). A theoretical approach to the Lockhart-Martinelli Correlation for stratified flow. *International Journal of Multiphase Flow*, 2, 591-595.
37. Taitel, Y., & Dukler A.E., (1976). A model for prediction flow regime transition in horizontal and near horizontal gas-liquid flow. *A.I.Ch.E. Journal*, 22(1), 47-55.
38. Taitel, Y., (1977). Flow pattern transitions in rough pipes. *International Journal of Multiphase Flow*, 3, 597-601.
39. Taitel, Y., Barnea, D., & Dukler, A.E., (1980). Modeling flow pattern transitions for steady upward gas-liquid flow in vertical tubes. *A.I.Ch.E. Journal*, 26(3), 345-354.
40. Barnea, D., Shoham, O., & Taitel, Y., (1982). Flow pattern transition for downward inclined two phase flow; horizontal to vertical. *Chemical Engineering Science*, 37(5), 735-740.

41. Barnea, D., Shoham, O., & Taitel, Y., (1982). Flow pattern transition for downward inclined two phase flow; horizontal to vertical. *Chemical Engineering Science*, 37(5), 741-744.
42. Barnea, D., Shoham, O., Taitel, Y., & Dukler, A.E., (1985). Gas-liquid flow in inclined tubes: flow pattern transitions for upward flow. *Chemical Engineering Science*, 40(1), 131-136.
43. Barnea, D., & Brauner, N., (1985). Holdup of the liquid slug in two phase intermittent flow. *International Journal of Multiphase Flow*, 11(1), 43-49.
44. Barnea, D., (1986). Transition from annular and from dispersed bubble flow - unified models for the whole range of pipe inclination. *International Journal of Multiphase Flow*, 12(5), 733-744.
45. Barnea, D., (1987). A unified model for predicting flow pattern transitions for the whole range of pipe inclinations. *International Journal of Multiphase Flow*, 13(1), 1-12.
46. Brauner, N., (2001). The prediction of dispersed flows boundaries in liquid-liquid and gas-liquid systems. *International Journal of Multiphase Flow*, 27(5), 885-910.
47. Cai, J., Nešić, S., & De Waard, C., (2004). Modeling of Water Wetting in Oil-Water Pipe Flow. Paper presented at *NACE CORROSION/04*, Houston, TX, paper #04663.
48. Batchelor, G.K., (1951). Pressure fluctuation in isotropic turbulence. *Proceedings of the Cambridge Philosophical Society*, 47, 359 .
49. Clay, P.H., (1940). The mechanism of emulsion formation in turbulent flow. *Proceedings, Akademie van Wetenschappen*, 43, 852-965.
50. Brodkey, R.S., (1969). *The phenomena of fluid in motion*. London: Addison-Wesley.
51. Bond, W.N., & Newton, D.A., (1927). Bubbles and Drops and Stokes' Law. *Philosophical Magazine*, 4, 889-898.
52. Bond, W.N., (1928). Bubbles and drops and Stokes' Law (paper2). *Philosophical Magazine*, 5, 794-800.

53. Efirid, K.D., & Jasinki, R.J., (1989). Effect of the crude oil on corrosion of steel in crude oil/brine production. *Corrosion Engineering*, 45(2), 165-171.
54. Neumann, H.J., Paczynska-Lahme, B., & Severin, D., (1985). *Geology of petroleum*. New York: Halsted Press, 125.
55. Wu, Y., (1995). Entrainment Method Enhanced to Account for Oil's Water Content. *Oil & Gas Technology*, 83-86.
56. De Waard, C., Smith, L., & Craig, B.D., (2001). The Influence of Crude Oil on Well Tubing Corrosion Rates. Paper presented at *EUROCORR 2001*, Italy.
57. Snyder, L.R., (1970). Petroleum nitrogen compounds and oxygen compounds. *Accounts of chemical research*, 3(9), 290-299.
58. Robbins, K., & Hsu, C.S., (1999). Composition. *Kirk-Othmer Encyclopedia of Chemical Technology* (Fourth Edition), 18, 351-370.
59. Deyab, M.A., Abo Dief, H.A., Eissa, E.A., & Taman, A.R., (2007). Electrochemical investigations of naphthenic acid corrosion for carbon steel and the inhibitive effect by some ethoxylated fatty acids. *Electrochimica Acta*, 52, 8105–8110.
60. Szyprowski, A.J., (2000). Relationship between chemical structure of imidazoline inhibitors and their effectiveness against hydrogen sulphide corrosion of steels. *British Corrosion Journal*, 35, 155.
61. Sun, Y., George, K., & Nešić, S., (2003). The Effect of Cl and Acetic Acid on Localized CO₂ Corrosion in Wet Gas Flow. Paper presented at *NACE CORROSION/03*, SanDiego, CA, paper #03327.
62. Foad El Sherbini, E.E., (1999). Effect of some ethoxylated fatty acids on the corrosion behaviour of mild steel in sulfuric acid solution. *Materials Chemistry and Physics*, 60, 286-290.
63. Fajardo, V., Canto, C., Brown, B., & Nešić, S., (2007). Effect of Organic Acids in CO₂ Corrosion. Paper presented at *NACE CORROSION/07*, Nashville, TN, paper #07319.

64. Jovancicevic, V., Ahn, Y.S., Dougherty, J., & Alink, B., (2000). CO₂ corrosion inhibition by sulfur-containing organic compound. Paper presented at *NACE CORROSION/00*, Houston, TX, paper #00007.
65. Ajmera, P., (2009) Effect of Asphaltene on Phase Wetting and Internal Corrosion in Oil-Water Two Phase Flow (Master Thesis, Ohio University, 2009).
66. Li, C., (2009). Effect of Corrosion Inhibitor on Water Wetting and Carbon Dioxide Corrosion in Oil-Water Two-Phase Flow (Doctoral dissertation, Ohio University, 2009).
67. Durnie, W., De Marco, R., Kinsella, B., Jefferson, A., & Pejicic, B., (2005). Predicting the Adsorption Properties of Carbon Dioxide Corrosion Inhibitors Using a Structure-Activity Relationship. *Journal of Electrochemical Society*, 152(1), 1-11.
68. Hackerman, N., & Cook, E.L., (1951). Dual Adsorption of polar organic compounds on steel. *The Journal of physical and colloid chemistry*, 56, 524-526.
69. Hackerman, N., & Roebuck, A.H., (1954). Adsorption of polar organic compound on steel. *Industrial and engineering chemistry*, 46(7), 1481-1485.
70. Hackerman, N., & Hurd, R.M., (1961). Corrosion inhibition and molecular structure. Paper presented at the *First International Congress on Metallic Corrosion*, London, England, 166-169.
71. Vosta, J., Pelikan, J., & Hackerman, N., (1980). Study of the Character of the Inhibition Reaction (in Corrosion). Paper presented at the *Fifth European symposium on corrosion inhibition*, Ferrara, Italy, 255-266.
72. Hackerman, N., (1990). Review of Corrosion Inhibition Science and Technology. *Material Performance*, 29(2), 44-47.
73. Khaled, K.F., Babic-Samardzija, K., & Hackerman, N., (2005). Theoretical study of the structural effects of polymethylene amines on corrosion inhibition of iron in acid solutions. *Electrochimica Acta*, 50(12), 2515-2520.
74. Srhiri, A., Etman, M., & Dabosi, F., (1996). Electro and physicochemical study of corrosion inhibition of carbon steel in 3% NaCl by alkylimidazoles. *Electrochimica Acta*, 41(3), 429-437.

75. Chatterjee, J., & Wasan, D.T., (1998). A kinetic model for dynamic interfacial tension variation in an acidic oil/alkali/surfactant system. *Chemical Engineering Science*, 53(15), 2711-2725.
76. Varadaraj, R., & Brons, C., (2007). Molecular origins of heavy crude oil interfacial activity. Part 2: Fundamental interfacial properties of model naphthenic acids and naphthenic acids separated from heavy crude oils. *Energy & Fuels*, 21(1), 199-204.
77. Adamson, A.W., (1990). *Physical Chemistry of Surfaces* (5th edition). New York: Wiley.
78. Lord, D., Hayes, K., Demond, A., & Salehzadeh, A., (1997). Influence of Organic Acid Solution Chemistry on Subsurface Transport Properties. 1. Surface and Interfacial Tension. *Science Technology*, 31, 2045-2051.
79. Xu, Y., (2005). Dynamic Interfacial Tension between Bitumen and Aqueous Sodium Hydroxide Solutions. *Energy & Fuels*, 9, 148-154.
80. Xuanping, T., (2010) Effect of Surface State on Water Wetting and Carbon Dioxide Corrosion in Oil-Water Two-Phase Flows (Doctoral dissertation, Ohio University, 2010).
81. Hoiland, S., Barth, T., Blokhus, A.M., & Skauge, A., (2001). The effect of crude oil acid fraction on wettability as studied by interfacial tension and contact angles. *Journal of Petroleum Science & Engineering*, 30, 91-103.
82. Dubey, S.T., & Doe, P.H., (1993) Base number and wetting properties of crude oils. *SPE Reservoir Engineering*, 195-200.
83. Anderson, W.G., (1986). Wettability literature survey. *Journal of petroleum technology*, 1125-1141.
84. Yang, S.Y., Hirasaki, G.J., Basu, S., & Vaidya, R., (2002). Statistical analysis on parameters that affect wetting for crude oil/brine/mica system. *Journal of Petroleum Science & Engineering*, 33, 203-215.